THE THREE-BODY PROBLEM WITH SHORT-RANGE INTERACTIONS

E. NIELSEN[a,b], D.V. FEDOROV[c], A.S. JENSEN[c], E. GARRIDO[d]

[a]*Institute of Physics and Astronomy, University of Aarhus, DK-8000 Aarhus C, Denmark*
[b]*Department of Physics, Kansas State University, Manhatten, KA 66506-2601, USA*
[c]*Institute of Physics and Astronomy, University of Aarhus, DK-8000 Aarhus C, Denmark*
[d]*Instituto de Estructura de la Materia, CSIC, Serrano 123, E-28006 Madrid, Spain*

ELSEVIER

AMSTERDAM – LONDON – NEW YORK – OXFORD – PARIS – SHANNON – TOKYO

ELSEVIER

Physics Reports 347 (2001) 373–459

PHYSICS REPORTS

www.elsevier.com/locate/physrep

The three-body problem with short-range interactions

E. Nielsen[a,b], D.V. Fedorov[c], A.S. Jensen[c], E. Garrido[d,*]

[a]*Institute of Physics and Astronomy, University of Aarhus, DK-8000 Aarhus C, Denmark*
[b]*Department of Physics, Kansas State University, Manhatten, KA 66506-2601, USA*
[c]*Institute of Physics and Astronomy, University of Aarhus, DK-8000 Aarhus C, Denmark*
[d]*Instituto de Estructura de la Materia, CSIC, Serrano 123, E-28006 Madrid, Spain*

Received August 2000; editor: G.E. Brown

Contents

* Corresponding author.
E-mail address: imteg57@pinar2.csic.es (E. Garrido).

0370-1573/01/$ - see front matter
PII: S0370-1573(00)00107-1

Abstract

The quantum mechanical three-body problem is studied for general short-range interactions. We work in coordinate space to facilitate accurate computations of weakly bound and spatially extended systems. Hyperspherical coordinates are used in both the interpretation and as an integral part of the numerical method. Universal properties and model independence are discussed throughout the report. We present an overview of the hyperspherical adiabatic Faddeev equations. The wave function is expanded on hyperspherical angular eigenfunctions which in turn are found numerically using the Faddeev equations. We generalize the formalism to any dimension of space d greater or equal to two. We present two numerical techniques for solving the Faddeev equations on the hypersphere. These techniques are effective for short and intermediate/large distances including use for hard core repulsive potentials. We study the asymptotic limit of large hyperradius and derive the analytic behaviour of the angular eigenvalues and eigenfunctions. We discuss four applications of the general method. We first analyze the Efimov and Thomas effects for arbitrary angular momenta and for arbitrary dimensions d. Second we apply the method to extract the general behaviour of weakly bound three-body systems in two dimensions. Third we illustrate the method in three dimensions by structure computations of Borromean halo nuclei, the hypertriton and helium molecules. Fourth we investigate in three dimensions three-body continuum properties of Borromean halo nuclei and recombination reactions of helium atoms as an example of direct relevance for the stability of Bose–Einstein condensates.

PACS: 21.45. + v; 31.15. − p

1. Introduction

The classical three-body problem, Moon–Earth–Sun, still contains unanswered questions [1,2]. Also the quantum mechanical three-body problem has been around almost as long as quantum mechanics [3] and still in general considered "unsolved". Both structure and dynamical behaviour of this problem arises in all subfields of physics including chemical physics [4–19].

Precise and rigorous solutions are highly desirable both for use directly as well as in high accuracy studies of three-body correlations within various many-body systems. New and efficient methods providing both insight and high precision are most welcome as that developed recently [20,21]. This method is applicable for short-range interactions and may prove useful in the future also when long-range interactions are involved [22]. In this report we shall describe the method, generalize to d dimensions, extract a number of analytical conclusions and investigate numerically several topical physical systems. Further details and discussions are available in [23].

1.1. The three-body problem in various branches of physics

The two-body problem is classified as "solved" due to angular momentum conservation, which effectively reduces the problem to that of one-dimensional radial motion. The energy is then still conserved and in both classical and quantum mechanics the task is to solve a second-order ordinary differential equation corresponding to constant energy. For the three-body problem the configuration space is six-dimensional in the centre of mass system. Again spherically symmetric interactions between each pair of particles imply total angular momentum conservation, but this only provides three constants of motion effectively leaving a three-dimensional problem. For classical mechanics we have three coupled second order non-linear differential equations. In quantum mechanics we have instead a three-dimensional partial second-order differential equation and no efficient general numerical procedure exists.

In atomic physics the constituent particles are to a very good approximation point particles and the long-range Coulomb interaction is known exactly. The stability of Coulomb interacting three-body systems is, apart from borderline cases and possible additional forces, completely understood [24]. The equation of motion can immediately be written down and the (sometimes very difficult) problem is to find the solutions [8,24,25]. These long-range interacting systems are abundant, but beyond the scope of the present report.

In molecular or chemical physics three-body systems effectively arise when the Born–Oppenheimer approximation is used to separate out the electron motion [17,26–30]. Mixed molecular and atomic systems also exist [18,19,31], e.g. muonic molecules, $dt\mu^-$, are of practical interest for muon catalyzed fusion [32]. In nuclear physics there are the three-nucleon systems [7] and the more complicated nuclear clusters approximately described by three-body models [5,22,33–37]. Finally we have the nucleons (three-quarks) themselves [4].

In both nuclear and molecular physics the decoupling into clusters is much less efficient than for atomic systems. The particles are composed of other particles like quarks, other nuclei or electrons. The interactions are not known exactly and may effectively depend on the relative position and motion of all three particles. In nuclear physics the experimental data is often used to determine the effective two-body interaction [7], which in molecular physics most often is calculated in the

Born–Oppenheimer approximation as the ground state energy of the electrons with frozen nuclear positions [17,26–30].

The dependence of observables on the potentials has been discussed both in two [38,39] and three dimensions [13,35–37,40–43]. This question of *model independence* is interesting in nuclear physics aiming at effective nucleon–nucleon potentials and consistent models with predictive power. In molecular physics complicated models might be approximated by use of simpler potentials providing better physical insight and easier to handle numerically. Model independence relates different physical systems within different subfields of physics.

Borromean systems [5] occur in both molecular and nuclear physics. The prominent nuclear examples, ^{11}Li and ^{6}He, are often called neutron *halos* [13–15], which in other publications [44] are used as synonymous with Borromean system. A more suitable distinction and a precise definition is given in [43,45], where halos denote systems with a substantial cluster decomposition and a significant part of the wave function outside the classically allowed region.

For short-range interactions the *Efimov effect* [46] may appear, i.e. a three-body system has infinitely many bound states if at least two of the two-body subsystems have an infinite s-wave scattering length. The Efimov effect is mathematically the same as the *Thomas effect* [47], i.e. a three-body system with zero-range two-body interactions has infinitely many bound states. Extremely large scattering lengths are necessary to obtain just a few Efimov states and only the first is predicted in the atomic helium trimer [17,30]. They may also appear by chance in neutron dripline [37].

1.2. Theoretical few-body methods

The various few-body methods are in general each optimized for computation of different quantities. *Quantum Monte Carlo variational computations* are most efficient in calculations of ground-state energies. The Green function Monte Carlo method gives high-precision and the quantum diffusion Monte Carlo version efficiently improves the ground-state energy of an approximately known wave function [48,49]. The method is less suited for spatially dilute systems [48], for wave functions with nodes and when derivatives are involved. It is easily generalized to a higher number of particles, e.g. 112 ^{4}He atoms [48], *thermodynamic* properties of helium liquids [50], the first excited state of the effective four-body molecular system SF_6–He_3 [51] and nuclear systems with mass numbers up to 7 [49,52]. For nuclei with very complicated two- and three-nucleon potentials the effects arising from uncertainties in the interactions and from deficiencies of the methods are not easily separated.

The sudden approximation applies for high-energy scattering of two- and three-body projectiles on a one-body target provided the reaction time is much faster than the intrinsic projectile motion [53], e.g. fragmentation of ^{11}Li on ^{12}C [54] and e^- on ^{6}He [55].

The Faddeev equations [56] were originally intended for momentum space, where the three Faddeev components are expanded on the partial angular momenta related to the Jacobi coordinates. Most applications have been within nuclear physics, bound states as well as scattering [6], but also applied on atomic helium trimers [57]. The Faddeev equations have also been generalized to N-body systems [58] and used in both momentum [59] and coordinate space [60]. The numerical problems are substantial already for the four-body problem, e.g. $p + {}^{3}\mathrm{H} \to p + {}^{3}\mathrm{H}$, $n + {}^{3}\mathrm{He}$ and $d + d$ [61]. There are also ongoing attempts to make realistic calculations for $N > 4$ [62].

The Faddeev procedure is off hand most suited for short-range interactions [36,63]. However, treating the large distance part of the Coulomb interaction as the kinetic energy avoids the large couplings between partial angular momenta related to different Jacobi coordinates allowing computations of e.g. bound state energies of $dt\mu^-$ [32] and scattering processes like $e^+ + \mathrm{H} \to \mathrm{Ps} + p$ [64]. The partial wave expansion may be avoided by directly solving the coupled three-dimensional equations for the lengths of the two Jacobi coordinates and the angle between their directions [65], e.g. $p + p\mu^-$, $d + d\mu^-$, $t + t\mu^-$, $d + t\mu^-$ and $t + d\mu$ [65] and $N + d$ [66]. Hard cores present different problems [67].

The *hyperspherical harmonics expansion* uses the eigenfunctions of the six-dimensional angular momentum operator as an angular basis for the three-body wave function. The expansion coefficients, depending on hyperradius, are then determined by a set of coupled differential equations. This approach is useful for simple two-body potentials [68] and especially for Borromean systems of relatively small spatial extensions. When a two-body subsystem has a bound state an increasing number of hyperspherical harmonics are needed for increasing hyperradius. Including the two-body bound state wave function explicitly in the basis introduces difficulties related to the two non-orthogonal parts of the new basis [69]. This expansion is also not very useful for complicated potentials with repulsive cores and for high-precision calculations.

Kohn's variational principle has been used for the recombination process $e^+ + \mathrm{H} \to Ps + p$ for energies below the threshold for three-body breakup [70] and in three-body nuclear scattering processes [71]. Extension to energies above the three-body threshold, also including Coulomb interactions, employs Faddeev type of components each expanded on hyperspherical harmonics modified with factors describing two-body correlations [72,73]. The effort is shifted from a large number of relatively simple basis states to fewer complicated basis states designed to describe parts of the correlations, e.g. the atomic helium trimer ground state [74] and nuclear scattering $n + d$ and $p + d$ [71,74].

The hyperspherical adiabatic expansion was originally introduced to describe the autoionizing states in the helium atom [75]. Although these states are sharp resonances in the continuum they appear as bound states or as shape resonances in the individual adiabatic potentials. The couplings between these states are responsible for the decays. The method is specifically powerful for low-energy scattering and bound states. It provides physical insight, e.g. H^- [76], but is less accurate than variational methods, which on the other hand cannot predict resonances such as the autoionizing states in helium. In atomic and chemical physics this method has been successfully applied to many reactions, e.g. scattering $e + \mathrm{He}^+$ [77], $e^\pm + \mathrm{Ps}$ [78], $\mathrm{H} + \mathrm{H}_2$ [79], and reactions $e^- + \mathrm{H} \to Ps + p$ [80,81], $p + \mu^-\mathrm{H}^+$, $\mathrm{H}_2 + \mathrm{F} \to \mathrm{HF} + \mathrm{H}$ [26] and $\mathrm{D}_2 + \mathrm{F} \to \mathrm{DF} + \mathrm{D}$ [27].

1.3. The philosophy and structure of the report

This report employs the hyperspherical adiabatic expansion allowing thorough, yet transparent, general analyses of a number of physical systems within essentially all subfields of physics. The analytic formulations of the method are directly suited for numerical implementations. The distinct advantages are accurate treatment of both large and small distances, in contrast to the generally accepted belief, and identical procedures for bound and continuum states. The method, first developed for *s*-states [21], proved its power by supplying numerical properties of the Efimov

states [20]. Detailed knowledge of the basic three-body method is used in applications to study few-body correlations within a number of genuine many-body systems [82–85].

The report is intended to describe the method in details and as complete as possible, on a level allowing all physics researcher to follow and judge the arguments. We have generalized the formulation to d dimensions and focused on the mathematical structure, especially at large distances, and extracted as many model independent results as possible. These are often concerned with weakly bound and spatially extended systems, where the details of the interactions are less important. The numerical examples are molecular and nuclear halos. Interesting effects are halo properties and Efimov occurrence conditions in d (not necessarily integer) dimensions. Comparison between properties in two and three dimensions are particularly interesting [39,86]. We believe the report will be useful due to the detailed basic descriptions, the general conclusions, the physical insight and the topical systems used as illustrations.

We shall first in Section 2 sketch a derivation of the angular and radial equations of motion. In Section 3 we explain analytical and numerical details of our method including improvements to deal with a strong repulsive core. In Section 4 we pay special attention to the (sometimes crucial [13,43,39,87,88]) large-distance structure of the Faddeev equations and derive analytically as far as possible the asymptotic behaviour of the corresponding adiabatic potentials and the couplings between them. The exotic Efimov effect is discussed in Section 5 for d (perhaps non-integer) dimensions and for arbitrary total angular momentum [11,39,46,86,89].

The practical examples begin with a brief sketch of the properties of two-dimensional systems in Section 6. Then we discuss in Section 7 the bound state energies and structures of the atomic helium trimers [17,30,67]. They provide severe tests of both the numerical method and the possible model independence as well as information about properties and occurrence of Efimov states [30,89]. In Section 8 we study the nuclear halo structures exemplified by ^{11}Li (^{9}Li and two neutrons) [54], ^{6}He (alpha particle and two neutrons) [90] and the hypertriton (proton, neutron and Λ-particle) [91]. Other examples could have been isospin and beta decay [92], the solar neutrino problem [93], the dense helium plasma changing the properties of the three-α system with strong consequences for the triple α-rate [94] or few-body correlations producing new structures on, or even outside, the neutron dripline [95,96].

Application to the continuum structure and scattering involving three particles in both initial and final states are discussed in Section 9. The examples are the continuum structure of nuclear halo systems [97–101]. Other examples could have been the high-energy fragmentation processes of ^{6}He and ^{11}Li [40,54,90,102–104]. We shall also discuss the atomic helium trimers. First subject to an external electric field as a way of controlling the Efimov effect [105]. Second by computing recombination rates of three helium atoms into a dimer and a third helium atom by employing hidden crossing theory [106] combined with the hyperspherical adiabatic expansion [107].

Finally, we included three appendices containing independent results used in the derivations while Section 10 contains a brief summary and the conclusion.

2. Hyperspherical description of three-body systems

Three points in a d-dimensional space always define a *plane*. A three-body problem is therefore basically a planar problem independent of the number of dimensions d of the space, provided

of course that $d \geq 2$. For $d < 2$ the internal configuration of the system is restricted. For $d \geq 2$ the number of available dimensions only influences the centrifugal barrier terms. This has profound effects on both structure and dynamics of the three-body system. These observations are valid for all types of interactions. The total number of degrees of freedom is $3d$ including the centre of mass.

As we shall see the three-body problem can then be formulated in general for any dimension $d \geq 2$. We shall use Jacobi and hyperspherical coordinates and exploit the hyperspherical adiabatic expansion. We shall assume that d is an integer in all the derivations, even though this restriction is unnecessary. In fact, it is possible to carry out analytic continuations of some of the final results and thereby provide the generalization to non-integer dimensions. Similar techniques are used other places, e.g. dimensional $1/d$ expansion in chemical physics [108,109], analytical continuations in the dimension parameter and dimensional regularization in mathematical and particle physics [110,111].

We shall restrict ourselves to consider systems with short-range two-body interactions as defined by Eq. (C.5). It is tedious, perhaps technically difficult, but straightforward to add three-body short-range forces as well as the spin-dependent spin–orbit, spin–spin and tensor forces. The present formulation may also be useful for long-range interactions.

2.1. Hyperspherical coordinates

Let us consider 3 particles in d-dimensions, i.e. $3d$ degrees of freedom of which d and $2d$ are related to centre of mass and relative motion, respectively. The masses, coordinates and momenta of the particles are m_i, $\boldsymbol{r}_i$ and $\boldsymbol{p}_i$, $i = 1, 2, 3$. The total mass and momentum are $M_t = m_1 + m_2 + m_3$ and $\boldsymbol{P}_t = \boldsymbol{p}_1 + \boldsymbol{p}_2 + \boldsymbol{p}_3$. The Hamiltonian is, after subtraction of the centre of mass energy, given by

$$H = \sum_{i=1}^{3} \frac{\boldsymbol{p}_i^2}{2m_i} - \frac{\boldsymbol{P}_t^2}{2M_t} + \sum_{i=1}^{3} V_i(|\boldsymbol{r}_j - \boldsymbol{r}_k|) + V_{3b}(\boldsymbol{r}_1, \boldsymbol{r}_2, \boldsymbol{r}_3) \,, \tag{1}$$

where $\{i, j, k\}$ is as an even permutation of $\{1, 2, 3\}$ such that i is associated with the particle pair (j, k). The two-body interaction between the pair (j, k) is then denoted V_i, which here is assumed to be central and short range as defined in Eq. (C.5). The three-body interaction V_{3b} is added for later use.

2.1.1. Definition of the coordinates

Let us for each $i = 1, 2, 3$ define the ith set of *Jacobi coordinates* $(\boldsymbol{x}_i, \boldsymbol{y}_i)$ as

$$\boldsymbol{x}_i = \mu_{jk}(\boldsymbol{r}_j - \boldsymbol{r}_k), \qquad \mu_{jk} = \sqrt{\frac{m_j m_k}{m(m_j + m_k)}} \,,$$

$$\boldsymbol{y}_i = \mu_{i(jk)}\left(\boldsymbol{r}_i - \frac{m_j \boldsymbol{r}_j + m_k \boldsymbol{r}_k}{m_j + m_k}\right), \qquad \mu_{i(jk)} = \sqrt{\frac{m_i(m_j + m_k)}{m(m_i + m_j + m_k)}} \,, \tag{2}$$

where m is a normalization mass. Each of the sets, $\{i, j, k\} = \{1, 2, 3\}$, $\{2, 3, 1\}$, $\{3, 1, 2\}$, combined with the centre of mass coordinate, describes the system. The space-fixed *hyperspherical coordinates*

$(\rho, \alpha_i, \Omega_{xi}, \Omega_{yi})$ are [112]

$$x_i = \rho \sin\alpha_i, \quad y_i = \rho \cos\alpha_i \ , \tag{3}$$

where ρ is the *hyperradius* and α_i is the *hyperangle* confined by $0 \le \alpha_i \le \pi/2$. The angular parts of $\boldsymbol{x}_i$ and $\boldsymbol{y}_i$ describing their directions are denoted Ω_{xi} and Ω_{yi}, each therefore representing $(d-1)$ angles. The total number of coordinates is thus $2d$ of which only one carries the dimension length. The total set of the $2d-1$ angular coordinates $(\alpha_i, \Omega_{xi}, \Omega_{yi})$ is denoted by Ω_i or simply Ω.

The volume element corresponding to the relative motion is given by

$$\mathrm{d}^d\boldsymbol{x}_i \mathrm{d}^d\boldsymbol{y}_i = \rho^{2d-1}\mathrm{d}\rho \sin^{d-1}\alpha_i \cos^{d-1}\alpha_i \mathrm{d}\alpha_i \mathrm{d}\Omega_{xi}\mathrm{d}\Omega_{yi} \equiv \rho^{2d-1}\mathrm{d}\rho\mathrm{d}\Omega \ . \tag{4}$$

The kinetic energy operator in the centre of mass system is now given by

$$T = \frac{\hbar^2}{2m}\left[-\frac{\partial^2}{\partial\rho^2} - \frac{2d-1}{\rho}\frac{\partial}{\partial\rho} + \frac{\hat{\Lambda}^2}{\rho^2}\right], \tag{5}$$

$$\hat{\Lambda}^2 = -\frac{\partial^2}{\partial\alpha_i^2} - 2(d-1)\cot(2\alpha_i)\frac{\partial}{\partial\alpha_i} + \frac{\hat{l}_{xi}^2}{\sin^2\alpha_i} + \frac{\hat{l}_{yi}^2}{\cos^2\alpha_i} \ , \tag{6}$$

and $\hat{l}_{xi}$ and $\hat{l}_{yi}$ are the angular momentum operators corresponding to $\boldsymbol{x}_i$ and $\boldsymbol{y}_i$ respectively, see Appendix B for definitions when $d \neq 3$. Here $\hat{\Lambda}^2$ is the square of the *grand angular momentum* operator in $2d$ dimensions, see Eq. (B.3).

2.1.2. The kinematic rotation

The connection between different sets of Jacobi coordinates are [113,114]

$$\boldsymbol{x}_j = -\boldsymbol{x}_i \cos\gamma_{ij} + \boldsymbol{y}_i \sin\gamma_{ij}, \qquad \boldsymbol{y}_j = -\boldsymbol{x}_i \sin\gamma_{ij} - \boldsymbol{y}_i \cos\gamma_{ij} \ , \tag{7}$$

where the rotation angle is confined by $-\pi/2 \le \gamma_{ij} \le \pi/2$ and given by

$$\gamma_{ij} = \arctan\left(\sigma\{i,j,k\}\sqrt{\frac{m_k(m_1+m_2+m_3)}{m_i m_j}}\right) \tag{8}$$

and $\sigma\{i,j,k\}$ is the sign of the permutation $\{i,j,k\}$. This transformation is usually called the *kinematic rotation* [115]. The six possible rotations corresponding to $i \to j$, $i \neq j$, and the identity operation form a group. Successive rotations of $1 \to 2$, $2 \to 3$ and $3 \to 1$ then return all vectors back to their initial positions and therefore $\gamma_{12} + \gamma_{23} + \gamma_{31} = \pi$.

The hyperradius ρ is independent of the choice of Jacobi coordinates whereas the different hyperangles α_i are related by

$$\sin^2\alpha_j = \sin^2\alpha_i \cos^2\gamma_{ij} + \cos^2\alpha_i \sin^2\gamma_{ij} - 2\cos\alpha_i \sin\alpha_i \cos\gamma_{ij} \sin\gamma_{ij} \cos\theta_i \ , \tag{9}$$

where θ_i is the angle between $\boldsymbol{x}_i$ and $\boldsymbol{y}_i$. For a fixed value of α_i, θ_i can assume any value in the interval between 0 and 2π. Then we obtain the constraints

$$||\gamma_{ij}| - \alpha_i| \le \alpha_j \le \frac{\pi}{2} - \left|\frac{\pi}{2} - \alpha_i - |\gamma_{ij}|\right| . \tag{10}$$

We may use a *body-fixed* set of coordinates, e.g. $(\rho, \alpha_i, \theta_i)$, where the angles describing the orientation of the plane of the particles, the three Euler angles for $d = 3$, are removed. A number of coupled equations increasing with angular momentum and particle spins appears with coordinate and frame singularities related to the Coriolis force for non-vanishing angular momentum [115]. We shall use the laboratory system and the hyperspherical coordinates. Restrictions on the total angular momenta and its partial wave decomposition arise instead from the choice of basis functions. The total number of basis functions needed presumably turn out to be roughly the same in both these procedures.

2.2. Hyperspherical adiabatic expansion

We shall use the *adiabatic hyperspherical* expansion [75], where we first solve the angular part of the Schrödinger equation and then expand the full wave function on the complete set of these angular basis functions. For fixed ρ the set of eigenvalues and eigenfunctions are then obtained as solutions to

$$\left[\hat{\Lambda}^2 - \lambda_0(\rho) + \frac{2m}{\hbar^2}\rho^2 \sum_{i=1}^{3} V_i(\mu_{jk}^{-1}\rho \sin\alpha_i)\right]\Phi_n(\rho,\Omega) = \lambda_n(\rho)\Phi_n(\rho,\Omega)\,, \tag{11}$$

where we assumed that V_{3b} only depends on ρ. We also introduced $\lambda_0(\rho)$ as an arbitrary function of ρ to be chosen later for numerical efficiency. Then we expand the total wave function Ψ on this complete set of solutions

$$\Psi = \sum_n \rho^{-(2d-1)/2} f_n(\rho)\Phi_n(\rho,\Omega)\,, \tag{12}$$

where we included the radial phase-space factor $\rho^{-(2d-1)/2}$. The spectrum arising from Eq. (11) is discrete due to the finite intervals confining the angular variables or, alternatively, their periodic nature. The corresponding set of solutions is complete for each value of ρ as shown directly for $d = 3$ in [116].

Inserting Eq. (12) into the Schrödinger equation with the Hamiltonian in Eq. (1) we obtain by use of Eqs. (5) and (11) the coupled set of hyperradial equations

$$\left(-\frac{\partial^2}{\partial\rho^2} + \frac{1}{\rho^2}\left(\lambda_n(\rho) + \lambda_0(\rho) + \frac{(2d-3)(2d-1)}{4}\right) - Q_{nn} - \frac{2m(E - V_{3b}(\rho))}{\hbar^2}\right) f_n(\rho)$$
$$= \sum_{n' \neq n}\left(2P_{nn'}\frac{\partial}{\partial\rho} + Q_{nn'}\right) f_{n'}(\rho)\,, \tag{13}$$

where E is the three-body energy and the functions P and Q are defined by

$$P_{nn'}(\rho) \equiv \left\langle \Phi_n(\rho,\Omega)\left|\frac{\partial}{\partial\rho}\right|\Phi_{n'}(\rho,\Omega)\right\rangle_\Omega\,, \tag{14}$$

$$Q_{nn'}(\rho) \equiv \left\langle \Phi_n(\rho,\Omega)\left|\frac{\partial^2}{\partial\rho^2}\right|\Phi_{n'}(\rho,\Omega)\right\rangle_\Omega\,, \tag{15}$$

where these angular matrix elements for an operator O are defined by

$$\langle \Phi|O|\tilde{\Phi}\rangle_\Omega \equiv \int \mathrm{d}\Omega\, \Phi^*(\Omega) O \tilde{\Phi}(\Omega)\,, \tag{16}$$

with $\mathrm{d}\Omega$ from Eq. (4). All $\Phi_n(\Omega)$ are normalized and $P_{nn} = 0$. The expansion in Eq. (12) is efficient when the effective diagonal potentials in Eq. (13),

$$V_{\mathrm{eff},n} \equiv \frac{\hbar^2}{2m}\left(\frac{\lambda_n(\rho) + \lambda_0(\rho) + (2d-3)(2d-1)/4}{\rho^2} - Q_{nn}\right) + V_{3b}(\rho)\,, \tag{17}$$

dominate over the coupling terms $P_{nn'}$ and $Q_{nn'}$, where $n \neq n'$.

The equations in Eq. (13) decouple completely in the *adiabatic limit* where

$$\frac{\partial}{\partial\rho}\Phi_n = \frac{\partial^2}{\partial\rho^2}\Phi_n = 0\,. \tag{18}$$

Therefore $V_{\mathrm{eff},n}$ can provide substantial insight [75] in close analogy to the corresponding potentials obtained in the Born–Oppenheimer approach [25].

Differentiating Eq. (11) with respect to ρ give $P_{nn'}$ and $Q_{nn'}$ as

$$P_{nn} = 0\,, \tag{19}$$

$$P_{nn'} = -\frac{\left\langle \Phi_n \left| \dfrac{\partial V}{\partial\rho} \right| \Phi_{n'} \right\rangle_\Omega}{\lambda_n - \lambda_{n'}} \quad \text{for } n \neq n'\,, \tag{20}$$

$$Q_{nn} = \sum_{m\neq n} P_{nm}P_{mn}\,, \tag{21}$$

$$Q_{nn'} = 2\sum_{m\neq n, m\neq n'} \frac{\lambda_n - \lambda_m}{\lambda_n - \lambda_{n'}} P_{nm}P_{mn'} - \frac{1}{\lambda_n - \lambda_{n'}}\left(\left\langle \Phi_n \left| \frac{\partial^2 V}{\partial\rho^2} \right| \Phi_{n'} \right\rangle_\Omega + 2P_{nn'}\frac{\partial(\lambda_n - \lambda_{n'})}{\partial\rho}\right) \quad \text{for } n \neq n'\,, \tag{22}$$

$$V(\rho,\Omega) \equiv \sum_{i=1}^{3}\left(\rho^2\frac{2m}{\hbar^2}V_i(\mu_{jk}^{-1}\rho\sin\alpha_i) - \frac{1}{3}\lambda_0(\rho)\right). \tag{23}$$

These equations can immediately be used numerically and analytically to obtain $P_{nn'}$ as described in Section 4.4. It is more difficult to compute $Q_{nn'}$ as the expression in Eq. (22) includes a sum over all the angular eigenstates.

When high numerical precision is needed, the *adiabatic hyperspherical* method may be modified into the *diabatic-by-sector* or *hyperspherical close coupling* method [8,27,78,80,81], where a set of a priori chosen values of ρ, $\{\rho_1, \rho_2, \ldots, \rho_N\}$, is selected and the wave function Ψ for a given ρ is expanded on the angular eigenfunctions corresponding to the closest point $k = k(\rho)$ in such a set.

2.3. Faddeev equations

We have so far assumed a procedure where we selected one of the three sets of hyperspherical or Jacobi coordinates defined in Eq. (2). One choice is the democratic coordinates providing a completely symmetric treatment of each Jacobi set [79,117]. We shall use the Faddeev equations and wave functions with three components related to the three sets of Jacobi coordinates, i.e.

$$\Phi(\rho,\Omega) = \phi_1(\rho,\Omega) + \phi_2(\rho,\Omega) + \phi_3(\rho,\Omega)\ , \tag{24}$$

where each component, $i = 1,2,3$, satisfies the angular Faddeev equations

$$(\hat{\Lambda}^2 - \lambda)\phi_i + \left(\frac{2m}{\hbar^2}\rho^2 V_i(\mu_{jk}^{-1}\rho\sin\alpha_i) - \frac{1}{3}\lambda_0(\rho)\right)[\phi_1 + \phi_2 + \phi_3] = 0\ , \tag{25}$$

where we omitted the index n introduced in Eq. (11) to distinguish different angular solutions. By adding the three equations in Eq. (25) we obtain the original angular Schrödinger equation (11).

A three-body state where the particles j and k are in a two-body bound state and particle i is far away is described by $\phi_j = \phi_k = 0$ and ϕ_i essentially as the two-body bound state wave function, see Section 4.3. In general, ϕ_i describes the correlations between particles j and k including the correct, sometimes crucial, behaviour at large hyperradii. In Fig. 1 is indicated how strong correlations between two particles suggest the use of coordinates including one describing the corresponding relative two-body motion. The necessary corresponding angular momenta could be dramatically smaller.

Beside the correct asymptotics, another advantage of the Faddeev equations over the Schrödinger equation is that couplings to higher partial angular momenta in each Faddeev component is of second order in the potentials. To understand this we partial-wave expand each angular Faddeev component on angular momentum eigenfunctions coupled to a total orbital angular momentum L and projection M. Omitting ρ as an argument we then get for $d = 3$

$$\phi_i^{LM}(\Omega) = \sum_{l_x,l_y} \phi_i^{(l_x,l_y)}(\alpha_i)\,[\,Y_{l_x}(\Omega_{xi})\otimes Y_{l_y}(\Omega_{yi})\,]_{LM}\ , \tag{26}$$

where $\phi_i^{(l_x,l_y)}(\alpha_i)$ are expansion coefficients and l_x and l_y are the partial angular momenta related to the directions Ω_{xi} and Ω_{yi} of the coordinates $\boldsymbol{x}_i$ and $\boldsymbol{y}_i$. This familiar coupling of angular momenta in three dimensions is generalized to $d \neq 3$ in Appendix B. Finite intrinsic spins are discussed in Section 3.4.

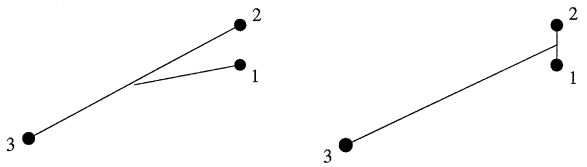

Fig. 1. When the two particles 1 and 2 are strongly correlated it is an advantage to use Jacobi set number 3 (right) rather than Jacobi set number 1 (left).

With Eq. (26) we rewrite Eq. (25) as

$$\left[-\frac{\partial^2}{\partial\alpha_i^2} - 2(d-1)\cot(2\alpha_i)\frac{\partial}{\partial\alpha_i} + \frac{l_x(l_x+d-2)}{\sin^2\alpha_i} + \frac{l_y(l_y+d-2)}{\cos^2\alpha_i} - \lambda \right]\phi_i^{(l_x,l_y)}(\alpha_i)$$
$$+ \left(\frac{2m}{\hbar^2}\rho^2 V_i(\mu_{jk}^{-1}\rho\sin\alpha_i) - \frac{1}{3}\lambda_0\right)\left(\phi_i^{(l_x,l_y)}(\alpha_i) + \sum_{j\neq i}\sum_{l'_x,l'_y}\hat{R}_{ij}^{(l_x,l_y)\,(l'_x,l'_y)}[\phi_j^{(l'_x,l'_y)}](\alpha_i)\right) = 0\ , \qquad (27)$$

where $\hat{R}_{ij}^{(l_x,l_y)\,(l'_x,l'_y)}$ is a projection operator transforming or "rotating" from the basis of Jacobi set j to that i [113,114], i.e.

$$\hat{R}_{ij}^{(l_x,l_y)\,(l'_x,l'_y)}[\phi_j^{(l'_x,l'_y)}](\alpha_i) = \int d\Omega_{xi}\int d\Omega_{yi}[Y_{l_x}(\Omega_{xi})\otimes Y_{l_y}(\Omega_{yi})]^*_{LM}$$
$$\times\,\phi_j^{(l'_x,l'_y)}(\alpha_j)[Y_{l'_x}(\Omega_{xj})\otimes Y_{l'_y}(\Omega_{yj})]_{LM}\ . \qquad (28)$$

In this integral $(\alpha_j,\Omega_{xj},\Omega_{yj})$ depend on $(\alpha_i,\Omega_{xi},\Omega_{yi})$ through Eqs. (7) and (9). The operator "rotating" from one set i to the same set i is the identity operator, i.e. $\hat{R}_{ii}^{(l_x,l_y)\,(l'_x,l'_y)}[\phi_i^{(l'_x,l'_y)}](\alpha_i) = \phi_i^{(l'_x,l'_y)}(\alpha_i)\delta_{l_x,l'_x}\delta_{l_y,l'_y}$.

In Eq. (27) $\phi_i^{(l_x,l_y)}$ is coupled to $\phi_j^{(l''_x,l''_y)}$ $(j\neq i)$ by a term of first order in the potential V_i and $\phi_j^{(l''_x,l''_y)}$ in turn is coupled to $\phi_i^{(l'_x,l'_y)}$ by a term of first order in V_j. Therefore the coupling between $\phi_i^{(l_x,l_y)}$ and $\phi_i^{(l'_x,l'_y)}$ is of second order in the potentials when $(l_x,l_y)\neq(l'_x,l'_y)$. This concludes the argument showing that the coupling of different angular momentum states in each of the Faddeev components at most is of second order in the two-body short-range potentials.

In this context we can now understand why the method is less suited for long-range Coulomb potentials where polarization effects are very important. Consider for example the system H^-. Let us assume a structure where one electron is bound to the proton and the other is far away. The hydrogen atom is significantly polarized and therefore excited into higher angular momentum states. In the Faddeev picture each partial angular momentum in the electron–electron system contributes substantially to the interaction causing the polarization. Thus the partial angular momentum convergence is very slow.

Returning now to short-range potentials. The coupling between different angular momentum states in the original Schrödinger equation is of first order in the potentials. Therefore to describe correlations arising from V_j and V_k a much larger number of partial angular momenta in Jacobi set i is often needed when the Schrödinger equation is used instead of the Faddeev equations, see Fig. 1. This is especially pronounced when more than one of the two-body subsystems has a bound state. The two simultaneously crucial two-body correlations are then much harder to describe with the Schrödinger equation. The asymptotic behaviour is decisive and is simply described with a few partial waves in the Faddeev equations. The extreme Efimov states [46,118] are in this way easily computed with only s-waves in all three Jacobi sets [20,37].

A disadvantage of the Faddeev equations is that the α_i equations are integro-differential equations, see Eq. (27). Another disadvantage is that Eq. (27) is not variational in the sense that the lowest angular eigenvalue λ_1 might be smaller than the exact eigenvalue when a limited number of partial angular momenta is included. For instance, if we do not include any basis states of the Faddeev component ϕ_3, the potential V_3 is not present in the Faddeev equations and the effects of

V_3 cannot be contained in their solution. Consequently, the computed lowest eigenvalue must be too small when V_3 is repulsive.

The advantage of variational equations can be regained by computing the energy as the expectation value of the Hamiltonian in the state obtained from the Faddeev equations. The variation should then consist of inclusion of different sets of basis functions. The numerical expense may easily be too high. It is more advantageous to parametrize the wave function in complete analogy to the Faddeev decomposition and use the Schrödinger equation directly.

All physical properties require computations of matrix elements. We therefore need to calculate the inner product between two wave functions in terms of the Faddeev components. Using the relation in Eq. (24) between the Schrödinger wave functions, Φ and Φ', and their Faddeev components we obtain

$$\langle \Phi | \tilde{\Phi} \rangle_\Omega = \left\langle \sum_{i=1}^{3} \phi_i \middle| \sum_{j=1}^{3} \tilde{\phi}_j \right\rangle_\Omega$$

$$= \sum_{i,j=1}^{3} \sum_{l_x,l_y,l'_x,l'_y} \int_0^{\pi/2} \mathrm{d}\alpha_i \sin^{d-1}\alpha_i \cos^{d-1}\alpha_i \phi_i^{(l_x,l_y)*}(\alpha_i) \hat{R}_{ij}^{(l_x,l_y)\,(l'_x,l'_y)} [\tilde{\phi}_j^{(l'_x,l'_y)}](\alpha_i) \,, \tag{29}$$

where the rotation operator $\hat{R}_{ij}$ is defined in Eq. (28).

Using the full space spanned by the three Faddeev components the resulting Schrödinger wave function may be vanishing, i.e. $\Phi = \phi_1 + \phi_2 + \phi_3 = 0$, even when the Faddeev components ϕ_i individually are non-zero [21,63,119]. These solutions with zero norm are unphysical and called *spurious* solutions. The corresponding Faddeev components may be obtained as eigenfunctions to the kinetic energy operator, since $\Phi = \phi_1 + \phi_2 + \phi_3 = 0$ implies that the potential term vanishes as seen from Eq. (25). Spurious states do not appear in momentum space Faddeev calculations [6] either because the total energy is negative or because the boundary conditions exclude vanishing wave functions.

In conclusion, the Faddeev equations provide a number of advantages although they also introduce complications. When all two-body interactions are of short range the angular Faddeev equations are simpler and more transparent to solve than the Schrödinger equation. We shall use the Faddeev equations and in the following illuminate the previous statements by numerical examples.

3. The hyperspherical adiabatic potentials

The key quantities in our adiabatic expansion are the angular eigenvalues $\lambda_n(\rho)$ defined by Eq. (11) or equivalently by Eq. (27), and the coupling constants $P_{nn'}(\rho)$ and $Q_{nn'}(\rho)$ defined by Eqs. (14) and (15). These quantities are needed as functions of the hyperradius ρ from zero to an upper limit $\rho_{\max}$ depending on the nature of the problem. This information is for short-range interactions most efficiently obtained by directly solving the Faddeev equations in Eq. (27). We shall concentrate on potentials where $r^2 V_i(r) \to 0$ for $r \to 0$. Then all $V_i(r)$ disappear from Eq. (27) in the limit $\rho = 0$. Moderately diverging potentials may also be treated, see [42] and Section 8.

3.1. The free angular solutions

Let us start with $\rho = 0$ and assume that $\rho^2 V_i(\mu_{jk}^{-1}\rho \sin\alpha_i) = 0$ for all i. Then the total angular wave functions as well as each of the Faddeev components are eigenfunctions of the kinetic energy operator for a constant ρ, see Eqs. (5), (11) and (25). These free solutions may be found from the partial-wave expansion in Eq. (27), which by defining $x = \cos 2\alpha_i$ reduces to the differential equation for the Jacobi functions in Eq. (A.1). The complete set of normalized free solutions to Eq. (25), regular at both $\alpha_i = 0$ and $\alpha_i = \pi/2$, are then for given quantum numbers l_x and l_y by use of Eq. (26) given as

$$\phi_i^{(L,M,K,l_x,l_y)}(\Omega_i) = \phi_i^{(l_x,l_y)}(\alpha_i)\,[\,Y_{l_x}(\Omega_{xi}) \otimes Y_{l_y}(\Omega_{yi})\,]_{LM}\ , \tag{30}$$

$$\phi_i^{(l_x,l_y)}(\alpha_i) = \mathcal{N}_n^{(l_x,l_y)} \sin^{l_x}\alpha_i \cos^{l_y}\alpha_i P_n^{((d-2)/2+l_x,\,(d-2)/2+l_y)}(\cos 2\alpha_i)\ , \tag{31}$$

$$\lambda = K(K+2d-2), \qquad K = 2n + l_x + l_y\ , \tag{32}$$

where n is a non-negative integer, $P_n^{((d-2)/2+l_x,\,(d-2)/2+l_y)}$ are Jacobi polynomials and the quantum numbers n (or K), l_x and l_y are non-negative integers limited by $l_x + l_y \le K$. The normalization constants $\mathcal{N}_n^{(l_x,l_y)}$ are derived from Eq. (A.4):

$$\mathcal{N}_n^{(l_x,l_y)} = \sqrt{\frac{(2n+d-1+l_x+l_y)\Gamma(n+1)\Gamma(n+d-1+l_x+l_y)}{2\Gamma(n+d/2+l_x)\Gamma(n+d/2+l_y)}}\ . \tag{33}$$

The free solutions in Eq. (30) form a convenient basis. They can be ordered into degenerate subspaces corresponding to each value of $K = 0, 1, 2, \ldots$ with the parity $(-1)^{l_x+l_y} = (-1)^K$, see Eq. (32) and Appendix B. The spectrum in Eq. (32) is the same as for the angular momentum operator for one particle in a space of dimension $2d$, see Appendix B. This is because the number of degrees of freedom determines the strength of the centrifugal barrier term as seen by transforming the kinetic energy operator from Cartesian to hyperspherical coordinates. The result is then obvious when the degrees of freedom are reduced by d effectively removing the centre of mass motion. The familiar example is the spectrum $K(K+4)$ for three particles in three dimensions.

3.1.1. Degeneracy of the free solutions

The eigenvalues are determined by the non-negative integer values of K obtained from n, l_x and l_y as in Eq. (32). The eigenstates related to each K-value are separated into states of given total angular momentum L. The remaining degeneracy related to each of the Faddeev components is denoted $D(d, L, K)$, where we do not include the trivial degeneracy of $2L+1$ due to angular momentum projection. From Eq. (32) we have in general that $l_x + l_y \le K$. For $d = 3$ each L-value, limited by $|l_x - l_y| \le L \le l_x + l_y$, corresponds to one state, where the different angular momentum projections still are not counted. For $d = 2$ the restrictions are instead $L = |l_x - l_y|$ or $L = l_x + l_y$, see Appendix B. For $d > 3$ the triangular inequalities and consequently the restrictions on K and L remain the same as for $d = 3$ [120].

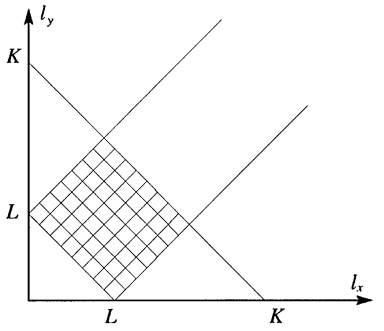

Fig. 2. The possible combinations of (l_x, l_y) for fixed values of the quantum numbers K and L are shown as every second of the points with integer coordinates within the rectangle defined by $|l_x - l_y| \le L \le l_x + l_y \le K$. Only every second point is allowed since $l_x + l_y$ must have the same parity as K. For $d = 2$ we have the restriction $L = |l_x - l_y|$ or $L = l_x + l_y$ implying that only points on three sides of the rectangle are possible. The number of states for $d \ge 3$ is thus $(L + 1)(K - L + 2)/2$ when $K + L$ is even and $L(K - L + 1)/2$ when $K + L$ is odd. For $d = 2$ we get instead the number of states $2\frac{1}{2}(K - L) + (L + 1) = K + 1$.

In Fig. 2 we sketch and compute the allowed sets of (l_x, l_y)-values for fixed K and L arriving at the number of states

$$D(d = 2, L, K) = K + 1 \,, \tag{34}$$

$$D(d, L, K) = \begin{cases} (L + 1)(K - L + 2)/2 & \text{for } K + L \text{ even} \,, \\ L(K - L + 1)/2 & \text{for } K + L \text{ odd} \,. \end{cases} \tag{35}$$

3.1.2. The kinematic rotation of the free solutions

The free solutions in Eq. (30) can be expressed in any of the three sets of Jacobi coordinates. The operator $\hat{R}_{ij}^{(l_x, l_y)\,(l'_x,\, l'_y)}$ describing this kinematic rotation from system j to system i is given in Eq. (28). The transformation relating the corresponding free solutions can be defined as an overlap matrix $\tilde{R}_{ij}$:

$$\tilde{R}_{ij}^{(LMKl_{xi}l_{yi},LMKl_{xj}l_{yj})} \equiv \langle \phi_i^{(LMKl_{xi}l_{yi})}(\Omega_i) \,|\, \phi_j^{(LMKl_{xj}l_{yj})}(\Omega_j) \rangle_\Omega \,, \tag{36}$$

which is diagonal in K, L and M due to (kinetic) energy and angular momentum conservation. The matrix elements are also independent of M. The remaining part, $\tilde{R}_{ij}^{(l_{xi}l_{yi},l_{xj}l_{yj})}$, is a square matrix of dimension $D(d, L, K)$.

The free solutions constitute a complete orthonormal basis for each of the Faddeev components as well as for the total wave function, i.e. the sum of the three Faddeev components. Each choice of Jacobi coordinate system selects the set of basis functions in Eq. (30). The transformation between these different sets must therefore be unitary and two subsequent transformations must be identical to one connecting the same initial and final basis sets, i.e.

$$\tilde{R}_{ij}\tilde{R}_{jk} = \tilde{R}_{ik}, \qquad \tilde{R}_{ij}^{-1} = \tilde{R}_{ij}^{\dagger}, \qquad \sum_{l_{xj}l_{yj}} \tilde{R}_{ij}^{(l_{xi}l_{yi},l_{xj}l_{yj})}\tilde{R}_{ji}^{(l_{xj}l_{yj},l'_{xi}l'_{yi})} = \delta_{l_{xi},\,l'_{xi}}\delta_{l_{yi},\,l'_{yi}} \,. \tag{37}$$

The matrix elements $\tilde{R}_{ij}^{(l_{xi}l_{yi},l_{xj}l_{yj})}$ for $d = 3$ are called the Raynal–Revai coefficients [113,121]. For $d = 2$ and $L = 0$ they can be found in [39].

The total wave function may be obtained from the three Faddeev components, expressed in any set of Jacobi coordinate, by use of the Hermitian matrix $\tilde{R}$ of dimension $3D(d,L,K)$ defined in terms of the matrices $\tilde{R}_{ij}$:

$$\tilde{R} = \begin{bmatrix} \tilde{R}_{11} & \tilde{R}_{12} & \tilde{R}_{13} \\ \tilde{R}_{21} & \tilde{R}_{22} & \tilde{R}_{23} \\ \tilde{R}_{31} & \tilde{R}_{32} & \tilde{R}_{33} \end{bmatrix}. \tag{38}$$

Using the group properties in Eq. (37) we then get $\tilde{R}^2 = 3\tilde{R}$ from which it follows that the eigenvalues of $\tilde{R}$ must be 0 or 3. Let us now for given (K,L,M) expand each Faddeev component ϕ_i of a wave function $\Phi = \phi_1 + \phi_2 + \phi_3$ on the free solutions in Eq. (30) with expansion coefficients $C_i^{(l_x,l_y)}$. The inner product in Eq. (29) between Φ and $\tilde{\Phi}$ is then

$$\langle \Phi | \tilde{\Phi} \rangle_\Omega = \sum_{i,i'=1}^{3} \sum_{l_x,l_y,l'_x,l'_y} C_i^{(l_x,l_y)*} \tilde{R}_{i,i'}^{(l_x,l_y)\,(l'_x,\,l'_y)} \tilde{C}_{i'}^{(l'_x,\,l'_y)} \equiv \langle C | \tilde{R} | \tilde{C} \rangle \,, \tag{39}$$

where $\tilde{R}$ is defined in Eq. (38) and $|C\rangle$ and $|\tilde{C}\rangle$ are the states described by the set of coefficients $C_i^{(l_x,l_y)}$ and $\tilde{C}_i^{(l_x,l_y)}$, respectively corresponding to Φ and $\tilde{\Phi}$.

Let us assume that $|C\rangle$ is a non-trivial eigenstate of $\tilde{R}$. Then its norm is zero according to Eq. (39) if the eigenvalue is 0 and non-zero if the eigenvalue is 3. Therefore the space spanned by the eigenstates corresponding to the eigenvalue 3 must be identical to the space of normalizable physical states. This space consisting of the free solutions to the Schrödinger equation has dimension $D(d,L,K)$. Since the full space has the dimension $3D(d,L,K)$ the remaining space spanned by eigenstates corresponding to the eigenvalue 0 must have the dimension $2D(d,L,K)$. This is then the space of non-normalizable states, identically vanishing functions named spurious solutions in Section 2.3.

The simplest example corresponds to $K = L = 0$, where the dimension is $D(d,0,0) = 1$ and the free solutions are constants independent of all angular coordinates. Expressing these constants in other coordinate systems give the same constants and the transformation matrix in Eq. (38) must then be

$$\tilde{R} = \begin{bmatrix} 1 & 1 & 1 \\ 1 & 1 & 1 \\ 1 & 1 & 1 \end{bmatrix}. \tag{40}$$

Thus, the unnormalized eigenfunctions of $\tilde{R}$ corresponding to the eigenvalue 3 is $(\phi_1,\phi_2,\phi_3) = (1,1,1)$ and a complete set corresponding to the eigenvalue 0 is for instance $(\phi_1,\phi_2,\phi_3) = (1,-1,0)$ and $(\frac{1}{2},\frac{1}{2},-1)$. Therefore, the physical space has dimension 1 and the space of spurious solutions has dimension 2.

3.2. Small distance solutions

We shall now formulate a method to solve the Faddeev equations in Eq. (27) for general short-range potentials for relatively small values of ρ, i.e. from zero and roughly up to the order of the ranges of the potentials.

3.2.1. Expanding on the free solutions

We shall expand each angular Faddeev component $\phi_i^{(LM)}(\Omega_i)$ on the complete set of free solutions in Eq. (30), i.e.

$$\phi_i^{(LM)}(\Omega_i) = \sum_{n,l_x,l_y} C_i^{(n,l_x,l_y)} \phi_i^{(L,M,K,l_x,l_y)}(\Omega_i) \,, \tag{41}$$

where L and M are the conserved angular momentum, $C_i^{(n,l_x,l_y)}$ are the expansion coefficients. The dependence and subsequent summation over n is needed, since non-vanishing interactions imply that $K = 2n + l_x + l_y$ no longer, in contrast to L and M, is a conserved quantum number.

Let C denote the column vector consisting of the expansion coefficients in Eq. (41) of all three Faddeev components sequentially ordered from $i = 1$ to 3. The angular Faddeev equations in Eq. (27) can then be written as

$$[\tilde{T} + \tilde{V}\tilde{R}]C = \lambda C \,, \tag{42}$$

where we assumed an appropriate truncation of the expansion in Eq. (41), used Eqs. (32) and (38), defined $\tilde{T}$ as the diagonal matrix with the matrix elements $K(K + 2d - 2)$ given by the eigenvalues of the kinetic energy operator and finally defined $\tilde{V}$ as the matrix form of the potentials

$$\begin{aligned}\tilde{V}_{i,i'}^{(n,l_x,l_y)\,(n',l'_x,l'_y)} \equiv{}& \delta_{i,i'}\delta_{l_x,l'_x}\delta_{l_y,l'_y}\mathcal{N}_n^{(l_x,l_y)}\mathcal{N}_{n'}^{(l'_x,l'_y)} \\ &\times \int_0^{\pi/2} \mathrm{d}\alpha_i \cos^{d-1}\alpha_i \sin^{d-1}\alpha_i \, P_n^{((d-2)/2+l_x,\,(d-2)/2+l_y)}(\cos 2\alpha_i) \\ &\times \left(\rho^2 \frac{2m}{\hbar^2} V_i(\mu_{jk}^{-1}\rho\sin\alpha_i) - \frac{1}{3}\lambda_0(\rho)\right) P_{n'}^{((d-2)/2+l'_x,\,(d-2)/2+l'_y)}(\cos 2\alpha_i) \,. \end{aligned} \tag{43}$$

In $\tilde{V}$ we omitted the indices for the conserved quantities L and M.

The matrix elements in Eq. (43) still remain finite for small ρ for Coulomb-like potentials, i.e. when $V_i(r) \propto r^{-1}$ for small r. Such an attractive potential must produce a Faddeev component similar to a Coulomb wave function for small α_i. Thus the components with $l_{xi} = 0$ must have a non-zero derivative at $\alpha_i = 0$. This behaviour is not present in any of the basis functions of the free solutions and the convergence as function of basis size is consequently considerably slower than for potentials that are finite at the origin.

For attractive potentials diverging for small r as $V_i(r) \propto r^{-2}$ this accuracy problem turns into a real divergence. Repulsive potentials with this behaviour at small α_i resemble a centrifugal barrier in α_i-space. The wave function is suppressed, but the behaviour is known and could then be incorporated. The accuracy is determined by two opposing effects, i.e. the wave function is small at small α_i, but the potential is large and the contribution to the energy therefore only needs a small probability to upset the accuracy. We shall treat strongly repulsive, non-diverging potentials numerically at small distances by using the freedom in $\lambda_0(\rho)$ in Eq. (42), see Section 7. A repulsive r^{-2}-potentials can also be used to remove Pauli blocked states when the three particles contain identical fermions [42], see Section 8.2.

3.2.2. Handling spurious solutions and symmetries

We showed in Section 3.1.2 that the eigenvalues of $\tilde{R}$ are 0 and 3, where the eigenfunctions corresponding to 0 are the spurious solutions. However, if the basis for a given K-value is incomplete, i.e. not all partial angular momenta with $l_x + l_y \leq K$ are included, the eigenvalues calculated using this truncated basis are no longer strictly 0 and 3, but somewhere in the interval $[0, 3]$.

To see this we denote the transformation $\tilde{R}$ in the reduced basis by $\tilde{R}_r$. The column vector C is assumed to be an eigenfunction with the eigenvalue x, i.e. $\tilde{R}_r C = xC$ and the norm $||C|| = 1$. Now we may write $C = C_3 + C_0$, where C_3 and C_0 are column vectors in the eigenspace of the full $\tilde{R}$ corresponding to the eigenvalues 3 and 0, respectively. Then $x = \langle C|\tilde{R}_r|C\rangle = \langle C|\tilde{R}|C\rangle = 3||C_3|| \in [0, 3]$. The eigenfunctions in the incomplete space corresponding to 0 are still unphysical, since the norm computed by Eq. (39) remains zero. Choosing an incomplete basis is highly desirable, because selection of basis states according to importance provide the flexibility of using high values of K and only the lowest angular momentum states, i.e. an incomplete basis.

Let us then introduce a new basis obtained as the eigenfunctions of $\tilde{R}$ diagonalized in the truncated basis. Rewriting the matrix equation in Eq. (42) in the new basis maintains the structure, since $\tilde{R}$ commutes with the diagonal kinetic energy matrix and these operators can therefore be simultaneously diagonalized. Now $\tilde{R}$ is diagonal with zero for all matrix elements corresponding to the eigenvalue zero. The new matrix $\tilde{V}\tilde{R}$ therefore completely decouples the spaces related to the eigenvalues 0 and 3. They can be solved independently and we can in the diagonalization of Eq. (42) discard the now uncoupled space corresponding to the eigenvalues 0. This procedure reduces the size of the matrix and removes at the same time the unphysical spurious solutions.

Another technically similar problem, although conceptually very different, is how to deal with the specific permutation symmetries necessary for systems of identical fermions or bosons. We first introduce $\tilde{P}$ as the operator projecting on the space of the desired permutation symmetry. We then replace $\tilde{R}$ in the above discussion by $\tilde{P}\tilde{R}$, i.e. we introduce a new basis as the eigenfunctions of $\tilde{P}\tilde{R}$ diagonalized in the old (truncated) basis. The matrix equation in Eq. (42) in this new basis maintains the same form, since both $\tilde{P}$ and $\tilde{R}$ commute with the kinetic energy operator. The space spanned by the eigenvalues of $\tilde{P}\tilde{R}$ corresponding to 0 then again decouples from the remaining space.

This (decoupled) space of functions of zero eigenvalue is identical to the space spanned by spurious solutions of zero norm and solutions of the wrong symmetry. This may be verified by writing any wave function as a sum of four terms corresponding to spurious–physical and right–wrong symmetry and by use of the properties of $\tilde{P}$ and $\tilde{R}$ as projection operators on correct permutation symmetry and physical states, respectively. Thus, the eigenfunctions with non-zero eigenvalues have both positive norm and the correct symmetry [63,119].

An example is identical particles 2 and 3 and the solutions classified as either symmetric or antisymmetric. The projection operator is then

$$P = \tfrac{1}{2}(1 \pm X_{23}) , \tag{44}$$

where X_{23} is the operator exchanging all coordinates of particles 2 and 3 and $(+)$ applies for bosons and $(-)$ for fermions. The matrix elements of X_{23} in the basis of Eq. (30)

are given by

$$X_{23}^{(i,n,l_x,l_y)\,(i',n',l'_x,l'_y)} = \delta_{n,n'}\delta_{l_x,l'_x}\delta_{l_y,l'_y}(-1)^{l_x}\begin{bmatrix}1 & 0 & 0\\ 0 & 0 & 1\\ 0 & 1 & 0\end{bmatrix}_{ii'}, \tag{45}$$

where we used that the effect of X_{23} are $\boldsymbol{x}_1 \mapsto -\boldsymbol{x}_1$ and the Jacobi coordinate systems 2 and 3 are interchanged, but with the opposite ordering of the two particles implying that the signs of the vectors $\boldsymbol{x}_2$ and $\boldsymbol{x}_3$ also are changed, see Eq. (2). Here we assumed that the truncation in the basis is symmetric for the components for identical particles 2 and 3, i.e. if one term in the expansion of Faddeev component number 2 is included the same term in the expansion of Faddeev component number 3 must also be included, and vice versa.

Similarly, if all three particles are identical the projection operator is

$$P = \tfrac{1}{6}(1 + X_{12}X_{23} + X_{23}X_{12} \pm X_{12} \pm X_{23} \pm X_{31}), \tag{46}$$

where the exchange operators X_{ij} are defined in analogy to X_{23} and $(+)$ again applies for bosons and $(-)$ for fermions. The corresponding matrix elements are obtained by use of Eq. (45). Clearly, the same basis truncation for all three Faddeev components are also required for this highly symmetric case.

It is here worth emphasizing that X_{23} in Eq. (45) is diagonal in the quantum number n and furthermore also independent of n. Therefore, X_{23} can easily be generalized when other basis function than Jacoby polynomials are used for the α_i motion. This illustrates that symmetry comes in quite naturally in the Faddeev equations. In contrast, symmetrization when using the Schrödinger equation is more difficult unless symmetric coordinates are chosen from the beginning, e.g. the Smith–Whitten coordinates in [122]. In any case the procedure described above simultaneously reduces the size of the matrix, removes the unphysical spurious solutions and restores the correct symmetries.

3.2.3. *Perturbative treatment for small ρ*

We can solve the Faddeev equations in Eq. (42) for small ρ in perturbation theory. Let us assume that the column vector C is a solution to Eq. (42) for $\tilde{V} = 0$ with an angular eigenvalue of $\lambda = K(K + 2d - 2)$. Then only components with this K are present in the perturbative solution. Then Eq. (42) reduces to

$$\tilde{V}\tilde{R}C = [\Delta\lambda - \lambda_0(\rho)]C, \tag{47}$$

where $\lambda = -\lambda_0(\rho) + K(K + 2d - 2) + \Delta\lambda$ and $\tilde{V}$ is diagonal and given by

$$\tilde{V}_{i,i'}^{(n,l_x,l_y)\,(n',l'_x,l'_y)} \simeq \delta_{i,i'}\delta_{l_x,l'_x}\delta_{l_y,l'_y}\delta_{n,n'}\left(\rho^2\frac{2m}{\hbar^2}V_i(0) - \frac{1}{3}\lambda_0(\rho)\right). \tag{48}$$

Let us for simplicity assume that $V_i(0) = V_0$. Then the diagonal part of $\tilde{V}$ is given by $\tilde{V} = (\rho^2(2m/\hbar^2)V_0 - \frac{1}{3}\lambda_0(\rho))$ and therefore

$$\tilde{R}C = \frac{\Delta\lambda - \lambda_0(\rho)}{(2m/\hbar^2)V_0\rho^2 - \frac{1}{3}\lambda_0(\rho)}C \equiv xC. \tag{49}$$

Thus, C is an eigenvector of $\tilde{R}$ with the eigenvalue x and consequently

$$\Delta\lambda = x\frac{2m}{\hbar^2}\rho^2 V_0 - \lambda_0(\rho)\left(\frac{x}{3} - 1\right). \tag{50}$$

If $x = 3$ the λ_0 dependence disappears and the expression is precisely the first order perturbation result derived directly from the Schrödinger equation in Eq. (11), provided $\lambda_0(\rho)$ is equivalently treated, i.e.

$$\lambda = -\lambda_0(\rho) + K(K + 2d - 2) + \frac{2m}{\hbar^2}\rho^2 \sum_{i=1}^{3} V_i(0)\,, \tag{51}$$

where we lifted the restriction of identical strengths of the potentials. The value $x = 3$ can only be obtained if the basis with the K-space is complete otherwise $x < 3$ and the eigenvalue will behave as if the potentials were weaker.

This derivation can rather easily be generalized for potentials diverging as r^{-1} when $r \to 0$. Then the α_i dependence remains as $\sin^{-1}\alpha_i$, the strength becomes proportional to ρ and vanishing in the limit of $\rho = 0$. The result is that the terms $\rho^2 V_i(0)$ in Eq. (51) must be replaced by the expectation value with the unperturbed wave function of the small ρ limit of $\rho^2 V_i(\mu_{jk}^{-1}\rho\sin\alpha_i)$.

Potentials diverging as r^{-2} when $r \to 0$ do obviously not vanish in the limit of $\rho = 0$. However, they approach a constant times $\sin^{-2}\alpha_i$. The solution in α_i space may then be obtained exactly in this limit. If the wave function is concentrated at small α_i the potential is simply adding a term proportional to α_i^{-2}, i.e. of the form as a centrifugal barrier or attraction. This may then be treated more precisely resulting in a non-vanishing constant to be added to the eigenvalue spectrum. If only one of the two-body potentials has this long-range behaviour on top of otherwise short-range interactions the constant simply redefines the partial angular momentum quantum number l_{xi} [42].

3.2.4. The minimal basis size

The final perturbation expression in Eq. (51) only holds if the eigenvalues of $\tilde{R}$ are 0 or 3. This is only fulfilled if the basis for each K-value is complete, i.e. all possible partial angular momenta must be included in the basis. Let us aim at computing all angular eigenvalues up to a certain limit, i.e. $\lambda + \lambda_0(\rho = 0) \leq \lambda_{\max} \equiv K_{\max}(K_{\max} + 2d - 2)$, where $K_{\max}$ is defined by this equation for $\rho = 0$. Then the bases are complete for all $K \leq K_{\max}$ for $\rho = 0$, provided the summation in Eq. (41) for each Faddeev component includes all $0 \leq l_x + l_y \leq K_{\max}$ and all $0 \leq n \leq n_{\max} = \frac{1}{2}(K_{\max} - l_x - l_y)$.

With increasing ρ, couplings between different K-values become important and first-order perturbation breaks down. This implies that values of n, l_x and l_y higher than for $\rho = 0$ are needed in the expansion in Eq. (41). On the other hand, compared to the potential energy term in Eq. (27) the repulsive angular momentum barriers become increasingly important as l_x and l_y increases. This suppresses the contributions from high partial waves and only the smaller partial angular momenta are needed for a given K-value. In fact, only the lowest partial angular momenta are needed for large ρ, see Section 4.

For finite ρ the basis then has to be complete for all $K \leq K_{\max}$, where $K_{\max}(K_{\max} + d - 2) \sim \lambda_{\max}$ roughly defines the largest angular eigenvalue $\lambda_{\max}$ we want to compute accurately. For a repulsive core the angular eigenvalues λ must become very large for small ρ-values. However, $K_{\max}$ is not necessarily large, since we can exploit the freedom in choosing $\lambda_0(\rho)$ close to the

anticipated ρ-dependent value of the most important (lowest) eigenvalue λ. In principle, the results are independent of $\lambda_0(\rho)$, even when we exploit the allowed ρ-dependence. This redefinition of zero point energy can reduce considerably the number of K-values in which a complete basis is needed.

The numerical procedure for highly repulsive cores is then to choose $\lambda_0(\rho)$ such that the lowest eigenvalue $\lambda_1(\rho)$ is as close to zero as possible. Then only eigenvalues $\lambda(\rho) \leq \lambda_{\max}$ corresponding to values of $K \leq K_{\max}$, where $K_{\max}(K_{\max} + d - 2) \sim \lambda_{\max} - \lambda_1(\rho)$, require a complete basis. This method is used in accurate computations of the atomic helium trimers discussed in Section 7. It could also be useful for hard-core nucleon–nucleon potentials.

Increasing ρ we see from Eq. (27) that the effective potential, $\rho^2 V(\mu_{jk}^{-1}\rho \sin\alpha_i)$, becomes both increasingly deeper and more narrow as a function of α_i. The wave function then must vary rapidly from zero for $\alpha_i = 0$ to a finite value at the edge of the short-range potential after which a smooth dependence is obtained in the (much larger) interaction free region of α_i-space. These potentials may also support bound states in an amount roughly independent of ρ, since the potential depth increases as ρ^2 while the range decreases as ρ^{-1}. Thus, to describe the strong variation and the possible nodes of the components $\phi_i^{(l_x,l_y)}(\alpha_i)$ in Eq. (41), we need a basis with an increasing number of polynomials (large n), but not necessarily with large partial angular momenta.

The overall conclusions are then that we must choose a complete basis for small K-values, for intermediate K we only need to include some of the possible partial angular momenta, and for high values of K we can decrease the number of partial angular momentum components and concentrate on the lowest partial angular momenta. This prescription of increasing the number of polynomials for each (l_x, l_y) as ρ increases is limited in practice to values of the hyperradius comparable to the ranges of the interactions.

3.3. Intermediate distance solutions

The three particles all simultaneously interact when the hyperradius is sufficiently small. Increasing ρ we arrive at intermediate distances corresponding to configurations where at least one particle must be outside the interaction ranges of both the other two, see Fig. 3. Overlapping

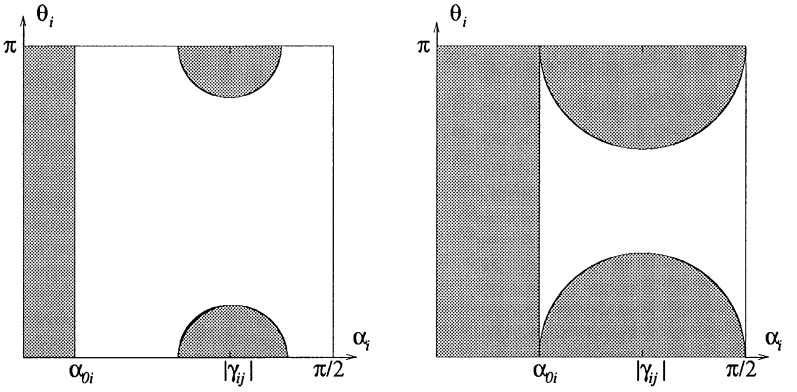

Fig. 3. The shaded areas of non-zero potentials in the (α_i, θ_i)-plane, where θ_i is the angle between $\boldsymbol{x}_i$ and $\boldsymbol{y}_i$. For a large value of the hyperradius (left) the potentials V_j and V_k are only non-zero close to the point $\alpha_j = 0$, i.e. $\alpha_i = |\gamma_{ij}|$ and $\theta_i = 0$ or $\theta_i = \pi$, see Eq. (7). For a smaller hyperradius the potentials start to overlap (right).

potentials require a definition, at least for anything else than schematic square well potentials, of a distance r_{0i} outside which the potential V_i is sufficiently small to be neglected in this context. We shall tentatively use Eq. (C.5) and assume that $V_i(r) \simeq 0$ for $r > r_{0i}$. The corresponding value α_{0i} outside which the potential $V_i(\mu_{jk}^{-1}\rho \sin\alpha_i)$ is negligible as function of α_i for fixed ρ is then given by

$$\alpha_{0i} = \arcsin(\mu_{jk} r_{0i}/\rho) \approx \mu_{jk} r_{0i}/\rho \ , \tag{52}$$

where the last approximation only is valid for large ρ.

The assumption that all three potentials do not overlap simultaneously for a given ρ may be expressed by the statement that if one point is inside the range of potential i, then it must be outside the ranges of both the potentials j and k, or, in an equivalent mathematical formulation, if $\alpha_i \leq \alpha_{0i}$ then $\alpha_j > \alpha_{0j}$ and $\alpha_k > \alpha_{0k}$, where (i,j,k) is a permutation of $(1,2,3)$. From Eq. (10) this implies that $\alpha_{0i} + \alpha_{0j} < \gamma_{ij}$ for all i and j, $i \neq j$. By use of Eq. (52) we then obtain a sufficient condition for non-overlapping potentials, i.e.

$$\rho > (\mu_{jk} r_{0i} + \mu_{ik} r_{0j})/\sin\gamma_{ij} \quad \text{for all pairs } (i,j) \text{ where } i \neq j \ , \tag{53}$$

which in the following shall serve as the definition of intermediate distances.

3.3.1. The Faddeev components outside the potentials

We can now solve the angular Faddeev equations in Eq. (27) for $\alpha_i > \alpha_{0i}$, i.e. in the regions where the potentials are zero. We shall from now on assume that $\lambda_0 = 0$, since we have no use for the associated flexibility at larger distances. The solutions, regular at $\alpha_i = \pi/2$, are then according to Appendix A given by

$$\begin{aligned}\phi_i^{(l_x,l_y)}(\alpha_i) &= A_i^{(l_x,l_y)} \sin^{l_x}\alpha_i \cos^{l_y}\alpha_i \Gamma(v+1) \\ &\quad \times P_v^{((d-2)/2+l_y,\,(d-2)/2+l_x)}(-\cos 2\alpha_i) \ ,\end{aligned} \tag{54}$$

where $A_i^{(l_x,l_y)}$ is an arbitrary constant and

$$v \equiv -\tfrac{1}{2}(d-1+l_x+l_y) + \tfrac{1}{2}\sqrt{(d-1)^2+\lambda} \tag{55}$$

or, equivalently, expressing λ in terms of v

$$\lambda = (2v+l_x+l_y)(2v+l_x+l_y+2d-2) \ . \tag{56}$$

If v is a non-negative integer Eq. (54) reduces to the free solutions of Eq. (31).

There is an ambiguity in the definition of v when λ assumes too negative values. We specify fully by choosing the branch of the square root in Eq. (55) such that v is either real or complex with positive imaginary value. In the following we shall maintain this definition of v as a function of λ, l_x and l_y.

The derivation assumed that the potential $V_i(\mu_{jk}^{-1}\rho \sin\alpha_i)$ is exactly zero for $\alpha_i > \alpha_{0i}$. The correction to the eigenvalue arising from this assumption is to first order in the deviation from zero

of $V_i(\mu_{jk}^{-1}\rho\sin\alpha_i)$ for $\alpha_i > \alpha_{0i}$ found as

$$|\delta\lambda| \le M_i^{(l_x,l_y)} \int_{\alpha_{0i}}^{\pi/2} \mathrm{d}\alpha_i \sin^{d-1}\alpha_i \cos^{d-1}\alpha_i \frac{2m}{\hbar^2}\rho^2 |V_i(\mu_{jk}^{-1}\rho\sin\alpha_i)|$$

$$\le M_i^{(l_x,l_y)} \mu_{jk}^d \rho^{2-d} \int_{r_{0i}}^{\rho/\mu_{jk}} \mathrm{d}r\, r^{d-1} \frac{2m}{\hbar^2} |V_i(r)| \,, \tag{57}$$

where we used the substitution $r = \mu_{jk}^{-1}\rho\sin\alpha_i$ and the definition

$$M_i^{(l_x,l_y)} \equiv |A_i^{(l_x,l_y)} \Gamma(\nu+1)|^2$$

$$\times \max_{\alpha_i \ge \alpha_{0i}} |\sin^{l_x}\alpha_i \cos^{l_y}\alpha_i\, P_\nu^{((d-2)/2+l_y,\,(d-2)/2+l_x)}(-\cos 2\alpha_i)|^2 \tag{58}$$

of the maximum probability for the solution in Eq. (54) for $\alpha_i \ge \alpha_{0i}$. Since $M_i^{(l_x,l_y)}$ is a finite number for a given ρ we can for short-range potentials make $\delta\lambda$ arbitrarily small by choosing r_{0i} sufficiently large, see Eq. (C.5). However, the accuracy is limited by ρ through the upper bound of r_{0i} defined in Eq. (53).

3.3.2. The Faddeev components inside the potentials

We now turn to the angular Faddeev equations in Eq. (27) for $\alpha_i < \alpha_{0i}$, i.e. in the regions where the potential V_i differs from zero while V_j and V_k for intermediate distances therefore must be vanishingly small. In other words, we have both $\alpha_j > \alpha_{0j}$ and $\alpha_k > \alpha_{0k}$. Then the two Faddeev components, ϕ_j and ϕ_k, are both eigenfunctions of the kinetic energy operator, see Eq. (25), i.e.

$$(\hat{\Lambda}^2 - \lambda)\phi_j(\alpha_i) = 0, \qquad (\hat{\Lambda}^2 - \lambda)\phi_k(\alpha_i) = 0 \,, \tag{59}$$

where the dependence of α_i indicates that we used the freedom to choose i as the most convenient Jacobi system. Then for $\alpha_i \le \alpha_{0i}$ we see that $\phi_i = -\phi_j - \phi_k$ is one particular solution to Eq. (25), since each of the potential and kinetic energy terms independently vanish due to the trivial factor of zero and by use of Eq. (59). Thus ϕ_i is an eigenfunction of the kinetic energy operator. We want to express this particular solution ϕ_i explicitly as function of α_i. Then we must transform the other two Faddeev components to Jacobi set i. We first note that ϕ_j and ϕ_k must be regular for $\alpha_i = 0$, because this point expressed in the other Jacobi coordinates must be within the regions $\alpha_j > \alpha_{0j}$ and $\alpha_k > \alpha_{0k}$, where both functions are regular solutions. Projection of these Faddeev components on the partial angular momentum states of Jacobi set i maintain these properties, i.e. the projected functions are still regular (at $\alpha_i = 0$) and eigenfunctions of the kinetic energy operator.

Thus the kinematic rotation operator in Eq. (28) acting on ϕ_j in Eq. (54) must be proportional to another eigenfunction, regular at $\alpha_i = 0$, of the kinetic energy operator. Using the properties in Eqs. (A.1) and (A.2) we then find

$$\hat{R}_{ij}^{(l_x,l_y)\,(l'_x,\,l'_y)}[\sin^{l'_x}\alpha_j \cos^{l'_y}\alpha_j \Gamma(\nu'+1) P_{\nu'}^{((d-2)/2+l'_y,\,(d-2)/2+l'_x)}(-\cos 2\alpha_j)\,](\alpha_i)$$

$$= R_{ij}^{(l_x,l_y)\,(l'_x,\,l'_y)}(\lambda)\sin^{l_x}\alpha_i \cos^{l_y}\alpha_i \Gamma(\nu+1) P_\nu^{((d-2)/2+l_x,\,(d-2)/2+l_y)}(\cos 2\alpha_i) \,, \tag{60}$$

where ν, ν' and λ are related by Eqs. (55) and (56) through energy conservation (same λ). The coefficients $R_{ij}^{(l_x,l_y)\,(l'_x,l'_y)}(\lambda)$ may depend on λ, but not on α_i. Using the definition in Eq. (28) of the operator $\hat{R}_{ij}^{(l_x,l_y)\,(l'_x,l'_y)}$ we find

$$\begin{aligned} &R_{ij}^{(l_x,l_y)\,(l'_x,l'_y)}(\lambda) \\ &\quad = \int \mathrm{d}\Omega_{xi} \int \mathrm{d}\Omega_{yi} \frac{\sin^{l'_x}\alpha_j \cos^{l'_y}\alpha_j \Gamma(\nu'+1) P_{\nu'}^{((d-2)/2+l'_y,\,(d-2)/2+l'_x)}(-\cos 2\alpha_j)}{\sin^{l_x}\alpha_i \cos^{l_y}\alpha_i \Gamma(\nu+1) P_{\nu}^{((d-2)/2+l_x,\,(d-2)/2+l_y)}(\cos 2\alpha_i)} \\ &\qquad \times [\,Y_{l_x}(\Omega_{xi}) \otimes Y_{l_y}(\Omega_{yi})\,]_{LM}^{*} [\,Y_{l'_x}(\Omega_{xj}) \otimes Y_{l'_y}(\Omega_{yj})\,]_{LM} \ , \end{aligned} \tag{61}$$

where $(\alpha_j, \Omega_{xj}, \Omega_{yj})$ are functions of $(\alpha_i, \Omega_{xi}, \Omega_{yi})$ through Eq. (7). This result formally depends on the value of α_i, but if the point of divergence $\alpha_j = 0$ is excluded from the integral in Eq. (61) the coefficients are independent of α_i. This condition of excluding $\alpha_j = 0$ is fulfilled for $\alpha_i < |\gamma_{ij}|$, see Eq. (10).

The coefficients in Eq. (61) are related to an analytic continuation to non-integer ν of the matrix elements $\tilde{R}$ defined in Eq. (39). For integer $\nu = n$ and $\nu' = n'$ we get the precise relation from Eqs. (30) and (A.7) to be

$$\begin{aligned} \tilde{R}_{i,j}^{(n,l_x,l_y)\,(n',l'_x,l'_y)} &= \delta_{2n+l_x+l_y,\,2n'+l'_x+l'_y} (-1)^{n'} \frac{\Gamma(n+1)\mathcal{N}_{n'}^{(l'_x,l'_y)}}{\Gamma(n'+1)\mathcal{N}_{n}^{(l_x,l_y)}} \\ &\quad \times R_{ij}^{(l_x,l_y)\,(l'_x,l'_y)}((2n+l_x+l_y)(2n+l_x+l_y+2d-2)) \end{aligned} \tag{62}$$

for $i \neq j$ and $n, n' \geq 0$. The Kronecker δ reflects the conservation of K.

We are now ready to express the above particular solution to Eq. (27), $\phi_i = -\phi_j - \phi_k$, explicitly in terms of α_i, i.e.

$$\begin{aligned} \phi_i^{(l_x,l_y)}(\alpha_i) = &-\left(\sum_{j\neq i} \sum_{l'_x,l'_y} R_{ij}^{(l_x,l_y)\,(l'_x,l'_y)}(\lambda) A_j^{(l'_x,l'_y)} \right) \\ &\times \sin^{l_x}\alpha_i \cos^{l_y}\alpha_i \Gamma(\nu+1) P_{\nu}^{((d-2)/2+l_x,\,(d-2)/2+l_y)}(\cos 2\alpha_i) \ . \end{aligned} \tag{63}$$

The complete solution to Eq. (27) for $\alpha_i \leq \alpha_{0i}$ is this particular solution added to the complete solution to the corresponding homogeneous equation, i.e.

$$\begin{aligned} &\left[-\frac{\partial^2}{\partial\alpha_i^2} - 2(d-1)\cot(2\alpha_i)\frac{\partial}{\partial\alpha_i} + \frac{l_x(l_x+d-2)}{\sin^2\alpha_i} + \frac{l_y(l_y+d-2)}{\cos^2\alpha_i} \right. \\ &\quad \left. + \frac{2m}{\hbar^2}\rho^2 V_i(\mu_{jk}^{-1}\rho\sin\alpha_i) - \lambda \right] \phi_i^{(l_x,l_y)}(\alpha_i) = 0 \ . \end{aligned} \tag{64}$$

A change of variable from α_i to $r \equiv \mu_{jk}^{-1}\rho\alpha_i$ changes Eq. (64) into

$$\begin{aligned} &\left[-\frac{\partial^2}{\partial r^2} - 2(d-1)\frac{\mu_{jk}\cot(2r\mu_{jk}/\rho)}{\rho}\frac{\partial}{\partial r} + \frac{l_x(l_x+d-2)}{(\rho^2/\mu_{jk}^2)\sin^2(r\mu_{jk}/\rho)} \right. \\ &\quad \left. + \frac{l_y(l_y+d-2)}{(\rho^2/\mu_{jk}^2)\cos^2(r\mu_{jk}/\rho)} + \frac{2m}{\mu_{jk}^2\hbar^2} V_i\left(\mu_{jk}^{-1}\rho\sin\left(\frac{r\mu_{jk}}{\rho}\right)\right) - \frac{\mu_{jk}^2\lambda}{\rho^2} \right] u_i^{(l_x,l_y)}(r) = 0 \ , \end{aligned} \tag{65}$$

$$\phi_i^{(l_x,l_y)}(\alpha_i) = B_i^{(l_x,l_y)} u_i^{(l_x,l_y)}(\mu_{ij}^{-1}\rho\alpha_i) \ , \tag{66}$$

where the arbitrary constant $B_i^{(l_x,l_y)}$ expresses the relative weight of the homogeneous solution in the ith Faddeev component. Eq. (65) reduces to the two-body radial equation in Eq. (C.3) when $\rho \gg r_{0i}$ with lowest order deviations proportional to r^2/ρ^2. The corresponding energy is then $(\hbar^2/2m)\lambda\rho^{-2}$. The solutions $u_i^{(l_x,l_y)}$ depend decisively on the interactions, e.g. whether two-body bound states with relative angular momentum l_x exist, see Section 4.

Finally, the complete solution of Eq. (27) for $\alpha_i \leq \alpha_{0i}$ is given by

$$\phi_i^{(l_x,l_y)}(\alpha_i) = B_i^{(l_x,l_y)} u_i^{(l_x,l_y)}(\mu_{ij}^{-1}\rho\alpha_i) - \left(\sum_{j\neq i}\sum_{l'_x,l'_y} R_{ij}^{(l_x,l_y)\,(l'_x,l'_y)}(\lambda) A_j^{(l'_x,l'_y)}\right) \times \sin^{l_x}\alpha_i \cos^{l_y}\alpha_i \Gamma(v+1) P_v^{((d-2)/2+l_x,\,(d-2)/2+l_y)}(\cos 2\alpha_i)\,. \tag{67}$$

However, the total wave function, $\Phi = \phi_i + \phi_j + \phi_k$, inside the region of potential i, i.e. for $\alpha_i \leq \alpha_{0i}$, is given by the even simpler expression

$$\Phi(\alpha_i, \Omega_{xi}, \Omega_{yi}) = \sum_{l_x,l_y} B_i^{(l_x,l_y)} u_i^{(l_x,l_y)}(\mu_{ij}^{-1}\rho\alpha_i)\,[\,Y_{l_x}(\Omega_{xi}) \otimes Y_{l_y}(\Omega_{yi})\,]_{LM}\,, \tag{68}$$

arising because $\phi_j + \phi_k$ precisely cancels the particular solution in Eq. (63).

3.3.3. Matching and solving the angular eigenvalue problem

The solutions in Eqs. (54) and (67) must be continuous at $\alpha_i = \alpha_{0i}$, i.e.

$$B_i^{(l_x,l_y)} \frac{u_i^{(l_x,l_y)}(\mu_{ij}^{-1}\rho\alpha_{0i})}{\sin^{l_x}\alpha_{0i}\cos^{l_y}\alpha_{0i}} = \Gamma(v+1) P_v^{((d-2)/2+l_y,\,(d-2)/2+l_x)}(-\cos 2\alpha_{0i}) A_i^{(l_x,l_y)} + \Gamma(v+1) P_v^{((d-2)/2+l_x,\,(d-2)/2+l_y)}(\cos 2\alpha_{0i}) \sum_{j\neq i}\sum_{l'_x,l'_y} R_{ij}^{(l_x,l_y)\,(l'_x,l'_y)}(\lambda) A_j^{(l'_x,l'_y)}\,. \tag{69}$$

By using Eq. (A.7) we can rewrite this condition in a more transparent form

$$B_i^{(l_x,l_y)} \frac{u_i^{(l_x,l_y)}(\mu_{ij}^{-1}\rho\alpha_{0i})}{\Gamma(v+1)\sin^{l_x}\alpha_{0i}\cos^{l_y}\alpha_{0i}} = -Q_v A_i^{(l_x,l_y)}\sin(\pi v) + P_v\left(A_i^{(l_x,l_y)}\cos(\pi v) + \sum_{j\neq i}\sum_{l'_x,l'_y} R_{ij}^{(l_x,l_y)\,(l'_x,l'_y)}(\lambda) A_j^{(l'_x,l'_y)}\right), \tag{70}$$

where $P_v \equiv P_v^{((d-2)/2+l_x,\,(d-2)/2+l_y)}(\cos 2\alpha_{0i})$ and $Q_v \equiv Q_v^{((d-2)/2+l_x,\,(d-2)/2+l_y)}(\cos 2\alpha_{0i})$.

Continuity of the derivative gives a similar equation obtained by deriving with respect to α_{0i} on both sides of Eq. (70). Eliminating $B_i^{(l_x,l_y)}$ from Eq. (70) gives a matrix equation for the coefficients $A_i^{(l_x,l_y)}$ valid for all $i = 1,2,3$, i.e.

$$\sin(\pi v)\left[\left(\frac{\rho}{\mu_{jk}}\frac{\partial \ln u_i^{(l_x,l_y)}}{\partial r} - l_x\cot\alpha_{0i} - l_y\tan\alpha_{0i}\right)Q_v - \frac{\partial Q_v}{\partial\alpha_{0i}}\right] A_i^{(l_x,l_y)} = \left[\left(\frac{\rho}{\mu_{jk}}\frac{\partial \ln u_i^{(l_x,l_y)}}{\partial r} - l_x\cot\alpha_{0i} - l_y\tan\alpha_{0i}\right)P_v - \frac{\partial P_v}{\partial\alpha_{0i}}\right] \times\left[\cos(\pi v) A_i^{(l_x,l_y)} + \sum_{j\neq i}\sum_{l'_x,l'_y} R_{ij}^{(l_x,l_y)\,(l'_x,l'_y)}(\lambda) A_j^{(l'_x,l'_y)}\right], \tag{71}$$

where $r = \mu_{jk}^{-1}\rho\alpha_{0i}$ in the logarithmic derivative of $u_i^{(l_x,l_y)}(r)$.

This equation is linear in the coefficients $A_i^{(l_x,l_y)}$ and the corresponding determinant must be zero to allow non-trivial solutions. This in turn defines a non-linear eigenvalue equation in λ. The information about the potentials is contained in the logarithmic derivative of $u_i^{(l_x,l_y)}$ at the energy $(\hbar^2/2m)\lambda\rho^{-2}$, which then in general has to be found numerically by solving Eq. (65). This has two important implications. First, solving Eq. (71) is reduced to finding solutions to a number of two-body equations. In practice, both angular eigenvalues and eigenfunctions can be computed by this procedure, see Section 7. Secondly, when ρ is a few times larger than r_{0i}, the angular eigenvalues are essentially *model independent* in the sense that they are identical for different potentials provided these logarithmic derivatives are identical. This can be rephrased by saying that potentials resulting in the same two-body phase shifts produce the same angular eigenvalues at large ρ.

3.4. Finite spins of the particles

For simplicity of notation we have so far assumed that the particles either were spin zero bosons or that the spin degrees of freedom were totally uncoupled and therefore could be ignored. However, this is not possible for a number of interesting systems, perhaps especially in nuclear physics, where the spin–orbit, spin–spin and tensor forces are very important two-body interactions. The previous chapters and sections demonstrated that the orbital part of the wave functions is decisive for the large-distance asymptotical behaviour. The essential ingredients are therefore already established. On the other hand, a two-body bound state located far away from a third particle must at least asymptotically conserve the total (not orbital) angular momentum of that two-body state. Thus the spins cannot simply be factorized away by including another coupling of the total spin to the orbital part in Eq. (26). Instead it is natural to employ the *ls* coupling scheme for the individual pairs of particles. Incorporating the corresponding couplings at smaller distances is then rather straightforward. Details can be found in [23]. Several practical examples are discussed in the published literature [40,91,100,123].

4. Large-distance asymptotic behaviour

The previous sections discussed solutions for intermediate distances roughly understood as hyperradii larger than the ranges of the two-body interactions r_{0i} or as defined by Eq. (58). In this section we shall discuss very large distances including the asymptotic limit of infinite hyperradii. The behaviour of the adiabatic potentials and the coupling terms in this limit is necessary in order to understand the method of the adiabatic expansion. In numerical calculations of bound state properties this knowledge is revealing but not essential, since the wave functions are exponentially decreasing with distance. However, for scattering problems the boundary conditions at $\rho = \infty$ define the process and the large-distance information is absolutely essential, see Section 9.

4.1. Expansion of eigenvalue equation

The overall assumption is that the hyperradius is much larger than the range of the potentials, i.e. $\rho \gg r_{0i}$. In addition, we shall assume $|\lambda| r_{0i}^2 \ll \rho^2$ corresponding to the energy $(\hbar^2/2m)\mu_{jk}^2\lambda\rho^{-2}$

asymptotically approaching zero, or at least not diverging, in the limit of $\rho = \infty$. Furthermore, we shall in the expansions in this section assume that the hyperradius also is much larger than all two-body scattering lengths $a_i^{(l_x)}$ corresponding to the angular momentum l_x of system i as defined in Eq. (C.6), i.e. $\rho \gg |a_i^{(l_x)}|$. In Section 5 we shall investigate the intriguing limit, where $r_{0i} \ll \rho \ll |a_i^{(l_x)}|$.

The approximation in Eq. (52) is now valid and $\alpha < \alpha_{0i}$ implies that $r \equiv \mu_{jk}^{-1}\rho\alpha_i \ll \rho$. Then Eq. (65) reduces to the two-body radial equation in Eq. (C.3) and the solution $u_i^{(l_x,l_y)}(r)$ becomes the two-body radial wave function at the energy $(\hbar^2/2m)\mu_{jk}^2\lambda\rho^{-2}$. *If* this energy is small $u_i^{(l_x,l_y)}$ is simply the two-body wave function at zero energy. The logarithmic derivative needed in Eq. (71) is therefore for small α_{0i} obtained by using the asymptotic form in Eq. (C.6) as

$$\begin{aligned}
&\frac{\rho}{\mu_{jk}}\frac{\partial \ln u_i^{(l_x,l_y)}}{\partial r} - l_x\cot\alpha_{0i} - l_y\tan\alpha_{0i} \\
&\quad = \frac{\rho}{\mu_{jk}}\frac{d-2+2l_x}{r_{0i}}\left(\left(\frac{r_{0i}}{a_i^{(l_x)}}\right)^{d-2+2l_x} - 1\right)^{-1} + \mathcal{O}\left(\frac{r_{0i}}{\rho}\right),
\end{aligned} \tag{72}$$

where $\mathcal{O}(f(\rho))$ is a function at most of the same order as $f(\rho)$ when $\rho \to \infty$.

Inserting Eqs. (72), (A.10) and (A.11) into Eq. (71) we obtain after a little algebra for odd dimensions d that

$$\begin{aligned}
&\sin(\pi\nu)\Bigg[-\cot\left(\frac{\pi d}{2}\right) + \frac{\Gamma\left(\frac{d-2}{2}+l_x\right)\Gamma\left(\frac{d}{2}+l_x\right)\Gamma\left(\nu+\frac{d}{2}+l_y\right)\Gamma(\nu+1)}{\pi\Gamma\left(\nu+\frac{d}{2}+l_x\right)\Gamma(\nu+d-1+l_x+l_y)} \\
&\qquad \times\left(\left(\frac{\rho}{\mu_{jk}a_i^{(l_x)}}\right)^{d-2+2l_x} + \mathcal{O}\left(\left(\frac{\rho}{r_{0i}}\right)^{d-4+2l_x}\right)\right)\Bigg]A_i^{(l_x,l_y)} \\
&\quad = \left(1+\mathcal{O}\left(\left(\frac{r_{0i}}{\rho}\right)^2\right)\right)\left[\cos(\pi\nu)A_i^{(l_x,l_y)} + \sum_{j\neq i}\sum_{l_x',l_y'} R_{ij}^{(l_x,l_y)\,(l_x',l_y')}(\lambda)A_j^{(l_x',l_y')}\right].
\end{aligned} \tag{73}$$

For even d and $d+2l_x \geq 4$ we obtain instead

$$\begin{aligned}
&\frac{\sin(\pi\nu)}{\pi}\frac{\Gamma\left(\frac{d-2}{2}+l_x\right)\Gamma\left(\frac{d}{2}+l_x\right)\Gamma\left(\nu+\frac{d}{2}+l_y\right)\Gamma(\nu+1)}{\Gamma(\nu+\frac{d}{2}+l_x)\Gamma(\nu+d-1+l_x+l_y)} \\
&\qquad \times\left[\left(\frac{\rho}{\mu_{jk}a_i^{(l_x)}}\right)^{d-2+2l_x} + \begin{cases}\mathcal{O}\left(\log\left(\frac{\rho}{r_{0i}}\right)\right) & \text{for } d+2l_x=4 \\ \mathcal{O}\left(\left(\frac{\rho}{r_{0i}}\right)^{d-4+2l_x}\right) & \text{for } d+2l_x>4\end{cases}\right]A_i^{(l_x,l_y)} \\
&\quad = \left(1+\mathcal{O}\left(\left(\frac{r_{0i}}{\rho}\right)^2\right)\right)\left[\cos(\pi\nu)A_i^{(l_x,l_y)} + \sum_{j\neq i}\sum_{l_x',l_y'} R_{ij}^{(l_x,l_y)\,(l_x',l_y')}(\lambda)A_j^{(l_x',l_y')}\right],
\end{aligned} \tag{74}$$

and for the last case of even d and $d+2l_x=2$ ($d=2$, $l_x=0$) we obtain

$$-\frac{\sin(\pi\nu)}{\pi}\left[2\gamma_\Gamma+\psi_\Gamma(\nu+l_y+1)+\psi_\Gamma(\nu+1)+2\log\left(\frac{\mu_{jk}a_i^{(0)}}{\rho}\right)\right]A_i^{(l_x,l_y)}$$

$$=\left[\cos(\pi\nu)A_i^{(l_x,l_y)}+\sum_{j\neq i}\sum_{l'_x,l'_y}R_{ij}^{(l_x,l_y)\,(l'_x,l'_y)}(\lambda)A_j^{(l'_x,l'_y)}\right], \tag{75}$$

which may be obtained either from Eq. (73) by approaching the limit $d\to 2$ from $d>2$ or by using Eq. (A.11) directly in Eq. (71).

The key quantities in these asymptotic equations, which immediately lead to the asymptotic eigenvalue equations, are the coefficients $R_{ij}^{(l_x,l_y)\,(l'_x,l'_y)}(\lambda)$ defined in Eq. (61). They are continuous functions of λ because both $\Gamma(\nu'+1)\times P_{\nu'}^{(d-2)/2+l'_y,\,(d-2)/2+l'_x}(-\cos 2\alpha_j)$ and $\Gamma(\nu+1)P_\nu^{(d-2)/2+l_x,\,(d-2)/2+l_y}(\cos 2\alpha_i)$ are continuous functions of ν and therefore of λ. Furthermore, the denominator in the integrand of Eq. (61) is not zero provided α_i is sufficiently small, see Eq. (A.10). Thus, we proceed by exercising our freedom to choose an α_i value close to zero.

Since ν is confined by Eq. (55) the right-hand side of Eq. (73) remains finite unless $\nu\to-\frac{1}{2}(d-1+l_x+l_y)+\mathrm{i}\,\infty$, whereas the left-hand side behaves as $\sin(\pi\nu)(\rho/a_i^{(l_x)})^{d-2+2l_x}A_i^{(l_x,l_y)}$ when $\rho\to\infty$. This means that non-trivial solutions to Eq. (73) only can exist if ν approaches an integer n, or if $\nu\to-(d-1+l_x+l_y)+\mathrm{i}\,\infty$. The first of these cases corresponds to continuum configurations with all three particles far away from each other, see Section 4.2. The second case corresponds to two of the particles in a two-body bound state and the third particle far away from these two, see Section 4.3.

This analysis of Eq. (73) also applies directly to Eqs. (74) and (75), except when $d=2$ where powers of the form x^{d-2} must be replaced by $\log x$, see [39].

4.2. Three-body continuum states

We shall extract the properties of those solutions to Eq. (73), where ν approaches an integer when $\rho\to\infty$, i.e. eigenvalues ν or λ and coefficients, $A_i^{(l_x,l_y)}$ and $B_i^{(l_x,l_y)}$, in the corresponding wave functions in Eqs. (54) and (67).

Let us first assume that one of the coefficients $A_i^{(l_x,l_y)}$ is non-zero in the limit $\rho=\infty$. Then the corresponding ν must approach an integer n, see Eq. (73). For another component of the same solution, but with partial angular momenta l'_x and l'_y, the related ν' must be $\nu'=\nu+\frac{1}{2}(l_x+l_y-l'_x-l'_y)$ as seen from Eq. (55), since the energy (λ) is unchanged. If $A_i^{(l'_x,l'_y)}$ is non-zero in the limit $\rho=\infty$, ν' also approaches an integer and $l_x+l_y-l'_x-l'_y$ must be an even number. Only components with the same parity contribute to a given solution.

For a coefficient $A_i^{(l_x,l_y)}$, non-vanishing at $\rho=\infty$, the related value of ν must in this limit behave as $\nu=n+\mathcal{O}(\rho^{2-d-2l_x})$, again seen from Eq. (73). Assuming $\nu=n+b\rho^{2-d-2l_0}$, where b is a constant and l_0 and n are integers, we get $\lambda=K(K+2d-2)+4(K+d-1)b\rho^{2-d-2l_0}$ with $K=2n+l_x+l_y$. For another contributing component $A_i^{(l'_x,l'_y)}$ we find the same form $\nu'=n'+b\rho^{2-d-2l_0}$ with $n'=n+\frac{1}{2}(l_x+l_y-l'_x-l'_y)$.

For a component with $l_x+l_y>K$ we have that $\nu\to n<0$. The right-hand side of Eq. (73) remains finite, but the left-hand side behaves as $\sin(\pi\nu)\Gamma(\nu+1)\rho^{d-2+2l_x}A_i^{(l_x,l_y)}=\mathcal{O}(\rho^{d-2+2l_x})A_i^{(l_x,l_y)}$,

since the first-order pole in the Γ-function cancels the zero point in $\sin(\pi v)$. Therefore, this coefficient must vanish accordingly as $A_i^{(l_x,l_y)} = \mathcal{O}(\rho^{2-d-2l_x})$ implying that $A_i^{(l_x,l_y)}(\infty) = 0$.

For a component with $l_x + l_y \leq K$ we have $v \to n \geq 0$ and Eq. (73) becomes

$$\frac{\Gamma\left(\frac{d-2}{2}+l_x\right)\Gamma\left(\frac{d}{2}+l_x\right)\Gamma\left(n+\frac{d}{2}+l_y\right)\Gamma(n+1)}{\Gamma(n+\frac{d}{2}+l_x)\Gamma(n+d-1+l_x+l_y)}\frac{b\rho^{2l_x-2l_0}}{(\mu_{jk}a_i^{(l_x)})^{d-2+2l_x}}A_i^{(l_x,l_y)}$$

$$= A_i^{(l_x,l_y)} + (-1)^n \sum_{j\neq i}\sum_{l'_x,l'_y} R_{ij}^{(l_x,l_y)\,(l'_x,l'_y)}(\lambda)A_j^{(l'_x,l'_y)}\,. \tag{76}$$

From this equation we see that $A_i^{(l_x,l_y)} = \mathcal{O}(\rho^{2l_0-2l_x})$ and $A_i^{(l_x,l_y)}(\infty) = 0$ for $l_x > l_0$. For $l_x < l_0$ the left-hand side of Eq. (76) vanishes for $\rho \to \infty$ and therefore the right-hand side must also vanish. Therefore we obtain

$$D_i^{(l_x,l_y)} \equiv \cos(\pi v)A_i^{(l_x,l_y)} + \sum_{j\neq i}\sum_{l'_x,l'_y} R_{ij}^{(l_x,l_y)\,(l'_x,l'_y)}(\lambda)A_j^{(l'_x,l'_y)} = \mathcal{O}(\rho^{2l_x-2l_0})\,. \tag{77}$$

We conclude that only components with $l_x \leq l_0$ and $l_x + l_y \leq K$ can be non-zero in the limit $\rho = \infty$. These results are summarized in Table 1.

We can now find the constant b by solving the equation in Eq. (76) at $\rho = \infty$ with inclusion of only the contributing components of $l_x \leq l_0$ and $l_x + l_y \leq K$. As v and λ are dimensionless and b has the dimension of length raised to the power $d-2+2l_0$ we must find that $b = a_0^{d-2+2l_0}$, where a_0 is an average over the only available lengths in the problem, i.e. the scattering lengths $a_i^{(l_0)}$, $i = 1,2,3$. The other scattering lengths cannot enter in the eigenvalue behaviour, because Eq. (76) dictates that those with $l_x < l_0$ disappear for large ρ and those with $l_x > l_0$ require that the coefficient $A_i^{(l_x,l_y)}$ vanishes.

For $K = L = l_0 = 0$ for three identical bosons in three dimensions a_0 turns out to be $12/\pi$ times the two-body scattering length [20,21]. We then get

$$v = n + \left(\frac{\rho}{a_0}\right)^{2-d-2l_0}\,, \tag{78}$$

$$\lambda = K(K+2d-2) + 2(K+d-1)\left(\frac{\rho}{a_0}\right)^{2-d-2l_0}\,. \tag{79}$$

These equations exhibit the asymptotic behaviour of the angular eigenvalues. The features of a given value are the specific ρ-dependence characterized by an angular momentum quantum number l_0 and the approach towards a constant recognized from the free spectrum.

Table 1
The asymptotic large-distance behaviour the Faddeev components in the limit $\rho \to \infty$, i.e. the coefficients $A_i^{(l_x,l_y)}$, $D_i^{(l_x,l_y)}$ and $B_i^{(l_x,l_y)}$ defined in Eqs. (54), (77) and (66). The eigenvalues behave as $\lambda = K(K+2d-2) + 2(K+d-1)b\rho^{2-d-2l_0}$. The integers K and l_0 characterize how the eigenvalues approach the asymptotic value at $\rho = \infty$

	$A_i^{(l_x,l_y)}$	$D_i^{(l_x,l_y)}$	$B_i^{(l_x,l_y)}$
$l_x + l_y \leq K$ and $l_x \leq l_0$	$\mathcal{O}(\rho^0)$	$\mathcal{O}(\rho^{2l_x-2l_0})$	$\mathcal{O}(\rho^{l_x-2l_0})$
$l_x + l_y \leq K$ and $l_x > l_0$	$\mathcal{O}(\rho^{2l_0-2l_x})$	$\mathcal{O}(\rho^0)$	$\mathcal{O}(\rho^{-l_x})$
$l_x + l_y > K$	$\mathcal{O}(\rho^{2-d-2l_x})$	$\mathcal{O}(\rho^0)$	$\mathcal{O}(\rho^{-l_x})$

With this knowledge we can now use Eqs. (67), (70), (A.10), (A.11) and the results in Table 1 to calculate the wave function inside the potential regions, i.e. the coefficients $B_i^{(l_x,l_y)}$ related to the region $\alpha_i \leq \alpha_{0i}$, see Table 1.

4.2.1. Normalization of the asymptotic wave function

The normalization of the asymptotic wave function, defined by Eqs. (54), (67) and (68), can now be computed when ν approaches an integer in the limit $\rho \to \infty$. All contributions from regions, $\alpha \leq \alpha_{0i}$, inside the potentials vanish, because the corresponding coefficients $B_i^{(l_x,l_y)}$ vanish or approach a constant as seen in Table 1 and the sizes of the intervals also approach zero, i.e. $\alpha_{0i} \to 0$. The norm is therefore entirely due to the contributions from the regions, $\alpha_i > \alpha_{0i}$, outside the potentials. From Eqs. (54), (30), (39), (A.7), (62), (77) and Table 1 we obtain for a solution $|\Phi\rangle$ characterized by l_0 that

$$
\begin{aligned}
&\langle \Phi|\Phi\rangle_\Omega \\
&\quad \approx \sum_{i,i'=1}^{3} \sum_{l_x,l_y} \sum_{l'_x,l'_y} (-1)^{n+n'} \frac{\Gamma(n+1)\tilde{R}_{i,i'}^{(n,l_x,l_y)\,(n',l'_x,l'_y)}\Gamma(n'+1)}{\mathcal{N}_n^{(l_x,l_y)}\mathcal{N}_{n'}^{(l'_x,l'_y)}} A_i^{(l_x,l_y)*} A_j^{(l'_x,l'_y)} \\
&\quad = \sum_{i=1}^{3} \sum_{l_x,l_y} A_i^{(l_x,l_y)*} (-1)^n \left(\frac{\Gamma(n+1)}{\mathcal{N}_n^{(l_x,l_y)}}\right)^2 \\
&\qquad \times \left((-1)^{n'} A_i^{(l_x,l_y)} + \sum_{j\neq i} \sum_{l'_x,l'_y} R_{ij}^{(l_x,l_y)\,(l'_x,l'_y)}(\lambda) A_j^{(l'_x,l'_y)} \right) \\
&\quad \approx \sum_{i=1}^{3} \sum_{l_y} \left(\frac{\Gamma(n+1)}{\mathcal{N}_n^{(l_0,l_y)}}\right)^2 (-1)^n A_i^{(l_0,l_y)*} D_i^{(l_0,l_y)} ,
\end{aligned}
\tag{80}
$$

where we used that $A_i^{(l_x,l_y)} D_i^{(l_x,l_y)}$ vanishes in this limit for $l_x \neq l_0$. The sum over l_y in Eq. (80) is restricted by $l_0 + l_y \leq K$, since $A_i^{(l_x,l_y)}$ vanishes in the large ρ-limit for $l_x + l_y > K$. From Eq. (76) we see that if $b = 0$ then also $D_i^{(l_0,l_y)} = 0$. In this case also components with $l_x = l_0$ do not contribute to the norm, which consequently vanish in this large-distance limit. Thus, solutions with $b = 0$ have zero norm and must be spurious.

We can now see that there must exist at least one non-vanishing component, $A_i^{(l_0,l_{y0})}$, with $l_0 + l_{y0} \leq K$. Otherwise no non-zero terms would be left in the sum in Eq. (80). The triangular inequalities $|l_0 - l_{y0}| \leq L \leq l_0 + l_{y0}$ imply that $l_{y0} \geq |l_0 - L|$, where L is the angular momentum obtained by coupling of l_0 and l_{y0}. Therefore we also have $K \geq l_0 + l_{y0} \geq l_0 + |l_0 - L|$ and $l_0 \leq \frac{1}{2}(K + L)$. If we now consider a component with $l_x + l_y > K$ then the triangular inequality gives us that $l_x \geq l_y - L > K - l_x - L$ and therefore $l_x > \frac{1}{2}(K - L) \geq \frac{1}{2}(l_0 + |l_0 - L| - L)$. Thus, for $L = 0$ all components with $l_x + l_y > K$ also have $l_x > l_0$.

For $L = 0$ states we can also conclude that inside the potential regions the Faddeev components with $l_x = l_0$ fall off slower with ρ than all other components. This is consistent with the fact that the scattering lengths $a_i^{(l_0)}, i = 1, 2, 3$, determine the low-energy properties of any given system at large distances. This conclusion does not hold in general for $L > 0$, where a component with minimum $l_x < l_0$ and $l_x + l_y > K$ could fall off even slower inside the potential regions. For such an l_x-value we have $l_y \leq L + l_x$ and $l_x = \frac{1}{2}(K - L) + 1 < l_0$, which corresponds to a slower fall off than for that of $l_x = l_0$, see Table 1.

4.2.2. The asymptotic degeneracy

The asymptotic states in the limit of $\rho = \infty$ are identical to the free states obtained without interactions. The angular spectrum of the free solutions are given by $\lambda(\infty) = K(K + 2d - 2)$ and the degeneracy for each of these values is $3D(d, L, K)$, but only $D(d, L, K)$ of these are physically acceptable while $2D(d, L, K)$ are spurious states, see Section 3.1.1.

We shall now try to find how many physical solutions are there for a given K and L for each l_0 between 0 and the maximum value $\frac{1}{2}(K + L)$. Let $T(k)$ denote the number of Faddeev components with $l_x \leq k$ and $l_x + l_y \leq K$, where each l_x-value in each Jacobi set has to be counted. Let $S(k)$ denote the number of spurious solutions, which can be obtained from these $T(k)$ Faddeev components by combining into identically vanishing total wave functions. The total number of components are $T(\frac{1}{2}(K + L)) = 3D(d, L, K)$ and the total number of spurious solutions are $S(\frac{1}{2}(K + L)) = 2D(d, L, K)$. A solution corresponding to $l_0 = k$ is a linear combination of the $T(k)$ components with $l_x \leq k$, see Section 4.2. The total number of solutions with $l_0 = 0, 1, \ldots, k$ is thus $T(k)$, but $S(k)$ of these are spurious. Therefore $P(k) = T(k) - S(k)$ is the number of physical solutions with $l_0 \leq k$ and thus $P(k) - P(k-1) = T(k) - S(k) - P(k-1)$ is the number of physical solutions with $l_0 = k$.

We may understand this by stepwise increasing l_0: the number of physical states with $l_0 = 0$ is the number of components with $l_x = 0$ minus the number of ways these can be combined into spurious states with zero norm. The number of physical states with $l_0 = 1$ is given by the number of components with $l_x \leq 1$ minus the number of spurious states obtained by combining components with $l_x \leq 1$ minus the number of physical states with $l_0 = 0$. We may continue in this way until we have obtained the total number of $D(d, K, L)$ physical states and $2D(d, K, L)$ spurious states, all found from $l_0 \leq \frac{1}{2}(K + L)$.

4.2.3. Numerical accuracy and the potential cutoffs r_{0i}

The accuracy of the numerical procedure is closely related to the choice of r_{0i}, i.e. the point outside which the potential V_i is assumed to be zero. Then $V_i(\mu_{jk}^{-1}\rho \sin\alpha_i) = 0$ for $\alpha_i > \alpha_{0i}$, see Section 3.3. Using the asymptotic wave function of a state characterized by l_0 and the approximation in Eq. (80) give

$$|\delta\lambda| \leq \sum_{i=1}^{3} \sum_{l_y} |A_i^{(l_0,l_y)}| \Gamma(n+1)^2 \int_{\alpha_{0i}}^{\pi/2} \sin^{d-2+2l_0}\alpha_i \cos^{d-2+2l_y}\alpha_i \times |P_n^{((d-2)/2+l_0,\,(d-2)/2+l_y)}(\cos 2\alpha_i)|^2 \left|\frac{2m}{\hbar^2}\rho^2 V_i(\mu_{jk}^{-1}\rho \sin\alpha_i)\right| |D_i^{(l_0,l_y)}| \,. \tag{81}$$

Using the asymptotic behaviour in Table 1 we obtain, after the change of integration variable to $r = \mu_{jk}^{-1}\rho \sin\alpha_i \leq \mu_{jk}^{-1}\rho$, the simple accuracy estimate

$$|\delta\lambda| \leq \begin{cases} \mathcal{O}(\rho^{2-d-2l_{\rm sh}}) \displaystyle\int_{r_{0i}}^{\infty} \mathrm{d}r\, r^{d-1+2l_{\rm sh}} \frac{2m}{\hbar^2} |V_i(r)| & \text{for } l_0 > l_{\rm sh} \,, \\ \mathcal{O}(\rho^{2-d-2l_0}) \displaystyle\int_{r_{0i}}^{\infty} \mathrm{d}r\, r^{d-1+2l_0} \frac{2m}{\hbar^2} |V_i(r)| & \text{for } l_0 \leq l_{\rm sh} \,, \end{cases} \tag{82}$$

where we introduced *the maximum short-range angular momentum* quantum number $l_{\rm sh} \geq 0$ for which the integrals in Eq. (82) are finite, see Eq. (C.5). These estimates can be as small as desired by choosing r_{0i} sufficiently large. Except for the solutions of $K = 0$, where $l_0 = 0$ and $\lambda = \mathcal{O}(\rho^{2-d})$, we can even conclude that both absolute and relative error $\delta\lambda/\lambda$ vanish when $\rho \to \infty$.

The freedom in the choice of r_{0i} can be exploited to obtain a faster convergence of the eigenvalues, i.e. faster vanishing of $\delta\lambda$ with increasing ρ. For r_{0i} increasing with ρ as $r_{0i} = \mathcal{O}(\rho^{1-\varepsilon})$, where ε is a small positive number, we use

$$\int_{r_{0i}}^{\infty} \mathrm{d}r\, r^{d-1+2l_0} \frac{2m}{\hbar^2} |V_i(r)| \leq r_{0i}^{2l_0-2l_{\mathrm{sh}}} \int_{r_{0i}}^{\infty} \mathrm{d}r\, r^{d-1+2l_{\mathrm{sh}}} \frac{2m}{\hbar^2} |V_i(r)| \tag{83}$$

and Eq. (82) to obtain the accuracy $\delta\lambda = \mathcal{O}(\rho^{2-d-2l_{\mathrm{sh}}+\bar{\varepsilon}})$ for $l_0 < l_{\mathrm{sh}}$, where $\bar{\varepsilon} = 2\varepsilon(l_{\mathrm{sh}} - l_0)$. For potentials with $l_{\mathrm{sh}} = \infty$, e.g. Gaussian, Yukawa and square well potentials, we can therefore choose $r_{0i} \propto \rho^{1-\varepsilon}$ causing $\delta\lambda$ to vanish faster than any power of ρ. Choosing r_{0i} as a function of ρ does not alter the leading-order terms in Table 1 and the ρ-dependent correction term in Eq. (79). The reason for this is that as long as $\alpha_{0i} \to 0$ and Eq. (73) consequently is valid the length scale decisive for the convergence of each solution is $|a_i^{(l_0)}|$.

The ρ-dependent term in Eq. (79), $2(K+d-1)(\rho/a_0)^{2-d-2l_0}$, vanishes faster than $\delta\lambda$ in Eq. (82) when $l_0 > l_{\mathrm{sh}}$. Dividing the solutions into categories according to the dominating l_0 at large distance is therefore only meaningful for $l_0 \leq l_{\mathrm{sh}}$. Other solutions with $l_0 > l_{\mathrm{sh}}$ and the same limiting value $\lambda = K(K+2d-2)$ couple and all contain a piece of the slowest converging component with the same resulting large-distance behaviour $\lambda = K(K+2d-2) + \mathcal{O}(\rho^{2-d-2l_{\mathrm{sh}}})$.

4.3. Two-cluster continuum states

Let us investigate solutions to Eq. (73) corresponding to large-distance configurations with a two-body bound state and the third particle far away. Then we have $\lambda = \mathcal{O}(-\rho^2)$, $\nu = -\frac{1}{2}(d-1+l_y) + \mathrm{i}t$ and from Eq. (56) therefore $\lambda = -4t^2 - (d-1)^2$, where $t \to +\infty$. We assume first that $l_x = 0$ and $d < 4$.

4.3.1. Weakly bound two-body states

The Γ-function for $|z| \to \infty$ and $|\arg z| < \pi$ may be approximated by [124]

$$\Gamma(z) \simeq \sqrt{2\pi} \exp\left(\left(z - \frac{1}{2}\right)\log z - z\right)[1 + \mathcal{O}(z^{-1})]\,, \tag{84}$$

which inserted into Eq. (84) along with the expression for ν leads to

$$\begin{aligned}
&\frac{\mathrm{i}}{2}\Bigg[-\exp\left(\pi t + \mathrm{i}\frac{\pi}{2}(d-1+l_y)\right)\cot\left(\frac{\pi d}{2}\right) \\
&\quad + \frac{\Gamma^2\left(\frac{d}{2}\right)}{\left(\frac{(d-2)}{2}\right)\pi} \exp\left(\pi t + \mathrm{i}\frac{\pi}{2}(1+l_y)\right)\left(\frac{\rho}{\mu_{jk} a_i^{(0)} t}\right)^{2-d}\Bigg] A_i^{(0,l_y)} \\
&= \frac{1}{2}\exp\left(\pi t + \mathrm{i}\frac{\pi}{2}(d-1+l_y)\right) A_i^{(0,l_y)} + \sum_{j\neq i} \sum_{l'_x, l'_y} R_{ij}^{(l_x,l_y)\,(l'_x,l'_y)}(-4t^2 - (d-1)^2) A_j^{(l'_x,l'_y)}\,.
\end{aligned} \tag{85}$$

The argument λ in $R_{ij}^{(l_x,l_y)\,(l'_x,l'_y)}(\lambda)$ diverges towards $-\infty$. By choosing α_i in Eq. (61) sufficiently small and using Eqs. (A.9), (A.10), (10) and (84) we get

$$R_{ij}^{(l_x,l_y)\,(l'_x,l'_y)}(-4t^2-(d-1)^2)=\mathcal{O}(\exp((\pi-2|\gamma_{ij}|+\varepsilon)t))\,, \tag{86}$$

where ε is an arbitrarily small positive number. The terms in Eq. (85) containing $R_{ij}^{(l_x,l_y)\,(l'_x,l'_y)}(-4t^2-(d-1)^2)$ therefore fall off faster than the other terms. Thus for non-zero coefficients $A_i^{(0,l_y)}$ we find to leading order that

$$t\approx C\frac{\rho}{\mu_{jk}a_i^{(0)}},\quad C\equiv\left[\frac{\Gamma^2\left(\frac{d}{2}\right)\sin\pi\left(\frac{d-2}{2}\right)}{\pi\left(\frac{d-2}{2}\right)}\right]^{1/(d-2)}. \tag{87}$$

Since t must be a positive real number also the scattering lengths must be positive, i.e. $a_i^{(0)}>0$. If $a_i^{(0)}<0$ a bound two-body state is not present in the subsystem, see Appendix C. Using Eq. (C.9) we now obtain

$$\lambda\approx -4C^2\left(\frac{\rho}{\mu_{jk}a_i^{(0)}}\right)^2=\rho^2\frac{2m}{\hbar^2}E_2\,, \tag{88}$$

where E_2 is the (small) two-body energy for angular momentum 0.

In this derivation we have assumed that $|\lambda|\rho^{-2}r_{0i}\ll 1$ to allow the use of $u_i^{(l_x,l_y)}$ appearing in Eq. (70) as the wave function of zero energy of subsystem i. The solution in Eq. (88) is only consistent with this assumption when $a_i^{(0)}\gg r_{i0}$, which however also is used to obtain Eq. (C.9), the energy of a weakly bound two-body state. Thus, the derivation is only valid for loosely bound states.

4.3.2. Bound two-body states

The result in Eq. (88) is general and applies to all two-body bound states for any dimension and any partial angular momentum. For each two-body bound state with energy $E_2<0$ one solution must approach $\lambda=(2mE_2/\hbar^2)\rho^2$ as $\rho\to\infty$.

Let $\psi_i^{(l_x)}(r)$ be the normalized radial wave function of a two-body bound state between particles j and k with angular momentum l_x. Then the function

$$\phi_j^{(l'_x,l'_y)}(\alpha_i)=\delta_{j,i}\delta_{l'_x,l_x}\delta_{l'_y,l_y}B_i^{(l_x,l_y)}\psi_i^{(l_x)}(\mu_{jk}^{-1}\rho\sin\alpha_i)(1+\mathcal{O}(\alpha_i^2)) \tag{89}$$

is a solution to Eq. (27) for large ρ for any l_y allowed by a given total L. ($\mathcal{O}(f(x))/f(x)$ is a function remaining finite as $x\to 0$.) To see this we first conclude that an exponential fall for large r of $\psi_i^{(l_x)}(r)$ implies that $\hat{R}_{ji}^{(l'_x,l'_y)\,(l_x,l_y)}[\phi_i^{(l_x,l_y)}](\alpha_j)=\mathcal{O}(\exp(-\rho\sqrt{-2mE_2/\hbar^2}))$ for $\alpha_j\leq\alpha_{0j}$. Thus for large ρ a trivial solution to Eq. (27) is $\phi_j^{(l'_x,l'_y)}=0$ with $j\neq i, l'_x\neq l_x$ or $l'_y\neq l_y$. Then we define $r=\mu_{jk}^{-1}\rho\sin\alpha_i$ and insert Eq. (89) into Eq. (27) arriving at

$$\left[\frac{\rho^2}{\mu_{jk}^2}\left(-\frac{\partial^2}{\partial r^2}-\frac{d-1}{r}\frac{\partial}{\partial r}+\frac{l_x(l_x+d-2)}{r^2}+\frac{2m\mu_{jk}^2}{\hbar^2}V_i(r)-\frac{\mu_{jk}^2\lambda}{\rho^2}\right)\right.$$
$$\left.+\left(r^2\frac{\partial^2}{\partial r^2}+(2d-1)r^2\frac{\partial}{\partial r}+l_y(l_y+d-2)\right)+\mathcal{O}(r^2\rho^{-2})\right]B_i^{(l_x,l_y)}\psi_i^{(l_x)}(r)\left(1+\mathcal{O}\left(\frac{r^2}{\rho^2}\right)\right)=0\,, \tag{90}$$

which is valid to leading order in ρ if $\lambda = (2m/\hbar^2)E_2\rho^2$ because $\psi_i^{(l_x)}$ is a solution to Eq. (C.3). Thus Eq. (89) is a solution to Eq. (27) with the desired properties.

That is for each two-body bound state of particles j and k with angular momentum l_x and for all possible values of l_y allowed by the restrictions imposed by the total angular momentum L, Eq. (27) has solutions, where only one component, $\phi_i^{(l_x,l_y)}$, is non-zero asymptotically for $\rho \to \infty$. Furthermore, the contributions from the other components fall off exponentially because the corresponding mixing only occurs through the kinematic rotation. The leading order eigenvalue related to this solution is $\lambda = (2m/\hbar^2)E_2\rho^2$ and the next order term may be derived from Eq. (90) by perturbation theory, i.e.

$$\lambda = \frac{2m}{\hbar^2}E_2\rho^2 + \int_0^\infty \mathrm{d}r\, r^{d-1}\psi_i^{(l_x)*}(r)\left(r^2\frac{\partial^2}{\partial r^2} + (2d-1)r^2\frac{\partial}{\partial r} + l_y(l_y+d-2)\right)\psi_i^{(l_x)}(r)\,. \tag{91}$$

Normalization of the total angular wave function, $\langle\Phi|\Phi\rangle_\Omega \equiv 1$, gives us that

$$\begin{aligned} 1 &= \int_0^{\pi/2} \mathrm{d}\alpha_i \sin^{d-1}\alpha_i \cos^{d-1}\alpha_i |B_i^{(l_x,l_y)}\psi_i^{(l_x)}(\mu_{jk}^{-1}\rho\sin\alpha_i)|^2 \\ &\simeq |B_i^{(l_x,l_y)}|^2\mu_{jk}^d\rho^{-d}\int_0^\infty \mathrm{d}r\, r^{d-1}|\psi_i^{(l_x)}(r)|^2 = |B_i^{(l_x,l_y)}|^2\frac{\mu_{jk}^d}{\rho^d}\,, \end{aligned} \tag{92}$$

because $\psi_i^{(l_x)}$ is normalized. Thus the coefficients are given by $B_i^{(l_x,l_y)} = \mu_{jk}^{-d/2}\rho^{d/2}$. For this solution we can now calculate the diagonal coupling term Eq. (15), i.e.

$$Q_{nn} = \frac{1}{\rho^2}\int_0^\infty \mathrm{d}r\, r^{d-1}\psi_i^{(l_x)*}(r)\left(r^2\frac{\partial^2}{\partial r^2} + \mathrm{d}r^2\frac{\partial}{\partial r} + \frac{d(d-2)}{4}\right)\psi_i^{(l_x)}(r)\,. \tag{93}$$

The diagonal effective potential in Eq. (17) is then given by

$$V_{\mathrm{eff},n} = E_2 + \frac{2m}{\hbar^2}\left(\frac{(d-1)(d-3)+4l_y(l_y+d-2)}{4\rho^2}\right) + \langle V_{3b}\rangle\,, \tag{94}$$

which is the same potential as in the two-body radial equation when the phase space factor is included in the wave function, see Eq. (C.4). Thus, the three-body system for large distance has solutions behaving as a two-cluster system with one of the clusters as a bound state of particles j and k and the other "cluster" being simply particle i. To leading order these solutions are independent of the properties of the short-range potentials relying only on the two-body wave function as exponentially falling off with distance [75].

4.4. Asymptotic behaviour of the non-diagonal coupling terms

Let us use Eq. (20) to calculate the asymptotic form of $P_{nn'}$, where n and n' are asymptotically either two-cluster states or three-body continuum states. Only the wave function in regions of non-zero potentials enters into Eq. (20). Eqs. (68) and (89) give for $\rho \to \infty$ inside the region of non-vanishing V_i that the total wave function (not the Faddeev components) to first order in α_i is

$$\Phi_n(\alpha_i,\Omega_{xi},\Omega_{yi}) = \sum_{l_x,l_y} B_{i,n}^{(l_x,l_y)}\psi_{i,n}^{(l_x)}(\mu_{ij}^{-1}\rho\alpha_i)\left[Y_{l_x}(\Omega_{xi})\otimes Y_{l_y}(\Omega_{yi})\right]_{LM}\,, \tag{95}$$

Table 2
The leading-order behaviour of the coupling terms $P_{nn'}$ between angular eigenstates n and n' for $\rho \to \infty$ for total angular momentum $L = 0$. The two-cluster states correspond to two-body bound states in system i and i' with partial angular momenta (l_x, l_y) and (l'_x, l'_y), respectively. The eigenvalues of the three-body continuum states, characterized by hyperspherical quantum numbers K and K' and dominated by the partial angular momentum l_0 and l'_0, approach $\lambda_n(\infty) = K(K + 2d - 2)$ and $\lambda_{n'}(\infty) = K'(K' + 2d - 2)$ for $\rho \to \infty$, see Section 4.2. These results are also valid for $L > 0$ if both $l_0 \leq \frac{1}{2}(K - L)$ and $l'_0 \leq \frac{1}{2}(K' - L)$

n	n'	Condition	$P_{nn'}$
Cluster	Cluster	$(i, l_x, l_y) = (i', l'_x, l'_y)$	$\mathcal{O}(\rho^{-1})$
		$(i, l_x, l_y) \neq (i', l'_x, l'_y)$	$\mathcal{O}(\exp(-\rho))$
Cluster	Continuum	$l_x \geq l'_0$	$\mathcal{O}(\rho^{-d/2-l_x-1})$
		$l_x < l'_0$	$\mathcal{O}(\rho^{-d/2-2l'_0+l_x-1})$
Continuum	Continuum	$K \neq K'$	$\mathcal{O}(\rho^{1-d-2\max(l_0,l'_0)})$
		$K = K'$	$\mathcal{O}(\rho^{-1-2\lvert l_0-l'_0\rvert})$

where the two-body wave functions $\psi_{i,n}^{(l_x)}$ correspond to the energy $(\hbar^2/2m)\lambda_n\rho^{-2}$. The quantities λ_n, $B_{i,n}^{(l_x,l_y)}$ and $\psi_{i,n}^{(l_x)}$ now carry the index n to discriminate between different angular solutions. Using Eq. (95) we then rewrite Eq. (20) as

$$
\begin{aligned}
P_{nn'} = & -\sum_{i=1}^{3}\sum_{l_x,l_y}\frac{B_{i,n}^{(l_x,l_y)*}B_{i,n'}^{(l_x,l_y)}}{\lambda_n-\lambda_{n'}}\int_0^{\alpha_{0i}} \mathrm{d}\alpha_i \sin^{d-1}\alpha_i \cos^{d-1}\alpha_i \\
& \times\frac{2m}{\hbar^2}\frac{\partial\rho^2 V_i(\mu_{jk}^{-1}\rho\sin\alpha_i)}{\partial\rho}\psi_{i,n}^{(l_x)}(\mu_{jk}^{-1}\rho\alpha_i)(1+\mathcal{O}(\alpha_i^2))^*\psi_{i,n'}^{(l_x)}(\mu_{jk}^{-1}\rho\alpha_i)(1+\mathcal{O}(\alpha_i^2)) \\
= & -\sum_{i=1}^{3}\sum_{l_x,l_y}\frac{B_{i,n}^{(l_x,l_y)*}B_{i,n'}^{(l_x,l_y)}}{\lambda_n-\lambda_{n'}}\frac{\mu_{jk}^d}{\rho^{d-1}} \\
& \times\left[\frac{2m}{\hbar^2}\int_0^{r_{0i}}\mathrm{d}r\, r^{d-1}\psi_{i,n}^{(l_x)}(r)^*\left(2V_i(r)+r\frac{\partial V_i}{\partial r}\right)\psi_{in'}^{(l_x)}(r)+\mathcal{O}(\rho^{-2})\right].
\end{aligned}
\tag{96}
$$

The leading-order behaviour of $P_{nn'}$ may now be obtained from Eqs. (79), (91), (92) and Table 1. We have furthermore for $L = 0$ that the components with $l_x = l_0$ exhibit the slowest fall off of $B_i^{(l_x,l_y)}$ as a function of ρ, see Section 4.2. These results are collected in Table 2, which also is valid for continuum states with $l_0 \leq \frac{1}{2}(K - L)$. For $L > 0$ and $l_0 > \frac{1}{2}(K - L)$ other components than $l_x = l_0$ may fall off even slower and therefore become dominant for sufficiently large ρ, see Section 4.2. Then the results in Table 2 do not apply. Less detailed results for the $L = 0$ and $d = 3$ are obtained in [116].

The coupling terms $Q_{nn'}$ in Eq. (22) corresponding to matrix elements of the second derivative are also needed. Unfortunately, they cannot be calculated in the same way because Eq. (22) contains a sum over all the angular eigenstates. It is however tempting to use $Q_{nn'} = \partial P_{nn'}/\partial\rho + \sum_{n''} P_{nn''}P_{n''n'}$ obtained by differentiating Eq. (14) as an analogue of the operator expression $Q = \partial P/\partial\rho + P^2$ found from [116]. Then we find the asymptotic behaviour to be $Q_{nn'} = \mathcal{O}(\rho^{-1})P_{nn'}$.

It should however be noted that the infinite sum hidden in P^2, $(P^2)_{nn} = \sum_{n'} P_{nn'} P_{n'n}$, in general *cannot* predict the $Q_{nn} \propto \rho^{-2}$ behaviour of the diagonal term for a two-cluster state as obtained in Eq. (93). As seen from Table 2, all couplings to a two-cluster state fall off faster than ρ^{-1} except the (first derivative) couplings to other two-cluster states corresponding to another two-body bound state in the same subsystem with the same angular momentum. Therefore, if the two-body subsystem does not have another bound state the diagonal Q_{nn} must from this argument fall off faster than ρ^{-2}. Since this is wrong, we can conclude that the infinite sum over angular eigenvalues in the expression for Q must be taken before the limit $\rho \to \infty$. Each of the coupling terms do converge for large ρ, but the convergence in ρ and the summation over the infinitely many angular eigenvalues cannot always be interchanged.

This problem is worse if one of the two-body systems has infinitely many bound states as for particles of both positive and negative charge. Then there must be infinitely many adiabatic potentials each corresponding to bound two-body subsystems behaving as $-\rho^2$ for large ρ. We cannot interchange the infinite sum in the adiabatic expansion of Eq. (12) with the limit $\rho \to \infty$. In practice, the hyperspherical adiabatic expansion cannot immediately be used to describe three-body scattering above the three-body breakup threshold for oppositely charged particles. On the other hand, the present treatment may be applicable to systems with the same charges on all particles.

5. The Efimov and Thomas effects in *d* dimensions

In 1970 Efimov discovered that a three-body system in three dimensions with short-range interactions and at least two of the two-body subsystems with an *s*-state of zero energy, must have infinitely many bound states [46]. A zero-energy two-body *s*-state is equivalent to an infinitely large *s*-wave scattering length $a_i^{(0)}$. However, less extreme conditions of finite scattering length and a resulting finite number of bound states are already interesting. These bound states with rather characteristic properties arise in systems where the absolute values of $a_i^{(0)}$ are much larger than the ranges of the potential r_{0i}.

The "Efimov limit" of infinitely many bound states is reached for $|a_i^{(0)}/r_{0i}| \to \infty$. It is only occasionally recognized [125,126] that this is exactly the same limit giving rise to the Thomas effect discovered already in 1935 [47]. This effect, occurring in three-body systems with zero-range two-body potentials, produces an infinite number of strongly bound states. Also here $|a_i^{(0)}/r_{0i}| = \infty$ simply because $r_{0i} \equiv 0$ for such potentials.

5.1. Three identical bosons in 3 dimensions

The analyses in Section 4 are valid in the limit of $\rho \gg |a_i^{(l_x)}|$ but the key equations, Eqs. (73)–(75), are correct already when $\rho \gg r_{0i}$. In this section we only need to assume that $|a_i^{(l_x)}| \gg r_{0i}$ and ρ and $a_i^{(l_x)}$ could consequently be of the same order of magnitude. The term $(\rho/a_i^{(l_x)})^{d-2+2l_x} \sin(\pi\nu)$ in these equations is therefore not necessarily large for $\rho \gg r_{0i}$ as exploited in Section 4. We want to solve Eq. (73) in the limit $\rho \gg r_{0i}$ for three identical bosons in 3 dimensions with zero total angular momentum. Let us here assume that only the *s*-wave scattering length is large such that $|a_i^{(l_x)}|$ for $l_x > 0$ is of the same magnitude as r_{0i}. We shall later discuss the other possibilities.

Under these conditions all solutions, dominated by non-zero angular momentum $l_0 > 0$, have already approximately reached the free eigenvalues when $\rho \gg r_{0i}$, see Eq. (79). The eigenfunctions are then constants. These solutions are therefore decoupled in the radial equation. The remaining solutions with $l_0 = 0$ are dominated by partial angular momentum 0. As $\rho/a_i^{(0)}$ is not necessarily large in Eq. (73) the coefficient $A_i^{(0,0)}$ may be non-zero when $\rho \gg r_{0i}$ even for non-integer ν-values. For components with $l_x > 0$ the coefficients $A_i^{(l_x,l_y)}$ must vanish as $(\rho/a_i^{(l_x)})^{2-d-2l_x}$ according to Eq. (73). Thus we only need to include components with $l_x = l_y = 0$ for these distances of $\rho \gg r_{0i}$.

To solve Eq. (73) we need $R_{ij}^{(0,0)\,(0,0)}$ and from Eqs. (61) and (A.12) we have

$$R_{ij}^{(0,0)\,(0,0)}(\lambda) = \int d\Omega_{xi} \int d\Omega_{yi} \left(\frac{1}{\sqrt{4\pi}}\right)^4 \times \frac{\Gamma(\nu+1)\sin[\,(\nu+1)(\pi-2\alpha_j)\,]}{(\nu+1)\sin(\pi-2\alpha_j)} \left(\frac{\Gamma(\nu+1)\sin(2(\nu+1)\alpha_i)}{(\nu+1)\sin(2\alpha_i)}\right)^{-1}, \tag{97}$$

where we can use $\alpha_i = 0$ according to Eq. (10). Then $\alpha_j = |\gamma_{ij}|$ and the integrand in Eq. (97) is independent of Ω_{xi} and Ω_{xi} immediately resulting in

$$R_{ij}^{(0,0)\,(0,0)}(\lambda) = \frac{\sin[\,(\nu+1)(\pi-2|\gamma_{ij}|)\,]}{(\nu+1)\sin(\pi-2|\gamma_{ij}|)}\,. \tag{98}$$

The three particles have the same mass, then $\gamma_{ij} = \pm\,\pi/3$, see Eq. (8) and we get

$$R_{ij}^{(0,0)\,(0,0)}(\lambda) = \frac{2\sin((\nu+1)\pi/3)}{(\nu+1)\sqrt{3}}\,. \tag{99}$$

We can further simplify Eq. (73) by using the boson symmetry, $A_1^{(0,0)} = A_2^{(0,0)} = A_3^{(0,0)}$, and the equal scattering lengths $a_1^{(0)} = a_2^{(0)} = a_3^{(0)}$. Then we obtain

$$\frac{\rho}{\mu_{jk} a_i^{(0)}} = \frac{2(\nu+1)\cos(\pi\nu) + \frac{8}{\sqrt{3}}\sin((\nu+1)\pi/3)}{\sin(\pi\nu)}\,. \tag{100}$$

The lowest solutions, $\lambda = 4\nu(\nu+2)$, to this equation are shown in Fig. 4 as a function of $\rho/|a_i^{(0)}|$ for negative as well as for positive scattering length. The free spectrum, $\lambda = K(K+4)$, is approached for $\rho \gg |a_i^{(0)}|$ with the exception of $\lambda = 12$ corresponding to $K = 2$ for which no completely symmetric state exists. For positive scattering length, $a_i^{(0)} > 0$, the lowest eigenvalue diverges as $\lambda = -(\rho/a_i^{(0)})^2(m/m_i)$ as given by Eq. (88) corresponding to a two-body bound state. At $\rho = 0$ the spectrum is shifted downwards compared to the free spectrum where the lowest solution then has $\nu = -1 + 0.503i$ and $\lambda = -5.01$.

The partial angular momenta are zero for the interesting component and the α-dependence of the angular wave function is found from Eqs. (A.12) and (54):

$$\Phi = -\sum_{i=1}^{3} A_i^{(0,0)} \frac{\Gamma(\nu+3/2)}{\Gamma(3/2)} \frac{\sin(\nu(\alpha_i - \pi/2))}{\sin(2\alpha_i)}\,. \tag{101}$$

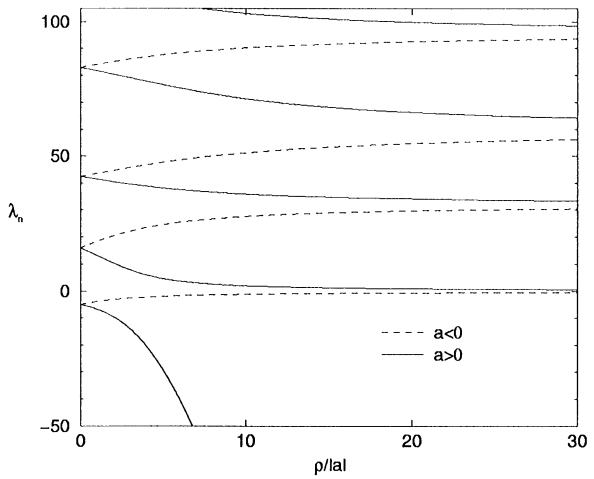

Fig. 4. The lowest angular eigenvalues for 3 identical bosons of mass m_1 in 3 dimensions interacting with zero-range potentials with scattering length $a \equiv a_i^{(0)}$. The unit mass in Eq. (2) is chosen as $m = \frac{1}{2}m_1$ such that $\mu_{jk} \equiv 1$. The plot contains both the solutions for positive a (full curve) where the two-body systems have bound states, and negative a (dashed curve). For $\rho \to 0$ the spectra for negative and positive scattering length are the same. The lowest eigenvalue is $\lambda_1(\rho = 0) = -5.01$. For $\rho \to \infty$ all the eigenvalues approach the values for no interactions, either from above (positive a) or from below (negative a).

The diagonal effective potential in Eq. (17) is $V_{\text{eff}} = (\hbar^2/2m)(15/4 + \lambda(\rho))\rho^{-2}$, where Q_{nn} is neglected as unimportant for the distances of interest in the present context, i.e. $r_{0i} \ll \rho \ll |a_i^{(0)}|$ where $\lambda = -5.01$. These neglected terms arise due to the variation of the angular wave functions, which in our case only vary slowly with ρ, because λ and v nearly are constants. In fact, all the couplings defined in Eqs. (14) and (15) are negligibly small, since the angular eigenvalues and therefore also the Faddeev components remain nearly constant over this large region of space.

These effective potentials are shown in Fig. 5, where the dominating feature is the strong variation for the interesting region of small ρ. From λ we then obtain the simple small distance behaviour of the effective potentials, i.e.

$$V_{\text{eff},1}(\rho) = \frac{\hbar^2}{2m}\frac{(-1.26)}{\rho^2} \equiv \frac{\hbar^2}{2m}\frac{(-\xi^2 - 1/4)}{\rho^2}\,, \tag{102}$$

where $\xi = 1.006$ corresponding to $\lambda_1 = -5.01$. The unnormalized radial wave functions for small energy are solutions for the potentials in Eq. (102), i.e.

$$f_1(\rho) = \sqrt{\rho}\sin(\xi\ln(\rho/r_{0i}) + \delta)\,, \tag{103}$$

where δ is a phase depending on the boundary condition at $\rho \sim r_{0i}$. These solutions are not coupled to components related to the higher potentials, since the coupling constants are negligibly small. We can therefore assume that $f_n = 0$ for $n \geq 2$. By counting the number of nodes between r_{0i} and $|a_i^{(0)}|$ in f_1 we get a fairly accurate estimate of the number N of bound states, i.e.

$$N \simeq \frac{\xi}{\pi}\ln\left(\frac{|a_i^{(0)}|}{r_{0i}}\right). \tag{104}$$

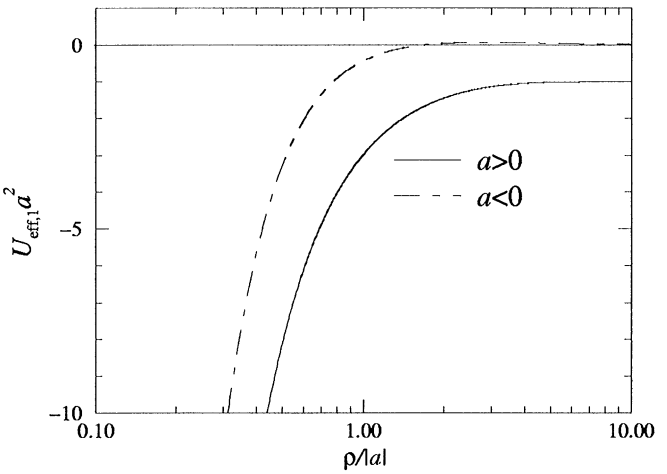

Fig. 5. The effective potential, $U_{\mathrm{eff}} = V_{\mathrm{eff}} 2m/\hbar^2$, corresponding to the lowest angular eigenvalue for 3 identical bosons of mass m in 3 dimensions interacting with zero-range potentials. The diagonal coupling term Q_{nn} is not included. The s-wave scattering length a is used to scale the axes into dimensionless quantities. The plot exhibits the solutions for both positive a, where the two-body systems have bound states, and negative a. For $\rho \ll |a|$ the potential approaches $-1.26\rho^{-2}$.

Thus for $a_i^{(0)} = \pm\infty$ or $r_{0i} = 0$ we have an infinite number of bound states. These two limits are precisely where the Efimov or Thomas effects occur.

Improved radial wave functions corresponding to these bound states with finite energies can be found by solving Eq. (13) with only one angular eigenfunction included, neglect of the coupling terms and use of the small distance expression in Eq. (102). We then get

$$f_1(\rho) = \sqrt{\rho} K_{\mathrm{i}\xi}(\kappa\rho), \quad \kappa \equiv \sqrt{\frac{2m(-E)}{\hbar^2}}\,, \tag{105}$$

where K_n is the modified Bessel function of the second kind, which is exponentially decreasing for large arguments. When the energy approaches zero the wave function in Eq. (105) reduces to Eq. (103). As the contributions from both small and large ρ are small we use Eq. (105) for every ρ in $]0, \infty[$ to obtain

$$\langle;\rho^2\rangle = \frac{2}{3}(1+\xi^2)\frac{\hbar^2}{2m(-E)}\,, \tag{106}$$

which is similar to Eq. (C.10) for two-body systems deviating only by the constant factor depending on ξ instead of d.

The binding energies may be determined as soon as an appropriate boundary condition is provided at a small ρ-value. Such a boundary condition is typically that $f_1(\rho_0) = 0$ for $\rho_0 = 0$ or that the logarithmic derivative of f_1 must equal a specific value for $\rho_0 \sim r_{0i}$ slightly outside the range of the short-range potential. With $K_{\mathrm{i}\xi}(\kappa\rho_0) = 0$ the bound state energies are found from $\kappa_n = z_n/\rho_0$, where z_n are the zero points of the Bessel functions, i.e. $K_{\mathrm{i}\xi}(z_n) = 0$, $n = 0, 1, 2 \ldots$. Using $\kappa\rho_0 \ll 1$ the wave function in Eq. (103) is an accurate approximation and we obtain that

$z_n \simeq z_0 \exp(-n\pi/\xi)$ and therefore

$$E_n = \exp\left(-\frac{2\pi}{\xi}n\right)E_0 \ , \tag{107}$$

where E_0 is the energy of the first of these Efimov state. Size and energy are related by Eq. (106) and the size therefore increase exponentially, i.e.

$$\langle\rho^2\rangle_n = \exp\left(\frac{2\pi}{\xi}n\right)\langle\rho^2\rangle_0 \ . \tag{108}$$

As λ_1 is almost constant over the region in ρ in which the Efimov states exist, they all have almost identical angular wave functions as given in Eq. (101). In other words, these three-body states exhibit the same angular correlations and differ essentially only by size and number of nodes in the radial wave function.

From a general non-relativistic Schrödinger equation of N particles,

$$\left[-\sum_{i=1}^{N}\frac{\hbar^2}{2m_i}\Delta_i + V(\boldsymbol{r}_1, \ldots, \boldsymbol{r}_N) - E\right]\Psi(\boldsymbol{r}_1, \ldots, \boldsymbol{r}_N) = 0 \ , \tag{109}$$

we see that the simultaneous transformations

$$\begin{aligned} &\boldsymbol{r}_i \mapsto \boldsymbol{r}_i', \quad E \mapsto E', \quad V \mapsto V' \ , \\ &\boldsymbol{r}_i' \equiv t\boldsymbol{r}_i, \quad E' \equiv t^{-2}E, \quad V'(\boldsymbol{r}_1, \ldots, \boldsymbol{r}_N) \equiv t^{-2}V(t^{-1}\boldsymbol{r}_1, \ldots, t^{-1}\boldsymbol{r}_1) \end{aligned} \tag{110}$$

leave the Schrödinger equation unchanged for any positive number t. Thus, the Schrödinger equation is invariant under scalings, where all lengths are multiplied by a number t and all energies are multiplied by t^{-2}.

The Efimov states follow these general scaling rules for length and energy in quantum mechanics, but now in addition also *within* the Efimov series, i.e.

$$E \mapsto E' = Et^{-2}, \quad \langle\rho^2\rangle^{1/2} \mapsto \langle\rho^2\rangle'^{1/2} = \langle\rho^2\rangle^{1/2}t \ , \tag{111}$$

where t only can be an integer power of $\exp(\pi/\xi)$, i.e. $t = \exp(n\,\pi/\xi)$. In this case the scaling applies within the spectrum itself *without* any scaling of the two-body potentials, i.e. by applying the scaling in Eq. (111) on energy and size of a single Efimov state, the same quantities of another Efimov state in the same Efimov series is obtained. The reason for this additional symmetry is that the kinetic energy and the effective potential in Eq. (102) both scale as t^{-2} under the transformation in Eq. (110). Only the cutoff at small ρ, which defines the energy of the lowest Efimov state, is not invariant under this scaling.

5.2. Occurrence conditions for the Thomas and Efimov effects

Let us now try to determine the restrictions on dimension, angular momenta and masses, which allow the Efimov and Thomas effects. The requirement is simply that the lowest radial potential is of the form given in Eq. (102) for $r_{0i} \ll \rho \ll |a_i^{(l_x)}|$. This is fulfilled if the lowest angular eigenvalue λ_1 is less than $-(2d-3)(2d-1)/4 - 1/4 = -(d-1)^2$ such that $\lambda_1 = -(d-1)^2 - \xi^2$, where ξ^2 is a positive number, see Eqs. (17) and (102). The number of Efimov states for a system of three bosons in three dimensions increases proportional to ξ for a given ratio between the

scattering length and the range of the potential. This dependence is expected to hold in general although ξ may differ from the value 1.006 found in Eq. (102). Also the angular part of the wave function of the Efimov states may differ from Eq. (101) in the general case.

5.2.1. Dimensional requirements

Let us return to Eq. (73) and again study the limit $\rho \gg r_{0i}$ without imposing the additional constraint of $\rho \gg |a_i^{(l_x)}|$. When $d + 2l_x > 4$, the term behaving as $(\rho/r_{0i})^{d-4+2l_x}\sin(\pi v)$ is then large unless v is an integer. Thus, the free spectrum is obtained even when $\rho \ll |a_i^{(l_0)}|$ unless the amplitude $A_i^{(l_x,l_y)}$ vanishes. The only difference compared to the result in Eq. (78) is that we now have $v = n + \mathcal{O}(\rho^{4-d-2l_x})$ instead of $v = n + \mathcal{O}(\rho^{2-d-2l_x})$. Analogously, for $d + 2l_x = 4$ we find from Eq. (74) that now $v = n + \mathcal{O}([\ln(\rho)]^{-1})$.

Therefore for a solution to Eq. (73), where a component with $l_x = l_0$ is non-zero for $\rho \gg r_{0i}$, the angular eigenvalues must approach the free spectrum for $\rho \gg r_{0i}$, i.e. $\lambda \to K(K + 2d - 2)$. This limit must be independent of the size of the scattering lengths $a_i^{(l_0)}$ provided either $l_0 \geq 1$ or $d \geq 4$ is valid. That is the Efimov and Thomas effects are only possible for dimensions less than 4. Furthermore, solutions with negative eigenvalues λ at large distance can only occur for very large *s-wave* scattering lengths, since $l_0 > 0$. The components with $l_x \geq 1$ of the corresponding eigenfunctions must fall off for $\rho \gg r_{0i}$ independently of the value of $a_i^{(l_x)}$. Thus, in our search for negative angular eigenvalues we only need to include components with $(l_x, l_y) = (0, L)$.

We then need to calculate the coefficients $R_{ij}^{(0,L)\,(0,L)}(\lambda)$ defined in Eq. (61). First we *choose* $\alpha_i = 0$ through Eqs. (7) and (9), then implying that $\boldsymbol{x}_j = \sin(\gamma_{ij})\boldsymbol{y}_i$, $\boldsymbol{y}_j = -\cos(\gamma_{ij})\boldsymbol{y}_i$, $[Y_0(\Omega_{xj})\otimes Y_L(\Omega_{yj})]_L = (-1)^L[Y_0(\Omega_{yi})\otimes Y_L(\Omega_{yi})]_L$ and $\alpha_j = |\gamma_{ij}|$. The integrals in Eq. (7) are now easily computed and we find

$$R_{ij}^{(0,L)\,(0,L)}(\lambda) = \frac{\Gamma(v+1)P_v^{((d-2)/2+L,\,(d-2)/2)}(-\cos 2\gamma_{ij})}{\Gamma(v+1)P_v^{((d-2)/2,\,(d-2)/2+L)}(1)}(-\cos\gamma_{ij})^L$$
$$= \frac{\Gamma\left(\frac{d}{2}\right)\Gamma\left(v+\frac{d}{2}+L\right)}{\Gamma\left(\frac{d}{2}+L\right)\Gamma\left(v+\frac{d}{2}\right)}F\left(-v,\,v+L+d-1;\frac{d}{2}+L;\cos^2\gamma_{ij}\right)(-\cos\gamma_{ij})^L\,, \tag{112}$$

where we used that Y_L is normalized and Eq. (A.2). We rewrite Eq. (73) as

$$\left[-\frac{\sin\left(\pi\left(v+\frac{d}{2}\right)\right)}{\sin\left(\pi\frac{d}{2}\right)} + \frac{\Gamma^2\left(\frac{d}{2}\right)\Gamma(v+1)\Gamma\left(v+\frac{d}{2}+L\right)\sin(\pi v)}{\pi\left(\frac{d-2}{2}\right)\Gamma\left(v+\frac{d}{2}\right)\Gamma(v+d-1+L)}\left(\frac{\rho}{\mu_{jk}a_i^{(0)}}\right)^{d-2}\right]A_i^{(0,L)}$$
$$= \sum_{j\neq i}\frac{\Gamma\left(\frac{d}{2}\right)\Gamma\left(v+\frac{d}{2}+L\right)}{\Gamma\left(\frac{d}{2}+L\right)\Gamma\left(v+\frac{d}{2}\right)}F\left(-v,\,v+L+d-1;\frac{d}{2}+L;\cos^2\gamma_{ij}\right)(-\cos\gamma_{ij})^L A_j^{(0,L)}\,, \tag{113}$$

where only components with $|a_i^{(0)}| \gg r_{0i}$ can have non-vanishing values of $A_i^{(0,L)}$ for $\rho \gg r_{0i}$.

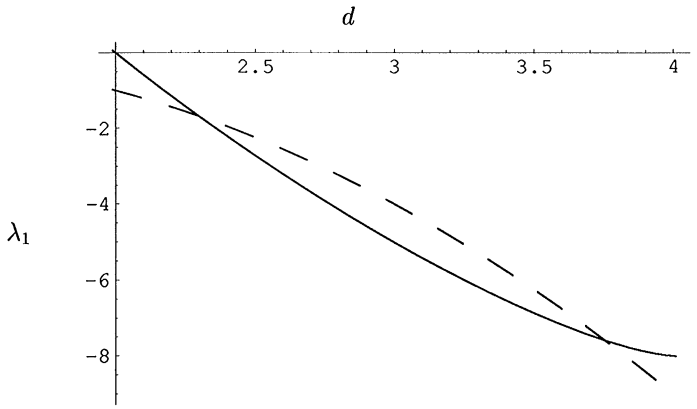

Fig. 6. The lowest angular eigenvalue $\lambda_1(\rho = 0)$ (full curve) for 3 identical bosons with total angular momentum $L = 0$ obtained from Eq. (113) is shown as a function of the dimension d and compared with $-(2d-1)(2d-3)/4 - 1/4 = -(d-1)^2$ (dashed curve). The Efimov effect occurs if $\lambda_1(0) < -(d-1)^2$, i.e. for $2.3 < d < 3.8$.

Again the dimension $d = 2$ needs special treatment. We can either take the limit of $d \to 2$ in Eq. (113) or equivalently insert Eq. (112) into Eq. (75). In both cases we obtain the same result for $d = 2$, i.e.

$$\left[\cos(\pi\nu) + \frac{\sin(\pi\nu)}{\pi}\left(\psi_\Gamma(\nu+1+L) + \psi_\Gamma(\nu+1) + 2\gamma + 2\ln\left(\frac{\rho}{\mu_{jk}a_i^{(0)}}\right)\right)\right]A_i^{(0,L)}$$
$$+ \sum_{j\neq i}\frac{\Gamma(\nu+1+L)}{L!\Gamma(\nu+1)}F(-\nu, \nu+L+1; 1+L; \cos^2\gamma_{ij})(-\cos\gamma_{ij})^L A_j^{(0,L)} = 0\,, \tag{114}$$

which is a generalization of the result for $L = 0$ obtained in [39]. Again the free spectrum is found for $\rho \gg |a_i^{(0)}|$ but also for $\rho \ll |a_i^{(0)}|$, because $\ln(\rho/(\mu_{jk}a_i^{(0)}))$ diverges in both cases. Therefore the lowest eigenvalue approaches 0 both when $\rho \gg a_i^{(0)}$ and when $r_{0i} \ll \rho \ll a_i^{(0)}$.

Thus, the Efimov and Thomas effects do not occur for $d = 2$. This is consistent with the general theorem that few-body systems with finite range potentials in one and two dimensions can only have a finite number of bound states [127]. Also other authors have argued that there are no Efimov and Thomas effects in $d = 2$ dimensions [128,129].

The overall general conclusion is then that the Efimov and Thomas effects are only possible for dimensions in the interval $2 < d < 4$. This includes only the integer value of $d = 3$, but allows also an interval of fractional dimensions. The extension of that interval may easily be found from Eq. (113) for three identical bosons with $L = 0$. The limit of $\lambda_1(\rho)$ for $\rho \to 0$ is then computed as the decisive quantity for obtaining a sufficiently attractive effective potential of the form in Eq. (17) for distances $r_{0i} \ll \rho \ll |a_i^{(l_x)}|$. To allow the effects $\lambda_1(\rho = 0)$ must be smaller than $-(2d-3)(2d-1)/4 - 1/4 = -(d-1)^2$. The two relevant functions are shown in Fig. 6 as function of the dimension. The effects can only occur for $2.3 < d < 3.8$.

5.2.2. Mass variations and requirements

We shall investigate the occurrence conditions for $d = 3$ and $L = 0$ as function of the masses of the three particles. Without loss of generality we assume that $m_1 \leq m_2 \leq m_3$. The mass-dependent

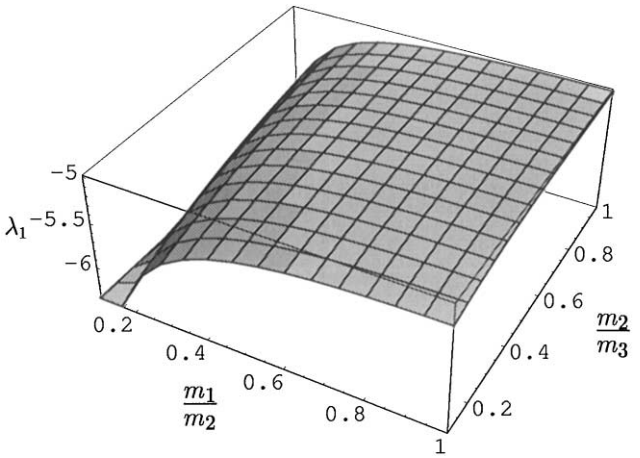

Fig. 7. The lowest angular eigenvalue $\lambda_1(\rho = 0)$ for a three-body system with total angular momentum $L = 0$ in $d = 3$ dimensions in the limit $r_{0i} \ll \rho \ll a_i^{(0)}$ as a function of the mass ratios m_1/m_2 and m_2/m_3 when $m_1 \leq m_2 \leq m_3$.

rotation angles γ_{ij} explicitly given in Eq. (8) are functions of the two mass ratios m_1/m_2 and m_2/m_3 both then between 0 and 1. We can solve Eq. (113) for $\rho \ll |a_i^{(0)}|$ for given $(m_1/m_2, m_2/m_3)$ assuming that all three s-wave scattering lengths are large compared to the ranges of the potentials. The resulting lowest eigenvalue is shown in Fig. 7.

Three equal masses correspond to the point $(m_1/m_2, m_2/m_3) = (1, 1)$, which has the largest (least negative) value of $\lambda_1(\rho = 0) = -5.01$, and the effects are then least pronounced. As one mass increases compared to the other two, i.e. m_2/m_3 decreases below 1, then $\lambda_1(\rho = 0)$ decreases. When one mass decreases compared to the other two, i.e. m_1/m_2 decreases below 1, $\lambda_1(\rho = 0)$ also decreases. As $m_1/m_2 \to 0$, $\lambda_1(\rho = 0)$ diverges to minus infinity, because both γ_{12} and γ_{31} then converge towards $\pi/2$ and $\gamma_{23} \simeq \sqrt{m_1/m_2}\sqrt{1 + m_2/m_3} \to 0$. This in turn leads to divergent off-diagonal terms in Eq. (113), cf. Eq. (98).

This confirms that the Efimov and Thomas effects are possible for all mass combinations in $d = 3$ dimensions, if all three subsystems have a resonance at zero energy or if all the potentials are of zero range. In addition, Fig. 7 illustrates that the most favourable condition, the largest value of ξ or equivalently the smallest $\lambda_1(\rho = 0)$, occurs when one of the particles is light compared to both the other two. Then the largest number of Efimov states is present for a given ratio of the scattering lengths to the range of the potentials.

5.2.3. Two resonant subsystems

From Eq. (104) we see that the scattering length must increase by a factor of $\exp(\pi/\xi) \sim 20$ to make room for one more Efimov state in a system of three identical bosons in 3 dimensions. That is to have, for example, 2 Efimov states the s-wave scattering length must be at least 400 times the range of the potential. In physical units this means for nuclei or atoms with potential ranges of about 5 fm or 5 Å that the scattering length must be at least 2000 fm or 2000 Å, respectively. The resonance energy of about $\hbar^2/(2\mu a^2)$ must correspondingly at least be smaller than about 1 eV or 10^{-10} eV, where we used a light nuclear mass of 5 nucleons. Thus, the resonance energy must be

extremely close to zero. To find systems where three different scattering lengths simultaneously are sufficiently large is very unlikely. However, the chances increase substantially if one or more of the two-body subsystems are identical. (The advantage is lost if all three particles are identical fermions, since then the totally symmetric Efimov states are not physically allowed.) The pertinent question in this connection is then how many of the two-body interactions must simultaneously produce resonances at extremely small energies.

To answer this question we first assume that only one scattering length is very large compared to the range of the potential. Then only the corresponding Faddeev component is non-zero for $\rho \gg r_{0i}$ and the 3×3 matrix equation for the A coefficients in Eq. (113) reduces to a 1×1 matrix equation for $\rho = 0$, i.e.

$$\frac{\sin\left(\pi\dfrac{v+d}{2}\right)}{\sin\left(\dfrac{\pi}{2}d\right)}A_i^{(0,L)} = 0\ . \tag{115}$$

Then v must be real and Eq. (56) gives $\lambda = (2v+L)(2v+L+2d-2) \geq -(d-1)^2$, which excludes occurrence of both the Efimov and Thomas effects. Therefore, at least two of the two-body subsystems must have an s-wave resonance at zero energy. This conclusion is valid for all dimensions and angular momenta.

The next step is to assume zero-energy resonances in precisely two subsystems, for example between particles 1, 2 and 1, 3, but not between 2, 3. Then $A_1^{(0,L)} = 0$ in Eq. (113), and the 2×2 determinant in the limit $\rho \to 0$ becomes

$$\left(\frac{\sin\left(\pi\left(v+\dfrac{d}{2}\right)\right)}{\sin\left(\pi\dfrac{d}{2}\right)}\frac{\Gamma\left(\dfrac{d}{2}+L\right)\Gamma\left(v+\dfrac{d}{2}\right)}{\Gamma\left(\dfrac{d}{2}\right)\Gamma\left(v+\dfrac{d}{2}+L\right)}\right)^2 - \left(F\left(-v,\, v+L+d-1;\frac{d}{2}+L;\cos^2\gamma_{23}\right)(-\cos\gamma_{23})^L\right)^2 = 0\ . \tag{116}$$

This equation in general and in particular the value of the lowest eigenvalue now only depends on the masses through $\gamma_{23} = \arctan\sqrt{m_1(m_1+m_2+m_3)/m_2m_3} \in [0, \pi/2]$. This decisive dependence is shown in Fig. 8 which exhibits $\lambda_1(\rho=0)$ as a function of γ_{23} for $d=3$ and both $L=0$ and $L=1$. For $L=0$ the $\lambda_1(\rho=0)$ function is always below the critical value of -4 except in the point $\gamma_{23} = \pi/2$. However, $\lambda_1(\rho=0) < -4$ only for $|\gamma_{23}| < 0.37$ for $L=1$.

We conclude that for all mass combinations the Efimov effect is possible in three dimensions except for $\gamma_{23} = \pi/2$ where $\lambda_1(\rho=0) = -4$. This value corresponds to particle 1 being infinitely heavy relative to at least *one* of the particles 2 and 3. Thus, the Efimov conditions are hard to meet for a light particle unless its interaction with one of the heavier particles produces a resonance at zero energy. Chances improve as $\lambda_1(\rho)$ diverge towards $-\infty$ as $\gamma_{23} \to 0$, i.e. in the limit when both $m_1 \ll m_2$ and $m_1 \ll m_3$.

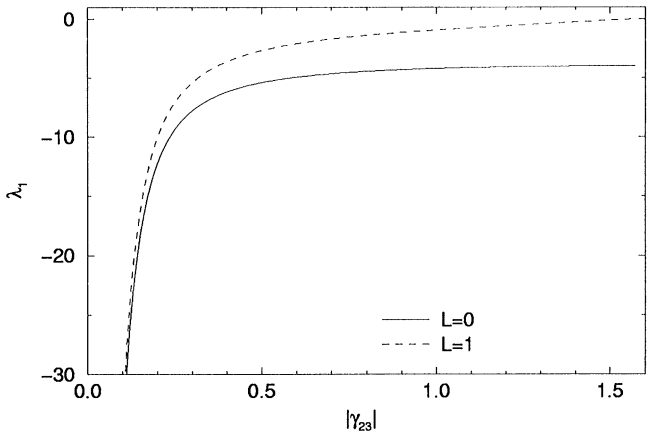

Fig. 8. The lowest angular eigenvalue extracted from Eq. (116) as a function of γ_{23} given by Eq. (8) for a three-body system with angular momentum $L = 0$ and 1 in three dimensions in the limit where $r_{0j} \ll \rho \ll |a_j^{(0)}|$ for $j = 2, 3$ and $\rho \gg |a_1^{(0)}|$.

The same trends are found for $L = 1$, where $\lambda_1(0)$ only is sufficiently negative ($\lambda_1(0) < -4$) to produce the Efimov effect when $\gamma_{23} < 0.37$. That is the Efimov effect only occurs for $L = 1$ when particle 1 is light enough, i.e. when $m_1 < \frac{1}{2}(-m_2 - m_3 + \sqrt{(m_2 + m_3)^2 + 0.60 m_2 m_3})$.

The obvious next question is now if we can derive similar conditions for arbitrary L. To achieve this we first try to find a value of γ_{23} such that $\lambda = -(2d-3)(2d-1) - 1/4 - \xi^2 = -(d-1)^2 - \xi^2$ is a solution to Eq. (116) for a value of $\xi > 0$. Then the related $\nu = -\frac{1}{2}(d - 1 + L) + i\xi$, see Eq. (55) and the derivation in Section 4.3. With this ν Eq. (116) can now be rewritten as

$$\pm \frac{\sin\left(\frac{\pi}{2}(1 - L + 2i\xi)\right)}{\sin\left(\pi\frac{d}{2}\right)} \frac{\Gamma\left(\frac{d}{2} + L\right)\Gamma\left(\frac{1-L}{2} + i\xi\right)}{\Gamma\left(\frac{d}{2}\right)\Gamma\left(\frac{1+L}{2} + i\xi\right)}$$

$$= (-\cos\gamma_{23})^L F\left(\frac{d-1+L}{2} - i\xi, \frac{d-1+L}{2} + i\xi; \frac{d}{2} + L; \cos^2\gamma_{23}\right), \tag{117}$$

where both sides of the equation are real when ξ is real, see Eq. (A.3). For $L \geq 1$ and any value of $\xi \geq 0$, Eq. (117) has a solution γ_{23} with one of the signs in Eq. (117). This follows, since the left-hand side is a constant in γ_{23} and the right-hand side is a continuous function of γ_{23}, which takes the value 0 for $\gamma_{23} = \pi/2$ and diverges towards $\pm\infty$ for $\gamma_{23} \to 0$. To compensate on the right-hand side when $\gamma_{23} \to 0$ we must have $\xi \to \infty$ and consequently $\lambda_1 \to -\infty$.

It is thus proven that an arbitrary low value of λ_1 can be obtained for any L by choosing the value of γ_{23} sufficiently small. The symmetry of the wave function must follow the sign in Eq. (117), because the corresponding coefficients in Eq. (113) must obey the relation $A_2^{(0,L)} = \pm A_3^{(0,L)}$. The interchange of particles 2 and 3 must therefore give the phase $(-1)^L$, i.e. even L for bosons and even or odd L for fermions depending on the symmetry of the spin wave function.

5.3. Conclusion

The Efimov and Thomas effects only exist in spaces with a dimension between 2 and 4 or more precisely between 2.3 and 3.8. Thus, the only integer dimension in which the effects exists is $d = 3$. At least two of the two-body subsystems must have infinite s-wave scattering lengths to obtain the Efimov effect, i.e. one of the particles must have infinite scattering length when interacting with both of the others. Let us call this particle the *resonant particle*. Large scattering length for higher angular momenta cannot produce the effect. The Thomas effect only occurs when at least two of the potentials are of zero range.

For given dimension, total angular momentum and mass ratios, all Efimov states only differ in size and number of nodes in the radial wave function. Within each Efimov series the mean square radius increases by a constant factor from one state to the next whereas the three-body binding energy decreases by the same factor. This factor is constant within each Efimov series, but otherwise it depends on dimension, angular momentum and mass ratios.

All mass combinations allow the effects for $d = 3$ and total angular momentum $L = 0$, but most Efimov states appear for a fixed ratio of scattering length and interaction range when the resonant particle is light compared to both the two others. In the opposite case, where the resonant particle is much heavier than one or both of the two others, the attractive effective potential is only barely above the critical value and therefore very few Efimov states are present. For $L > 0$ the Efimov effect only exists when the mass of the resonant particle is sufficiently small compared to the other two masses.

Turning this argument around the maximum total angular momentum, where an infinite Efimov series exists for a given set of mass ratios, increases with decreasing mass of the resonant particle. For molecular systems with two heavy particles and one light resonant particle an Efimov series exists for each total angular momentum up to a maximum value depending on the mass ratios.

6. Three-body systems in two dimensions

In this section we shall briefly review the most pertinent universal properties for two dimensional systems and illustrate with atomic helium trimers. Further details and discussions can be found in [39].

For $d = 2$ we conclude from Eq. (114), valid for $\rho \gg r_{0i}$, that the angular spectrum depends on the scattering lengths $a_i^{(0)}$ as for $d = 3$. The free spectrum emerges both when $r_{0i} \ll \rho \ll |a_i^{(l_x)}|$ and when $\rho \gg |a_i^{(l_x)}|$ such that the lowest eigenvalue λ_1 vanishes in these limits. Therefore the lowest effective radial potential must, in these ρ-intervals, behave as $V_{\mathrm{eff},1}(\rho) \propto (\frac{3}{4} + \lambda_1)\rho^{-2} \simeq \frac{3}{4}\rho^{-2}$. This small distance repulsion is now dominating in contrast to the $-1.26\rho^{-2}$ behaviour in three dimensions. The low-energy wave functions therefore concentrate at $\rho \gg r_{0i}$, where the adiabatic potentials only depend on the scattering lengths. In the limit of large scattering lengths and low energy, both the angular spectrum and the total wave function are then independent of the shapes of the two-body potentials.

Three identical bosons in the weak binding limit give two bound states, ground (g) and excited states (ex), with energies E and root mean square radii R, i.e.

$$\mathrm{E}^{(\mathrm{g})} = 16.52E_2, \quad E^{(\mathrm{ex})} = 1.267E_2, \quad E_2 = -4\exp(-2\gamma)\frac{\hbar^2}{2\mu a^2},$$

$$R^{(\mathrm{g})} = 0.111a, \quad R^{(\mathrm{ex})} = 0.927a, \tag{118}$$

where a is the s-wave scattering length, μ the reduced mass and γ as Euler's constant, see Eq. (C.9). Hence, the properties of the bound states only depend on the scattering length contrary to the Efimov states in 3 dimensions, where the range of the two-body potentials also enters, see Section 5.1. This *model independence* in two dimensions implies that the same scattering length produces approximately identical states. The generalization to systems with three different particles requires more parameters. However, a similar model independence still arises in the limit of weak binding, but the number of bound three-body states could now be one as well as two. The three-body binding energies still only depend on the inverse square of a scattering length, but the exact combination could be a complicated function of the ratios of masses and scattering lengths.

All short-range potentials, except a central attraction and an outer repulsive barrier, cannot produce bound three-body states unless one of the two-body subsystems has a bound state. Thus, Borromean systems are unlikely in two dimensions and their properties differ very much from those in 3 dimensions.

As examples we use the atomic helium trimers with the realistic LM2M2 potential [130]. The energies of the three-body bound states are given in Table 3. Both $^4\mathrm{He}_3$ and $^3\mathrm{He}_3$ have two bound states. The ratios between the three-body binding energies and the two-body binding energies are smaller than predicted in Eq. (118). The scattering lengths of ^{4}He–^{4}He and ^{3}He–^{3}He are then too small to produce the model-independent results.

The asymmetric systems, $^3\mathrm{He}^4\mathrm{He}_2$ and $^4\mathrm{He}^3\mathrm{He}_2$, each only have one bound state with $L^\pi = 0^+$. When one of the atoms in $^4\mathrm{He}_3$ is replaced by ^{3}He the kinetic energy is increased whereas the potential energy is unchanged. Therefore, the very weakly bound excited state of $^4\mathrm{He}_3$ must move to an energy above the two-body threshold, which also remains unchanged. When another ^{4}He is

Table 3
Bound state energies for the four helium trimers in 2 dimensions in absolute values in units of mK and relative to the binding energy of the most strongly bound two-body subsystem, which therefore provides the threshold. The second and third columns give the smallest s-wave scattering length (in atomic units) and the two-body energy (in mK) of that two-body subsystem. The ^{3}He atom is treated as a spin 0 boson and $^3\mathrm{He}_3$ is in a fully symmetric state. The symmetric trimers each have two bound states whereas the asymmetric systems only have one

System	$a^{(0)}_{\min}$	$E_{2,\min}$ (mK)	E_3 (mK)	$E_3/E_{2,\min}$
$^4\mathrm{He}_3$	42.312	− 38.384	− 172.1	4.48
			− 38.61	1.0059
$^3\mathrm{He}^4\mathrm{He}_2$	42.312	− 38.384	− 68.06	1.773
$^3\mathrm{He}^4_2\mathrm{He}$	131.96	− 3.8190	− 12.57	3.29
$^3\mathrm{He}_3$	2343.4	− 0.013134	− 0.1884	14.32
			− 0.01616	1.230

replaced by ^{3}He the most strongly bound two-body subsystem is ^{3}He–^{4}He, which is far less bound than $^4He_2$. Therefore, there is still room for a bound state in $^4He^3He_2$ although it lies above the two-body breakup threshold in $^3He^4He_2$.

The $^3He_3$ system is symmetric with two bound states. When one of the ^{3}He atoms is replaced by ^{4}He the two-body threshold decreases. The lowest angular eigenvalue is then much lower, but receives asymptotically only contributions from those two Faddeev components corresponding to the two identical ^{3}He–^{4}He subsystems, see Section 4. In contrast a symmetric system receives contributions from all three components. Therefore the attractive pocket in the corresponding effective radial potential has to be more shallow for asymmetric than for symmetric systems. In the present case this difference is sufficient to remove the three-body excited state.

7. Helium trimers: accurate numerical calculations

The examples in this section are the weakly bound atomic helium trimers in three dimensions [17,29,30,67,131]. Precise calculations of the energies and wave functions should first of all reveal detailed information about the structure of these small molecules and in particular of the suggested Efimov state. Second, such investigations should provide insight into the general structure of weakly bound three-body systems and of the nature of Efimov states. Third, it is a severe test of our method for two reasons, i.e. the very long-range correlations present in Efimov states are naturally described in our method, but very hard to obtain numerically with conventional methods, and also the strong repulsion at short distance in the two-body interactions increases the numerical difficulties.

These computations provide a good starting point for investigations of the possibility of adjusting the two-body interactions by an external field designed to sweep the region close to infinite scattering length. This would allow controlled observation of the Efimov effect. In this report we shall build on [30,105] and restrict the detailed discussions to illustrate the method and to extract the universal properties.

7.1. The two-body phenomenological potentials

The atomic helium–helium interaction is extremely weak and of the van der Waals type. It is therefore at large distance dominated by induced dipole–dipole interactions behaving as r^{-6}, where r is the inter-atomic distance, i.e. the potential is of short range and the maximum short-range angular momentum is $l_{sh} = 1$ according to Eq. (C.5).

The dimer, $^4He_2$, is bound [132,133] and the size measured to be $\langle |\boldsymbol{r}_1 - \boldsymbol{r}_2| \rangle = 120 \pm 20$ a.u. (atomic units of length, 1 a.u. $= 0.524177$ Å), which is consistent with the theoretical predictions for the wave function and the binding energy of around $1\,\mathrm{mK} = 0.0861735\,\mu\mathrm{eV} = 3.16679 \times 10^{-9}$ a.u. Such a small number requires high precision and the interaction is very difficult to calculate with sufficient accuracy from first principles. The atomic interaction models used in this context are therefore often fits to various measured thermal properties of the helium dimer.

We shall use the LM2M2 potential [130], which has an extremely large short-range repulsion, $V(0) = 2.1 \times 10^6\,\mathrm{K} = 6.6$ a.u., compared to the attractive minimum, $V(5.6\,\mathrm{a.u.}) = -10.97\,\mathrm{K} = 3.47 \times 10^{-5}$ a.u. The narrow attractive pocket is followed by a quickly decreasing tail. We shall also

Table 4
The s-wave scattering length $a^{(0)}$ and effective range $r_{\rm eff}$ of the LM2M2 interaction [130] in 3 dimensions for three atomic dimers

^{4}He–^{4}He		^{4}He–^{3}He		^{3}He–^{3}He	
$a^{(0)}$	$r_{\rm eff}$	$a^{(0)}$	$r_{\rm eff}$	$a^{(0)}$	$r_{\rm eff}$
189.054	13.843	− 33.261	18.564	− 13.520	25.717

use simpler model potentials, i.e. Gaussian $V(r) = S_0 \exp(-r^2/b^2)$, exponential $V(r) = S_0 \exp(-r/b)$ and square well $V(r) = S_0 \Theta(r < b)$, to study the model dependence and especially the effect of the repulsive core. These simple potentials have shallow attractions extending all the way to the center in contrast to the repulsive core and the narrow attractive pocket for the LM2M2 potential.

The potential strength and range parameters are adjusted to give the same s-wave scattering length, $a^{(0)}$, and effective range, $r_{\rm eff}$, as for the LM2M2 potential shown in Table 4. These parameters [30] depend on the reduced mass of the two-body system and therefore on the isotope content of the dimer even though the initial two-body interaction remains unchanged. The large positive scattering length for $^4He_2$ reflects the presence of a barely bound state whereas the other two negative scattering lengths show that these two-body systems are unbound. The effective ranges are roughly 3–5 times larger than the diameter of the atoms. How far the simple potentials can be exploited is an interesting question, i.e. which accuracies can be obtained with the corresponding relatively fast estimates.

In dimers and trimers with more than one ^{3}He we should account for the Pauli principle. With only two of these fermions we can treat the systems as consisting of spin zero bosons, since the ignored spin degree of freedom, having exceedingly little influence on the interaction, is taking care of the antisymmetry. For the $^3He_3$ system this is no longer possible, but now the proper symmetry results in a system far from being bound. To learn more about general structures we study instead the artificial system of three identical spin zero bosons with the mass as ^{3}He.

The three-body interaction in Eq. (1) is very small [134,135] and does not contribute at the present level of accuracy. We shall neglect it in the investigations of the atomic helium trimers.

7.2. The adiabatic potentials

We can now solve the angular part of the three-body problem for different isotope combinations and different potentials. For $\rho < 100$ a.u. we solve Eq. (42) whereas for $\rho > 100$ a.u. we solve Eq. (71), where we only include components with $l_x = 0$. For the Gaussian and exponential potentials we switch to Eq. (71) at $\rho = 300$ a.u. The sizes of the bases in the expansion in Eq. (41) give full convergence for the 4 most significant digits of the ground state binding energy. We need to include partial angular momenta up to $l_x = 14$ for LM2M2 and 4 for Gaussians. For $l_x = 0$ we use 150 and 80 basis states for the two interactions. For LM2M2 and $l_x = 14$ we use 20 polynomials and 30 for the Gaussian for $l_x = 4$. For $L = 0$ the total number of basis states is 840 and 1500 for $^4He_3$ and $^3He^4He_2$ with LM2M2 and 405 and 590 with Gaussians.

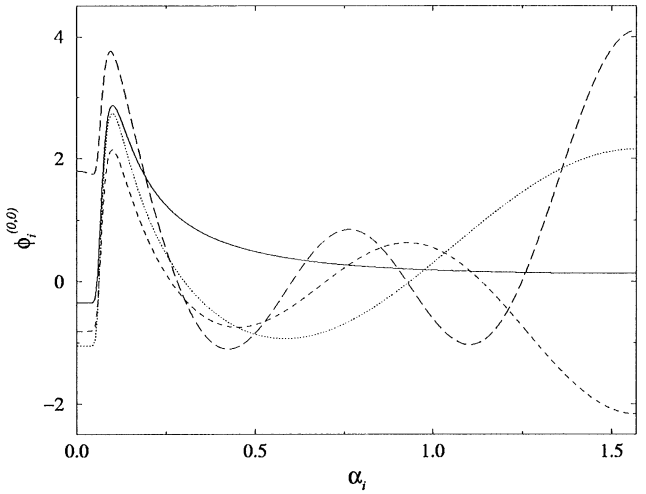

Fig. 9. The four lowest normalized s-wave angular Faddeev components as functions of α_i for $^4He_3$ in three dimensions at $\rho = 100$ a.u. for the LM2M2 potential and the total angular momentum $L = 0$. All three Faddeev components are identical.

For illustration $\phi_{i,n}^{(0,0)}$ corresponding to the four lowest angular eigenvalues is plotted in Fig. 9. The wave function for the lowest of these λ-values has a peak at small α and falls rapidly off reflecting the bound two-body state. The higher lying eigenfunctions exhibit an increasing number of oscillations in α.

The angular eigenvalues are all extremely large for small hyperradii reflecting the strongly repulsive core, see the examples in Figs. 10 and 11. One eigenvalue diverges parabolically for $^4He_3$ and $^3He^4He_2$ when $\rho \to \infty$ due to the two-body bound state, see Eq. (91). The downwards divergence begins shortly before $\rho = 1000$ a.u. in agreement with the value of $a_0 = 12/\pi a^{(0)} \approx 760$ a.u in Eq. (78). The remaining eigenvalues approach $K(K+4)$ in agreement with Eq. (79). Only odd (even) values of K appear as the free spectrum at large distance due to the odd (even) parity. Furthermore, there is no totally symmetric states with $K = 1, 2$ for $^4He_3$.

For $^4He_3$ one eigenvalue corresponding to $l_0 = 0$ approaches each $K(K+4)$ value from above, because all 3 Faddeev components are identical. Thus, only one component couples to itself. For $^3He^4He_2$ we now find a much denser spectrum due to fewer symmetry restrictions. In other words, additional levels are present. These "extra" eigenvalues approach their asymptotic values from below due to the negative scattering length of the ^{3}He–^{4}He subsystem. For $^4He^3He_2$ the features of the previous spectra remain except that now the diverging level has disappeared, since no more bound subsystem is present. All two-body scattering lengths are negative and therefore all the eigenvalues approach their asymptotic values from below, compare with Eq. (76).

The eigenvalues corresponding to the LM2M2 potential have many avoided crossings and increase dramatically for small ρ due to the repulsive core in that potential. The Gaussian potential is finite at the center and the eigenvalues obtain instead their free value according to Eq. (51) for $\rho = 0$. This should in principle also occur for the LM2M2 potential, but the value of this potential at $\rho = 0$ is extremely large and in practise an almost diverging potential appears.

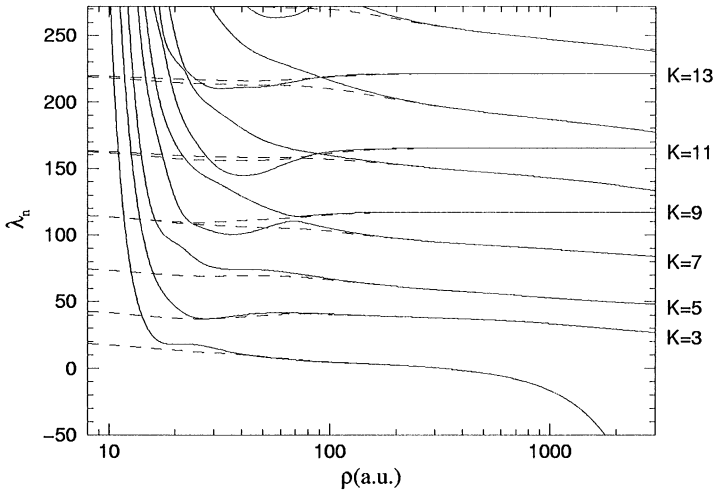

Fig. 10. The angular eigenvalues as function of hyperradius for the $^4He_3$-trimer calculated with the LM2M2 potential (solid curves) and the Gaussian model potentials (dashed curves) for angular momentum and parity $L^\pi = 1^-$.

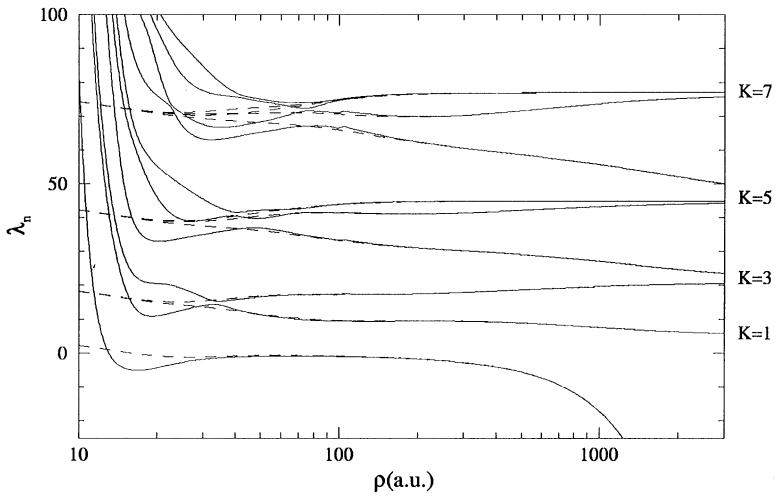

Fig. 11. The angular eigenvalues as function of hyperradius for the $^3He^4He_2$-trimer calculated with the LM2M2 potential (solid curves) and the Gaussian model potentials (dashed curves) for angular momentum and parity $L^\pi = 1^-$.

The angular eigenvalue spectra for the Gaussian potential coincide with those of the LM2M2 potential for approximately $\rho > 100$ a.u. strongly indicating that only the low-energy scattering properties are important when ρ is larger than a few times the range of the potentials. At distances outside the effective range the two spectra of these wildly different potentials are remarkably similar as predicted. On the other hand, for $\rho < 100$ a.u. major differences occur.

Clearly, finite and smooth two-body potentials allow much faster and more accurate numerical computations. Whether this is realistic and sufficient for a given problem has to be evaluated for each case.

We can analyze the degeneracy of $L^\pi = 0^+$ for the asymptotic spectrum for the asymmetric systems, ^{3}He^{4}He$_2$ and ^{4}He^{3}He$_2$, by noting that for each K, which must be even due to parity, we have $K/2+1$ possible values of $l_x = l_y$ varying from 0 to $K/2$, since $0 \le l_x + l_y \le K$. If we now choose Jacobi system i such that particle j and k are identical we can see that l_x has to be even. Therefore the degeneracy is the nearest integer below $K/4+1$. Due to symmetry we have only two *different* s-wave Faddeev components, $\phi_i^{(0,0)}(\alpha_i)$ and $\phi_j^{(0,0)}(\alpha) = \phi_k^{(0,0)}(\alpha)$. Therefore at most two of the $K/4+1$ asymptotic states are of the type $l_0 = 0$. Similarly, we have one Faddeev component with $l_x = l_y = 1$ (one is forbidden due to symmetry), two with $l_x = l_y = 2$ etc. We can therefore fill up each K-level asymptotically: First we have two states of the type $l_0 = 0$, then one of the type $l_0 = 1$, then two with $l_0 = 2$, etc., until the number of possible $K/4+1$ states is reached.

For ^{4}He$_3$ the degeneracy is somewhat more complicated, because of the higher symmetry requirements. Formal group theory must be used to obtain the degeneracy for each K-level. However, the degeneracy for each l_0 within each K-level is simple, because only even values of $l_x = l_y$ are allowed for all the Faddeev components and furthermore all components must be identical. Therefore we have one state with $l_0 = 0$, none with $l_0 = 1$, one with $l_0 = 2$, none with $l_0 = 3$, etc., until the entire K-level is full.

The recipe for finding the degeneracy and l_0-splitting at $\rho = \infty$ for $L^\pi = 1^-$ is the same as for $L = 0$. Let us first study ^{3}He^{4}He$_2$. To write a basis for the wave function it is simplest to choose the Jacobi system with the x-coordinate connecting the two ^{4}He. The allowed components in this system are now $(l_x, l_y) = (0, 1), (2, 1), (2, 3), \ldots$ up to $l_x + l_y = K$ for each value of odd K-values. That is each K-level has $(K+1)/2$ physical solutions. These solutions can be built up of two independent components with $(l_x, l_y) = (0, 1)$, one component with $(l_x, l_y) = (1, 0)$ which asymptotically couples to one with $(l_x, l_y) = (1, 2)$, two with $(l_x, l_y) = (2, 1)$ which couples to the two with $(l_x, l_y) = (2, 3)$, etc. Hence, there will be two states with $l_0 = 0$, two with $l_0 = 1$, four with $l_0 = 2$, two with $l_0 = 3$, etc., until $(K+1)/2$ states are reached. For ^{4}He$_3$ this derivation is again more complicated, but we can conclude that the solutions are a subset of the solutions for ^{3}He^{4}He$_2$, simply due to the increased symmetry requirements. Specifically, we see that components with odd l_x and thus solutions with odd l_0 are forbidden.

7.3. *Bound states*: *energy and structure*

The calculated angular eigenvalues and coupling constants are now used in Eq. (13) to obtain the bound state energies and wave functions. In three dimensions ^{4}He$_3$ has two bound state with angular momentum and parity $L^\pi = 0^+$, ^{3}He^{4}He$_2$ has one bound state with $L^\pi = 0^+$ and ^{4}He^{3}He$_2$ is unbound. If treated with proper account of the Pauli principle also ^{3}He$_3$ is unbound. None of these trimers are bound for $L^\pi = 1^-$ and it is therefore also expected that none are bound for $L^\pi = 1^+$ and for higher total angular momenta. The computed energies of the bound states are given in Table 5.

In the numerical procedure to solve the radial equation we need more adiabatic potentials for ^{3}He^{4}He$_2$ than for ^{4}He$_3$ due to the denser angular spectrum. We also need many more adiabatic potentials to obtain the same precision for the LM2M2 potential than for the Gaussian and the exponential potentials. This is directly related to the repulsive core which introduces extra avoided crossings into the angular eigenvalues. The radial wave function must be very small under the small distance repulsive barrier. Unfortunately, the contribution to the energy is still not negligibly small,

Table 5
Bound state energies in mK for the helium trimers in 3 dimensions using various two-body potentials. The number in the brackets, { }, is the minimum number of adiabatic potentials included in the calculation to obtain this result. The $^4He_3$ has two bound states whereas $^3He^4He_2$ has only one. No other trimer with stable isotopes has bound states in 3 dimensions. For the LM2M2 potential we give the results for only one adiabatic potential to compare with the result in [17]

Potential	$^4He_3$				$^3He^4He_2$	
LM2M2	− 105.9	{1}	− 2.121	{1}	− 9.682	{1}
	− 125.2	{8}	− 2.269	{8}	− 13.66	{10}
Ref. [17]	− 106.1	{1}	− 2.118	{1}	− 10.22	{1}
Gaussian	− 150.7	{3}	− 2.485	{3}	− 18.82	{5}
Exponential	− 174.2	{3}	− 2.731	{3}	− 24.61	{5}

since the small probability has to be multiplied by the large values of the adiabatic potentials. High-accuracy therefore requires careful treatment also of this region. To improve the accuracy we have here exploited the arbitrary ρ-dependent constant $\lambda_0(\rho)$ appearing in Eq. (13) and discussed in Section 3.2.4.

In Table 5 we compare our results, where only the lowest adiabatic potential is included, with those of [17] obtained with the same approximations. For $^4He_3$ we find very good agreement for both ground a excited state, while the result for $^3He^4He_2$ deviates by 6% of the three-body energy of about − 10 mK. A much bigger basis for the asymmetric systems confirmed that our results are converged and our computations are more accurate than this discrepancy.

In [17,29] it was concluded that the excited state of $^4He_3$ behaves as an Efimov state. If the strength of the LM2M2 potential is decreased by 3%, i.e. multiplied by 0.97, the potential is no longer strong enough to bind this state. On the other hand, if the potential is increased by 20% stronger, i.e. multiplied by 1.2, the state moves into the continuum. Of course, this state becomes more bound as the potential is strengthened, but the binding energy of the two-body bound state increases even faster. Consequently, the continuum threshold catches up with the energy of the excited state, which then becomes unbound with respect to disintegration into a dimer and a free helium atom. Therefore, by studying this excited state, the ground state and the bound state of $^3He^4He_2$ we expect to obtain valuable information about Efimov states.

The geometric structure of the ground states of $^4He_3$ and $^3He^4He_2$ both resemble equilateral triangles where $^3He^4He_2$ is slightly prolonged in one direction. The distribution of the ^3He atom in $^3He^4He_2$ is qualitatively similar to that of one of the ^4He atoms in $^4He_3$. The lighter mass of ^3He, the resulting larger reduced masses or the larger kinetic energies, explains why $^3He^4He_2$ is less bound than $^4He_3$ and simultaneously twice as big. The ^3He atom has a tendency to be further away than ^4He causing an extra asymmetry and an additional prolongation of $^3He^4He_2$.

The excited state of $^4He_3$, the Efimov state, is about 10 times as spatially extended as the ground state and the size is of the same order as the two-body scattering length of 189 a.u. This is in agreement with the interpretation of the state as the least bound Efimov state in a potential similar

to that of Fig. 5. According to Eq. (108) this size should approximately be 23 times the size of the ground state. Similarly from Eq. (107) we conclude that the binding energy should be $23^2 = 520$ times less than that of the ground state. In fact, by replacing 23 by 10 we obtain very comparable numbers for both size and energy. This is a rather good agreement, since the approximations used in deriving Eqs. (107) and (108) are not really valid in the present case, where the state both is the first and the last of the Efimov series.

7.4. Helium trimers in external fields

We have seen in the previous subsection that even in the ^{4}He trimer, where the two-body scattering length is 10 times the effective range, there is only room for one Efimov state. It is therefore very unlikely that nature should provide systems with more than a few Efimov states. External fields may provide manipulation possibilities as for Bose–Einstein condensates [84,136] of ^{85,87}Rb and Na, where an external magnetic field via the hyperfine structure of the atoms moves down a resonant state in one of the higher lying two-body channels thereby producing a Feshbach resonance at zero energy in the two-body system [137,138]. For Efimov states one major problem is that these two-body subsystems have a lot of bound states below the resonance at zero energy. Then the Efimov states are must appear as resonances above these two-body thresholds and slightly below the three-body threshold.

7.4.1. Sweeping the threshold region with a perturbing potential

A static external electric field $\mathscr{E}$ polarizes an atom and induces a dipole $\beta\mathscr{E}$, where β is the polarizability of the atom. To lowest order the two-body potential then receives an additional contribution [105]

$$\Delta V^{(1)}(\boldsymbol{r}) = -\beta_1\beta_2|\mathscr{E}|^2\sqrt{\frac{16\pi}{5}}\frac{Y_{20}(\theta)}{r^3}\,, \tag{119}$$

where $\boldsymbol{r}$ is the vector separating the two atoms, θ is the angle between $\mathscr{E}$ and $\boldsymbol{r}$, and β_1 and β_2 are the polarizabilities of the two atoms.

The two atoms within our three-body system are in a relative s-state. Therefore the first-order contribution from the potential $\Delta V^{(1)}$ vanishes, since it is proportional to $\langle Y_{00}|Y_{20}|Y_{00}\rangle = 0$. The contribution in second-order perturbation arising from $\Delta V^{(1)}$, which then is fourth order in both $\mathscr{E}$ and polarizability, always lower the ground-state energy. Therefore, the potential in Eq. (119) only contributes to second order and decreases always the ground-state energy.

This means that higher order correction terms to the potential itself might produce lower order changes (in polarizability and field strength) to the ground-state energy. The terms arise as the field induces a dipole in one atom, which in turn induces a dipole in the other atom and these two dipoles interact [105]:

$$\Delta V^{(2)}(\boldsymbol{r}) = -\beta_1\beta_2(\beta_1+\beta_2)\sqrt{4\pi}\frac{Y_{00}(\theta)+(1/\sqrt{5})Y_{20}(\theta)}{r^6}|\mathscr{E}|^2\,, \tag{120}$$

which is second order in $\mathscr{E}$, but third order in the polarizabilities. The contribution, proportional to the matrix element $\langle Y_{00}|\Delta V^{(2)}|Y_{00}\rangle$, is now negative. Thus, to move a resonance of two helium

atoms towards the threshold of zero energy, we must use the unbound systems $^3He_2$ or $^3He^4He$. Here $^3He^4He$ is closer to the threshold and the most promising combination of helium trimers is therefore $^4He^3He_2$, where a resonance at zero energy in the two identical ^4He–^3He subsystems would produce an infinite Efimov series of bound states.

The unperturbed LM2M2 potential is now modified by adding $\Delta V^{(1)}$ and $\Delta V^{(2)}$ with a cutoff at distances smaller than about 1 a.u. The s-wave scattering length $a^{(0)}$ of ^4He–^3He is first calculated as a function of the field strength. We integrate the coupled two-body equations of the different angular momentum channels from a small distance $r_0 \approx 1$ a.u. to a large distance r_1 outside the effective range. Then we match the s-wave function to the form $\psi_0(r) \propto 1 - a^{(0)}/r$ and the higher angular momentum wave functions to $\psi_l(r) \propto r^{-l-1}$. The value of r_1 as well as the number of angular momenta included is varied in the computation to reach stability for $a^{(0)}$.

For $^3He^4He$ the scattering length decreases from $a^{(0)} = -33.261$ a.u., the value without field, to $-\infty$ as the field strength increases to $|\mathscr{E}| = 0.053$ a.u., where the system becomes bound. Increasing $|\mathscr{E}|$ above 0.053 a.u. the scattering length decreases from $+\infty$ towards zero. For $^3He_2$ the divergence is at $|\mathscr{E}| = 0.067$ a.u.

The three-body binding energies are remarkably similar for the LM2M2 and Gaussian potentials, see Table 5. We shall therefore use the Gaussian potential in the calculations of the $^4He^3He_2$ trimer in the external electric field, i.e. $V(r) = S_0(|\mathscr{E}|)\exp(-r^2/b^2)$ with constant range and the depth as function of the strength of the field adjusted to reproduce the computed scattering length.

The three-body system becomes bound at $|\mathscr{E}| = 0.045$ a.u. while the two-body subsystems still remain unbound below $|\mathscr{E}| = 0.05319$ a.u. For this strength interval we then have a Borromean system. Increasing the field strength above 0.045 a.u. we obtain an excited state in the three-body spectrum at $|\mathscr{E}| = 0.053$ a.u. This strength is very close to the two-body threshold of $|\mathscr{E}| = 0.05319$ and it is rather difficult to determine accurately the energies of the infinitely many excited states, which successively must appear below this threshold.

We find the first excited three-body state at $|\mathscr{E}| = 0.05315$ a.u., at $|\mathscr{E}| = 0.05316$ a.u. there are both a two-body bound state and two excited states of the trimer. At $|\mathscr{E}| = 0.05319$ a.u. the second excited three-body state is no longer found in the computations. Its binding energy is less than -3×10^{-9} mK, beyond which our calculations are unreliable.

7.4.2. Appearance of Efimov states in external electric fields

The characteristic features of Efimov states around the two-body threshold are obtained numerically, but disappointingly only a few of these states are found. The reason is that only two of the subsystems are close to having a resonance at zero energy and furthermore these identical subsystems correspond to two light and one heavy particle. Let us in the following label the ^4He atom by 1. The decisive parameter is in Section 5.2.3 found to be $\gamma_{23} = \arctan\sqrt{4.003(4.003 + 2\cdot 3.016)/3.016^2} = 1.127$.

According to Eq. (116) the lowest angular eigenvalue is $\lambda_1 = -4.118$ when $r_{0i} \ll \rho \ll |a_i^{(0)}|$ and therefore the critical parameter determining the distance between the Efimov states is $\xi = 0.343$ as discussed in Section 5. Hence, a new Efimov state would occur when the scattering length is increased by a factor $\exp(\pi/\xi) = 9442$. This clearly demonstrates that an extreme fine tuning is required to allow a larger number of Efimov states. Since a field strength of 0.053 a.u. corresponds to the very high value of 2.7 V/Å, we conclude that it is rather unrealistic to hope for more than one Efimov state in this system.

The knowledge and experience collected so far may, however, be used to determine the optimum requirements for observing Efimov states by fine tuning with an external electric field. First, the atoms or molecules should interact via short-range interactions, which undisturbed almost are able to bind the dimers. Second, the atoms should have a large polarizability, but not so large that the dimers become bound via the generated attractive van der Waals forces. Third, according to Fig. 8 it would be an advantage, if one of the atoms is light compared to the other two, while these two heavier atoms should be unable to form a two-body bound state. Under these special circumstances the trimer of one light particle and two heavy particles would be a good candidate for observing the Efimov states.

An alternative is to relax the restrictions and search for Efimov states as resonances instead of bound states [139]. Then there are many more possibilities to find tunable systems both with a static electric field through the polarization of the atoms and with magnetic fields through a Feshbach resonance.

8. Nuclear three-body halos

The examples in this section are nuclear halos in three dimensions, i.e. the hypertriton ${}^{3}_{\Lambda}\mathrm{H}$ (n + p + Λ), a three-body system weakly bound below the n + p bound subsystem [91], and the Borromean halos ${}^{6}\mathrm{He}$ (n + n + ${}^{6}\mathrm{He}$) and ${}^{11}\mathrm{Li}$ (n + n + ${}^{9}\mathrm{Li}$) without bound subsystems [5,40,54,123]. The hypertriton provides information about the strange sector of the strong interaction. Neutron halos are found at the neutron dripline [13–15,43,45,87]. They have been rather successfully described in terms of few-body models [5,33–36]. Antisymmetrization between core (${}^{6}\mathrm{He}, {}^{9}\mathrm{Li}$) particles and the neutrons is treated by adding a short-range two-body potential behaving as r^{-2} at short distances [42]. This strictly diverging repulsion, the small binding and the large spatial extension all require careful treatment and our method is designed for that.

8.1. *Hypertriton*: *the simplest strange halo*

The hypertriton (${}^{3}_{\Lambda}\mathrm{H}$) is the lightest nucleus with finite strangeness [91]. This three-body system may roughly be described as a Λ-particle bound to a deuteron, where the binding energy is $B_{\Lambda} = 0.13 \pm 0.05\,\mathrm{MeV}$ and the total angular momentum and parity are $J^{\pi} = \frac{1}{2}^{+}$. If the spatial extension of a two-body system is large compared to the range of the interaction the root mean square radius is given by $\langle r^2 \rangle^{1/2} \approx \hbar/\sqrt{4\mu B_{\Lambda}} = 10.2$ fm, where μ is the reduced mass and the parameters are for the Λ-deuteron system. Thus, $\langle r^2 \rangle^{1/2}$ is roughly 5 times larger than the deuteron root mean square radius of about 2 fm. The hypertriton is the most pronounced nuclear halo found so far.

8.1.1. *Two-body potentials*

We need two-body interactions reproducing the low-energy properties of the potentials, i.e. basically scattering length and effective range. For the nucleon–nucleon interaction the main component corresponds to the quantum numbers of the deuteron, i.e. the triplet *s*- and *d*-states

with the total angular momentum and parity $J^\pi = 1^+$, but also nucleon–nucleon relative p-states are possible in ${}^3_\Lambda$H. For the Λ-nucleon interaction we also include s, p and d-states. For each isospin we parametrize the spin dependence of the interactions with central, spin–spin, tensor and spin–orbit terms each with Gaussians as the radial shapes. We use GC1 for $T = 0$ (N–N) and G5r for $T = \frac{1}{2}$(N–Λ) both from [91] and $T = 1$ (N–N) from [90].

This set of parameters reproduce the nucleon–nucleon scattering lengths and effective ranges for the singlet and triplet s-states. In addition, the computed deuteron properties, binding energy $B_d = 2.224575\,\mathrm{MeV}$, root mean square radius $R_d = 1.967\,\mathrm{fm}$, d-state admixture $P_d \sim 5.66\%$, asymptotic ratio of the d to s-wave component $\eta_d = 0.0233$, and the electric quadrupole moment $Q_d = 0.273\,\mathrm{fm}^2$, are all in agreement with the experimental data. The Λ-nucleon potential is adjusted to the *Nijmegen SC* interaction [140], but with the strength of the central potential reduced by 10% to reproduce the all important ${}^3_\Lambda$H binding energy [91].

8.1.2. The hypertriton structure

Only s, p and d-waves contribute. The partial wave Faddeev components are first chosen consistent with parity, angular momentum coupling and isospin conservation or symmetries of the system. We include up to 100 basis states for each component. The angular eigenvalues are then for small hyperradii computed by solving Eq. (42) with the basis modified to include spins as indicated in Section 3.4. For large hyperradii we use the diagonal part of the large-distance asymptotic expansion [23,91].

The angular spectrum equals the free spectrum $K(K+4)$ at both $\rho = 0$ and $\rho = \infty$, since the potentials are finite and of short range. In the Jacobi system, where the x-coordinate connects the nucleons, we find one level for $K = 0$ corresponding to $(l_x, l_y, L, s_x, S) = (0, 0, 0, 1, 1/2)$. For $K = 2$ we get five levels related to $(l_x, l_y, L, s_x, S) = (0, 0, 0, 1, 1/2)$, $(1, 1, 0, 0, 1/2)$, $(1, 1, 1, 0, 1/2)$, $(2, 0, 2, 1, 3/2)$, $(0, 2, 2, 1, 3/2)$. All eigenvalues decrease for small ρ consistent with Eq. (51) reflecting the overall attraction. The lowest eigenvalue diverges parabolically for $\rho \to \infty$ as $\lambda = -2B_d m_N \rho^2/\hbar^2$, due to the bound state in the neutron–proton two-body subsystem. The free spectrum is recovered for $\rho \to \infty$, since one eigenvalue originating from each of the higher values at $\rho = 0$ decreases and replaces the missing level at infinity.

The calculated angular eigenvalues and the related coupling constants are now used in Eq. (31) to obtain the bound state energies and radial wave functions. The hypertriton binding energy is determined with a relative accuracy of about 10^{-3} already by including the lowest three adiabatic potentials. We obtain then $B_\Lambda = 0.108\,\mathrm{MeV}$, root mean square radii $\langle r^2 \rangle^{1/2} = 5.88\,\mathrm{fm}$ for the three-body system and $\langle r^2_{\Lambda d} \rangle^{1/2} = 11.73\,\mathrm{fm}$ for the Λ–deuteron two-body system. The main contribution to the wave function is by far given by the lowest component, which is peaked at around 3 fm with a rather slow exponential decay at larger distances. Significant probability is still found at 30 fm strongly indicating the need for an accurate treatment at these relatively large distances.

The total wave function is a sum of the three Faddeev components, where each is expressed in its Jacobi coordinates. Transforming all components into the Jacobi coordinates of the set, where the Λ-particle is a spectator (x-coordinate between the two nucleons), we find that 95% of the probability is from the component with $l_x = 0$. The remaining 5% almost completely arises from the component with $l_x = 2$ representing the d-wave contribution to the deuteron. The deuteron structure is almost maintained in the presence of the Λ-particle.

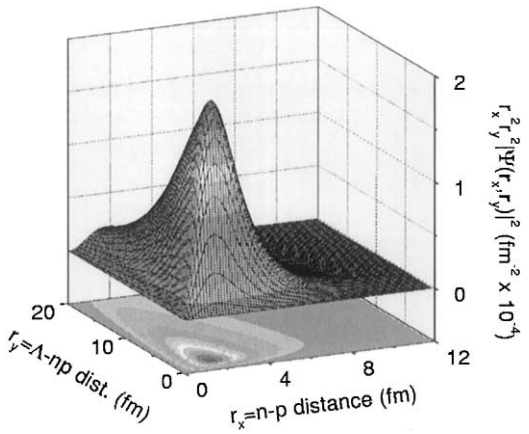

Fig. 12. The hypertriton probability arising from the dominating component. The coordinates are the nucleon–nucleon distance r_x and the Λ–deuteron distance r_y. The volume element is included in the probability.

Transforming the total wave function into one of the other sets of Jacobi coordinates, where one of the nucleons is the spectator, we find that components $(l_x, l_y, L, s_x, S) = (0,0,0,0,1/2)$, $(0,0,0,1,1/2), (1,1,0,0,1/2), (1,1,0,1,1/2)$ contribute by 55.0%, 18.5%, 18.7% and 6.0% of the probability in the wave function, respectively. All of these correspond to s or p-waves, and the Λ-nucleon relative angular momentum 2 therefore gives negligible contributions.

The dominating component (95%) in the hypertriton wave function corresponds to a relative neutron–proton s-state, and a relative Λ–deuteron s-state. The contribution of this component to the hypertriton probability distribution is shown in Fig. 12 as a function of the neutron–proton distance r_x, and the Λ–deuteron distance r_y. This distribution is elongated along the r_y-direction, reflecting the large value of the Λ-deuteron root mean square radius compared to the deuteron root mean square radius. In other words, the Λ-particle is essentially always found far outside the deuteron.

8.1.3. Information about the strange strong interaction

The previous conclusions all arise from the chosen set of two-body interactions. However, they are not completely determined by the imposed constraints and small uncertainties are present especially in the theoretical Λ–nucleon interaction. We have therefore varied the shapes of the radial formfactors still maintaining the same scattering lengths and effective ranges. The hypertriton properties are only marginally affected. The binding energy at most changes by 50 keV and usually much less. This is a substantial fraction of the hypertriton binding energy of 130 keV, but very insignificant in comparison with the strengths of the two-body interactions typically 10–100 MeV.

The singlet s-wave in the Λ-nucleon potential is the dominating component. Thus, the corresponding scattering length $a_{\Lambda N}^{(1)}$ is the most significant individual parameter. To maintain the measured binding energy within an acceptable uncertainty interval we can at most vary $a_{\Lambda N}^{(1)}$ by about 10% around the value -1.85 fm. It is then tempting to conclude that the hypertriton binding energy, via these accurate calculations, determines this parameter with this precision.

This is also a rather safe conclusion, but we want here to emphasize that an additional uncertainty should be included from a possibly more realistic weaker attraction producing the usual small underbinding, which subsequently is compensated by the three-body attractive potential. In any case precise experimental values and accurate computations of the hypertriton give access to information about the strong interaction, both the off-shell behaviour and the strange sector. Again it is worth emphasizing that the precision must be very high, because otherwise only the simplest low-energy properties like scattering lengths can be extracted.

8.2. *Borromean two-neutron halo nuclei*: ^{6}He *and* ^{11}Li

Large interaction cross-sections of some light nuclei close to the neutron dripline [141] are indications of a spatially extended neutron halo around an ordinary nuclear core [142]. Large Coulomb and nuclear two-neutron dissociation cross-sections [142–145] and narrow momentum distributions of the fragments after breakup [54,146] are other signs of this peculiar structure. The neutrons are mainly in classically forbidden regions at distances much larger than the range of the neutron-core interaction. Examples of Borromean two-neutron halo nuclei are ^{6}He ($\alpha + n + n$) and ^{11}Li (^{9}Li + n + n) [5]. Their three-body binding energies or equivalently their two-neutron separation energies, 973.4 ± 1.0 keV [147] and 295 ± 35 keV [148], are much larger than for beta-stable nuclei. Unlike the hypertriton, these systems have no two-body bound subsystems. On the other hand, the presence of neutrons within the core forbids some of the additional three-body neutron states due to the Pauli principle. This has to be carefully considered.

8.2.1. *Two- and three-body potentials*

The neutron–neutron potential is the isospin 1 part of the nucleon–nucleon interaction given in [90]. The neutron–^{4}He interaction reproduces the *s*, *p* and *d* phase shifts from zero and up to 20 MeV [42,98]. The experimental data on neutron–^{9}Li is much more limited and uncertain than that of neutron–^{4}He. There is strong evidence for a low-lying *p*-resonance at 500 ± 60 keV with a width of 400 ± 60 keV [149–151]. There is also accumulating evidence for an even lower lying somewhat uncertain virtual *s*-state approximately at 0.15 ± 0.15 MeV [150,151]. Both these states are necessary to explain some of the fragmentation data [40,54,144,145,152,153].

The ^{9}Li-core has a spin of $\frac{3}{2}$, which inevitably produces two levels for each orbital angular momentum arising from the neutron spin of $\frac{1}{2}$. The measurements refer to these actual (spin-split) levels. We then choose a realistic model with spin splitting reproducing the available data [102,123]. To benefit from the fairly accurate approximation assuming zero core spin we then simply reduced the spin splitting parameter to zero [42,98]. This implies a *p*-resonance at 0.75 MeV and an *s*-state energy of 0.58 MeV, which then necessarily must be above the measured values.

Accurate computions with these sets of two-particle interactions lead to three-body binding energies of ^{6}He and ^{11}Li too small by 0.5 MeV and 150 keV compared to the experimental values [7]. Unfortunately, the correct three-body binding energy is crucial, since essentially all other properties are strongly correlated with this energy. Adjusting the two-body interactions simultaneously alter the two-body continuum properties like resonances. Three-body continuum properties therefore cannot be expected to be described correctly [101].

To fine tuning the energy we use a three-body interaction as in Eqs. (1) and (13). This is not a genuine three-body force, but a phenomenological way of accounting for those polarizations of

the particles, which are beyond that described by the two-body interactions. Thus, this interaction must be of short range, since it only contributes when all three particles interact simultaneously.

So far our model assumed complete decoupling of relative and intrinsic particle degrees of freedom. This assumption is inconsistent with the full antisymmetrization required when the different particles contain identical fermions. Using the same deep neutron-core s-wave potential as appropriate for the neutrons in the core, the halo neutrons would naturally occupy these s-states, which already are occupied by the neutrons within the core.

To overcome this problem one should project out the undesired overlap of the three-body wave function with the Pauli-forbidden two-body neutron-core state [42,90]. To achieve this we investigated three methods, which only differ insignificantly for weakly bound systems. The first consists of excluding the lowest adiabatic potential, which essentially entirely otherwise would support the forbidden state. The second consists of modifying the two-body interaction to exclude the lowest bound forbidden two-body states, while still maintaining the scattering length and effective range of the potential. The third consists of adding a short-range two-body potential with a specific r^{-2} divergence at small distance still maintaining the same phase shifts for all energies, but without the undesired Pauli-forbidden two-body bound states in the resulting "phase-equivalent" two-body potential [42]. The third method basically removes the lowest adiabatic potential both at large and at small distances.

In the numerical computations we shall use the third method for s-waves while the $p_{3/2}$-states for the ^{9}Li-core are removed from the active space by a strong repulsion incorporated as an unphysically large spin–orbit interaction. The different methods produce almost indistinguishable results, but the computing time could differ substantially. The interaction parameters are from [42,98] resulting in binding energy and root mean square radius of 1.0 MeV and 2.50 fm for ^{6}He, and 0.30 MeV and 3.35 fm for ^{11}Li. The energies agree clearly with the measured values and the radii are consistent with 2.57 ± 0.10 fm [154] and 3.1 ± 0.3 fm [155] obtained from the data for ^{6}He and ^{11}Li, respectively.

8.2.2. The two-neutron halo structure

We include s, p and d-waves for ^{6}He and only s and p-waves for ^{11}Li, where we furthermore assume zero spin for the ^{9}Li-core. The basis size of up to 50 states in the expansion in Eq. (41) is substantially smaller than for the hypertriton, since the spatial extension is much smaller and no Pauli allowed two-body bound states are present. The angular eigenvalues are first computed by solving Eq. (42) with the basis modified to include spins as in [23,98].

The five lowest eigenvalues of the calculated spectrum are shown in Fig. 13 for the three-body halo nuclei ^{6}He and ^{11}Li. The use of the phase equivalent potential for the s-wave neutron-core interaction automatically excludes the λ-function originating from $\rho = 0$ and diverging towards $-\infty$ for large ρ. This excluded level corresponds to the Pauli forbidden bound states occupied by core neutrons. Therefore, the lowest λ originates instead from 12. This λ-function is mainly of p-wave character in the neutron-core relative wave function. The eigenvalues approach the values of the free spectrum for large distances. The lowest of these converges towards zero at $-\infty$.

The lowest decisive eigenvalue for ^{6}He is around the minimum dominated by the $K = 2$ contribution. For ^{11}Li one of the levels originating from 32 at $\rho = 0$ decreases very fast, passes through one sharp and one smooth avoided crossing, and becomes the lowest level at values of ρ larger than 2 fm [42]. This eigenvalue is of s-wave character in the neutron-core relative wave

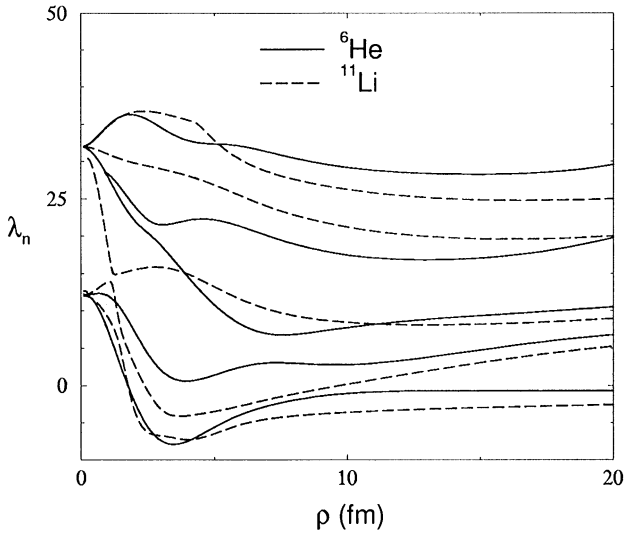

Fig. 13. The angular eigenvalues as function of hyperradius for ^{6}He (solid lines) and ^{11}Li (dashed lines) calculated from the interactions specified in [42,98,90].

function. Therefore, the ^{11}Li wave function is dominated by contributions originating from the $K = 4$ level with one node, i.e. mainly of s-wave character. The variation in the small distance behaviour is consistent with Eq. (51) when we consider the moderate p-wave attraction and the strong s-wave attraction overcompensated at short distances by the r^{-2} repulsion. The degeneracy 2 for the bunch originating from 12 arises from s or p-waves coupled to 0 or 1.

The calculated angular eigenvalues and the related coupling constants are now used in Eq. (13) to obtain the bound state energies and radial wave functions of these two Borromean systems. The binding energies are obtained with a relative accuracy of about 10^{-3} by including only the lowest two adiabatic potentials in Fig. 13. We find the energies and root mean square radii given above in agreement with the measured values. The radial wave functions for the lowest two adiabatic potentials are shown in Fig. 14. These radial wave functions related to the lowest adiabatic potential give for both nuclei more than 90% of the total probability. The wave function is spatially more extended for ^{11}Li than for ^{6}He, reflecting the smaller binding energy and the s-wave versus the more confined p-wave character.

To investigate the spatial distribution we again transform two of the Faddeev components into the Jacobi coordinates of the third. Using the Jacobi coordinates, where the core is the spectator, the main contributions for both ^{6}He and ^{11}Li correspond to relative s-states both between the two neutrons and the core and the dineutron centre of mass. This component contributes 90% and 83% of the ^{6}He and ^{11}Li total probability, respectively. In the other Jacobi coordinate, where one of the neutrons is the spectator, ^{6}He receives 90% of the total probability from components with relative p-waves in the α-neutron motion. For ^{11}Li the ^{9}Li-neutron relative s-state gives 60% of the probability and the relative p-state provides the remaining 40%.

The probability distribution of the dominating component in the total three-body wave function for ^{6}He is shown in Fig. 15 as a function of the neutron–neutron distance r_x and the core-nn

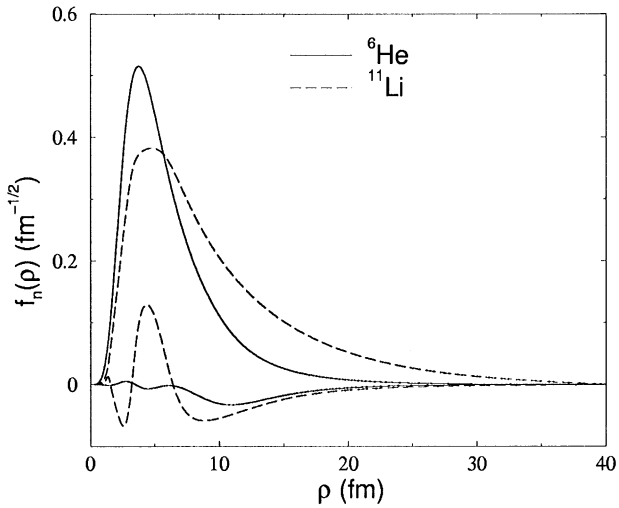

Fig. 14. The radial wave functions as functions of hyperradius for ^{6}He (solid lines) and ^{11}Li (dashed lines) corresponding to the lowest two adiabatic potentials in Fig. 13. The relative normalization is correct.

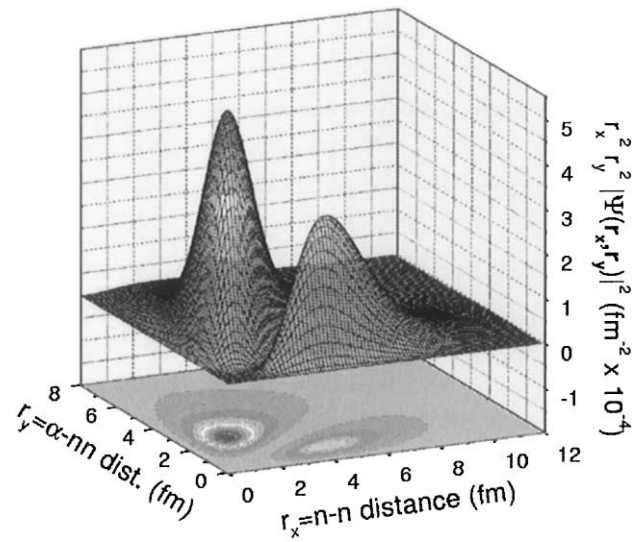

Fig. 15. The ^{6}He probability distribution arising from the dominating component of s-waves in the Jacobi coordinate system where the neutron–neutron distance is r_x and the α–nn distance r_y. The volume element is included in the probability.

distance r_y. We observe two maxima, where the position of the highest corresponds to a triangular three-body geometry with the two neutrons separated by about 2 fm and the α-particle slightly more than 2 fm away from the two-neutron centre of mass. The second maximum is close to an aligned geometry with the two neutrons around 4 fm apart and the α-particle at the centre of mass of the two neutrons.

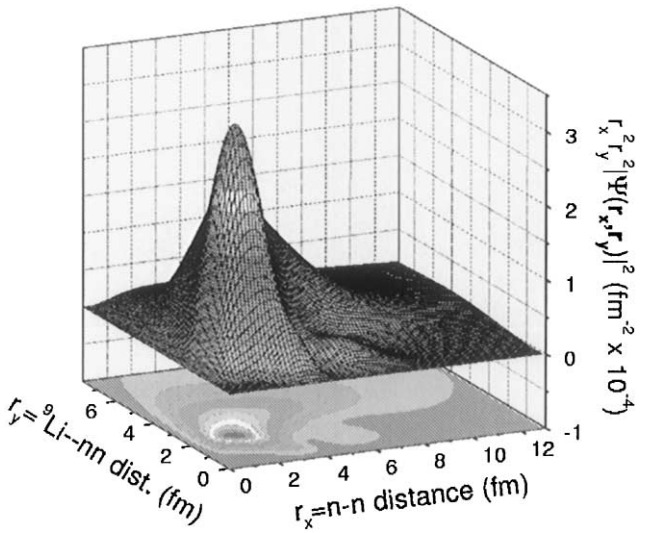

Fig. 16. The ^{11}Li probability distribution arising from the dominating component of s-waves in the Jacobi coordinate system where the neutron–neutron distance is r_x and the α–nn distance r_y. The volume element is included in the probability.

In Fig. 16 we show the completely analogous probability distribution for ^{11}Li. Only one dominating maximum appears, but the distribution is in general more irregular. The position of this maximum again corresponds to a triangular three-body geometry with a separation between the neutrons of around 2 fm and the same distance between the ^{9}Li-core and the centre of mass of the neutrons. The maximum is clearly wider for ^{11}Li than for ^{6}He and consequently the three particles in ^{11}Li have a larger probability of being far apart than in the ^{6}He case. This reflects again, as in Fig. 14, the different binding energies and the difference in partial wave character for these systems.

9. Continuum structure and scattering

The hyperspherical adiabatic expansion is in the previous sections applied in investigations of bound state properties. The method is also well suited for studies of low-energy continuum spectra and scattering processes. When at most one particle is charged the method is directly applicable and in particular exploited for Borromean systems [98–100] and Λ-scattering on a deuteron [91]. When more than one particle is positively charged the Coulomb interaction is inevitable and the detailed picture of Section 4.2 is not applicable. Still the general numerical method can be used as seen in a three-alpha model calculation of wave function and resonance position and width of the astrophysically interesting second 0^+ state of ^{12}C [22].

Other processes like neutral atom *three-body recombination*, $B + B_2 \leftrightarrow 3B$, influences the stability of Bose–Einstein condensates. A full three-body calculation must include all bound two-body subsystems, e.g. 1464 bound states in $^{87}Rb_2$ when each atom is in a triplet state [156]. To gain physical insight we shall use the method to investigate the recombination rate for the reactions

$^4\mathrm{He} + {}^4\mathrm{He}_2 \leftrightarrow 3{}^4\mathrm{He}$ in three dimensions. Other applications are tempting both in molecular, atomic and nuclear physics. However, before specific applications we must formulate the general procedure.

9.1. Scattering in the hyperspherical adiabatic approach

The radial wave functions must be labeled by two channel indices n, the usual index on the components, and n_i, an additional index labeling different total wave functions in Eq. (12). We have to solve the hyperradial equation (13) with the boundary conditions at large distance given by [99,158], i.e.

$$f_{n,n_i}(\rho) = \begin{cases} \sqrt{\dfrac{m\rho}{4\hbar^2}}\left(\delta_{n,n_i} H^{(-)}_{\mu_n}(\kappa_n\rho) - S_{n,n_i} H^{(+)}_{\mu_n}(\kappa_n\rho)\right) & \text{for } E \geq E_n\ , \\ \sqrt{\dfrac{m\rho}{4\hbar^2}} K_{\mu_n}(|\kappa_n|\rho) & \text{for } E < E_n\ , \end{cases} \tag{121}$$

where E is the energy of the three-body system, $E_n \equiv \lim_{\rho\to\infty}(\hbar^2/2m)\lambda_n\rho^{-2}$ is the asymptotic energy of channel n, $\kappa_n^2 \equiv (E - E_n)2m/\hbar^2$, $H^{(\pm)}_\mu(x)$ is the Hankel function, $K_\mu(x)$ the modified Bessel function of the second kind and S_{n,n_i} are the elements of the S-matrix. The order μ_n of the Bessel and Hankel functions is $\mu_n = K + 2$ if channel n is a continuum channel with the angular eigenvalue asymptotically approaching $\lambda_n = K(K + 4)$ and $\mu_n = \frac{1}{2} + l_y$ if channel n is a two-cluster channel where the third particle has orbital angular momentum l_y relative to the remaining two-body system. The energy E is always larger than E_n when the two-body system is unable to form bound states. The coupling constants $P_{nn'}$ between two-cluster states in Eq. (13) only fall off as ρ^{-1}, see Table 2. Therefore numerical integration is necessary up to a very large hyperradius before reaching the asymptotic form in Eq. (121).

Scattering experiments involving only the three particles in a Borromean system are not possible. However, positions and widths of resonances in the continuum spectrum often carry information about physical reaction processes. The importance is amplified for Borromean systems, where only one or perhaps a few bound states are present. Resonances can be computed from the energy dependence of the phase shifts of the radial wave functions. The S-matrix is first calculated and diagonalized for each energy resulting in eigenfunctions and eigenvalues. The eigenvalues are then converted into eigenphases δ_n by assigning the form $\exp(2\mathrm{i}\delta_n)$. The identifying feature of a resonance is a rapid variation of the eigenphase shifts with energy while passing the value of $\pi/2$ [157]. This procedure is rather difficult and not very accurate due to the inherent ambiguities of such phase analyses in multichannel systems.

A more precise and robust method is to solve the radial equations in Eq. (13) directly by using a complex energy $E = E_0 - \mathrm{i}\Gamma/2$ with the boundary conditions in Eq. (121). These solutions correspond to poles of the S-matrix at these complex energies [158]. For Borromean systems no two-cluster channels are present, i.e. we have always $E \geq E_n$. The resonances are then those solutions, where only the $H^{(+)}$ function of Eq. (121) is present in the asymptotic region, where $H^{(+)}$ turns into an outgoing (hyper)spherical wave, i.e.

$$\sqrt{\rho}H^{(+)}_{K+2}(\kappa\rho) \to \sqrt{\frac{2}{\pi\kappa}}\exp\left(+ \mathrm{i}\kappa\rho + \mathrm{i}\frac{\pi}{2}\left(K + \frac{3}{2}\right)\right). \tag{122}$$

The complex energy E and the corresponding wave number $\kappa = \kappa_0 - i\gamma$ produce time and large-distance spatial wave functions proportional to

$$\exp(iEt/\hbar) = \exp[(iE_0 - \Gamma/2)t/\hbar], \quad \exp(i\kappa\rho) = \exp[(i\kappa_0 + \gamma)\rho], \tag{123}$$

which routinely is interpreted as a spontaneously decaying, $\exp(-\Gamma t/2\hbar)$, pre-formed state with the constituents escaping towards infinity and their probability distribution therefore increasing asymptotically with the distance ρ.

The complex energy method can be further supplemented with the phase shift analysis. Narrow resonances with small imaginary values of the energy must necessarily result in rapid variations of the phase shifts. On the other hand, large imaginary values of the energy produce smooth variations of the phase shifts. The three-body poles obtained in this way reveal properties of the three-body system and may therefore contribute to measurable quantities. The connection between the three-body continuum structure and the underlying continuum structure of the two-body subsystems is not properly established.

9.2. Continuum structure of nuclear halos

The bound state properties were discussed in connection with the hypertriton ${}^{3}_{\Lambda}\mathrm{H}$ and the two Borromean nuclei ${}^{6}\mathrm{He}$ and ${}^{11}\mathrm{Li}$. The hypertriton has the deuteron as one bound two-body subsystem, ${}^{6}\mathrm{He}$ and ${}^{11}\mathrm{Li}$ have spin zero or $3/2^-$, respectively of both the core and the three-body ground states.

Scattering of a Λ-particle on a deuteron provides further information about the Λ–nucleon interaction. For energies below the deuteron breakup threshold the radial functions $f_n(\rho)$ decrease exponentially except of that corresponding to the lowest adiabatic eigenvalue. This function is at large distances turning into a phase-shifted sine function in the variable $|\kappa|\rho$. When the Λ–deuteron relative kinetic energy approaches zero we obtain the scattering length $a_{\Lambda d} \approx 18\,\mathrm{fm}$ and the effective range $r_{\Lambda d} \approx 4\,\mathrm{fm}$, where we used the interaction in Section 8.1 for this spin 1/2 scattering channel. When μ is the Λ–deuteron reduced mass we have the approximate connection to the binding energy of $B_\Lambda \approx 0.13\,\mathrm{MeV}$ as

$$B_\Lambda = \frac{\hbar^2}{2\mu a_{\Lambda d}^2} \frac{1}{1 - r_{\Lambda d}/a_{\Lambda d}} . \tag{124}$$

The Borromean two-neutron halo nuclei ${}^{6}\mathrm{He}$ and ${}^{11}\mathrm{Li}$ are easily excited into the continuum by distant Coulomb collisions. The dipole mode is then the leading-order excitation and the 1^- continuum structure becomes decisive for the size of the corresponding Coulomb dissociation cross sections [14,98]. None of these nuclei have documented 1^- resonances, but ${}^{6}\mathrm{He}$ has a narrow 2^+ resonance at $0.82 \pm 0.025\,\mathrm{MeV}$ with the width $0.113 \pm 0.020\,\mathrm{MeV}$ [159].

We first compute the angular eigenvalue spectra for the $J^\pi = 2^+$ and $J^\pi = 1^-$ channels for ${}^{6}\mathrm{He}$ with the interactions specified in [42,98,90]. There is a pronounced attractive pocket in the lowest adiabatic potential for $J^\pi = 2^+$ and a smaller pocket for $J^\pi = 1^-$ [98]. The spin dependence of the two-body interactions is responsible for that difference. The lowest poles of the S-matrix is computed as $E = (0.82 - i0.093/2)\,\mathrm{MeV}$ for $J^\pi = 2^+$ (consistent with measurements) and $E = (0.95 - i0.38/2)\mathrm{MeV}$ for $J^\pi = 1^-$.

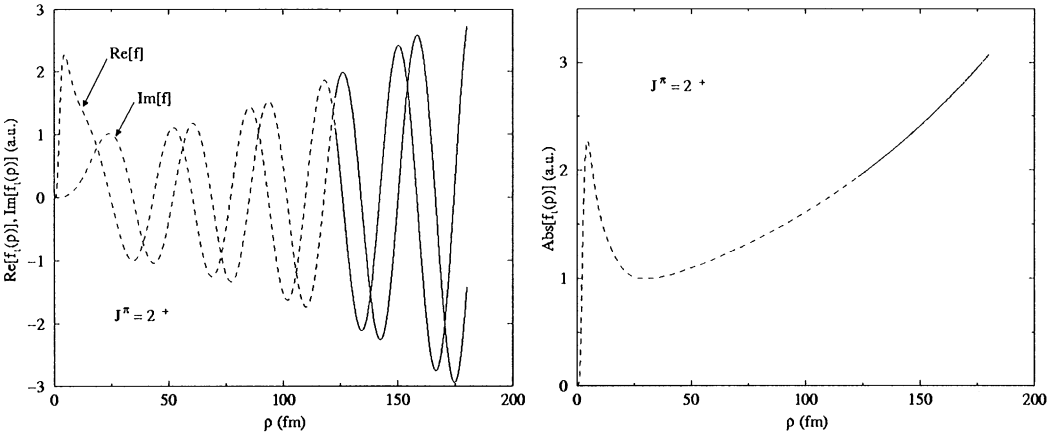

Fig. 17. Real and imaginary parts (left) and absolute square (right) of the radial wave function of ^{6}He for $J^\pi = 2^+$ for the energy $E = (0.82 - i0.093/2)$MeV, where the S-matrix has a pole. The dashed lines are full numerical calculations and the solid lines are the asymptotic Hankel functions $H_n^+(\kappa\rho)$. Courtesy of A. Cobis [160].

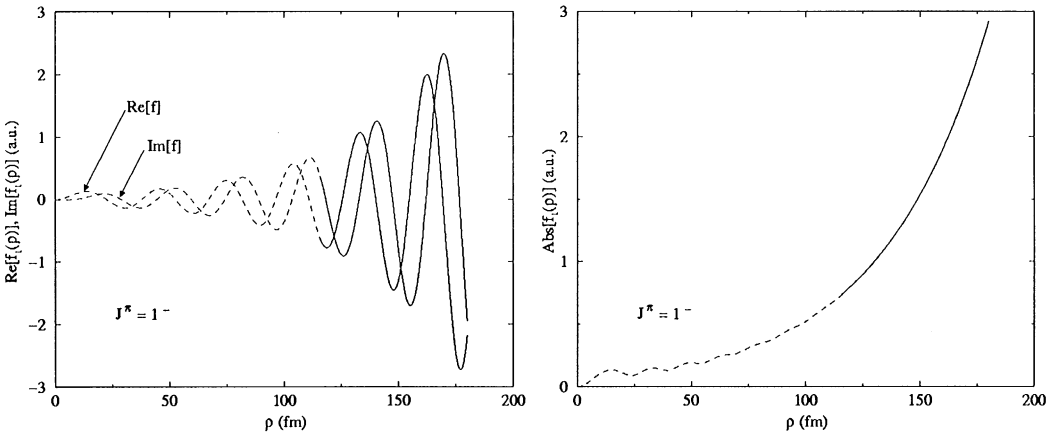

Fig. 18. The same as Fig. 17, but for $J^\pi = 1^-$ and the S-matrix pole energy of $E = (0.95 - i0.38/2)$MeV. Courtesy of A. Cobis [160].

In Fig. 17 we show the dominating component of the radial wave function for the relatively narrow $J^\pi = 2^+$ resonance. The wave function resembles that of a bound state with a large concentration of probability at small distances in the pocket region of the potential. The wave function begins to fall off outside the pocket and only then the exponential growth, characteristic for decaying states, takes place. The absence of nodes inside the potential pocket indicates that this is the ground state for $J^\pi = 2^+$. A small increase of the potential pocket converts this resonance into a bound state with the corresponding pole shifting first towards zero and then taking a real negative value.

We show in Fig. 18 the corresponding wave function for the lowest pole of $J^\pi = 1^-$, where the attractive region disappears in the total effective radial potential leaving an extended flat part at

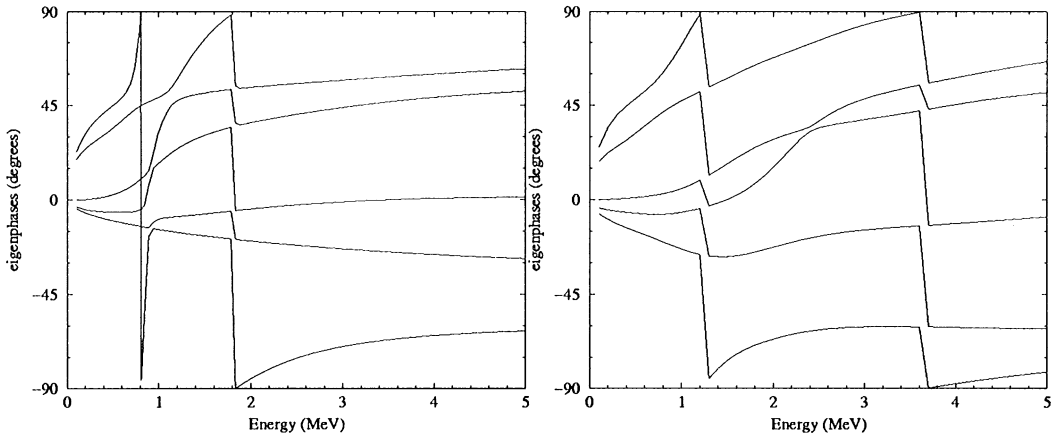

Fig. 19. The eigenphases corresponding to the lowest angular eigenvalues for ^{6}He obtained after diagonalization of the S-matrix for the $J^\pi = 2^+$ (left) and $J^\pi = 1^-$ (right) channels. Courtesy of A. Cobis [160].

distances above $\rho = 5$ fm [98]. Any resonance width should therefore be large. The concentration of probability in the pocket region is now much smaller reflecting the much larger width. Still a small bump is found at small hyperradii. This rather modest enhancement is responsible for a substantial increase of the $J^\pi = 1^-$ strength function [98].

We also calculate the S-matrix and extract the related eigenphases shown in Fig. 19. For $J^\pi = 2^+$ the rapid rise of the phase and the crossing of $\pi/2$ is a convincing confirmation of the resonance at about 0.9 MeV found in the complex energy method. Another pole in this channel appears around 1.8 MeV producing many avoided crossings, but now the phases are rather smooth at the crossings consistent with the large imaginary value of the corresponding complex energy. The $J^\pi = 1^-$ channel shows the same general picture, although now the energy variations are less strong, but still it is possible to connect the lowest resonance unambiguously to a complex energy solution.

The ^{11}Li halo nucleus has ground-state spin and parity $3/2^-$ and electric dipole excitations can therefore produce states of $J^\pi = 1/2^+, 3/2^+, 5/2^+$. If the ^{9}Li core with $J^\pi = 3/2^-$ is truly inert in the process and all interactions are spin independent the resulting spectra must be highly degenerate. However, the two-body interactions depend on the spin couplings of the core and the neutron resulting in ground-state spins of ^{10}Li of either 1 or 2. Both states are expected to be present as resonances in the low-energy two-body spectrum. This means that the continuum spectrum of ^{11}Li could be rather complicated. With a modest spin splitting of the $J^\pi = 1^-, 2^-$ of ^{10}Li the channels with $J^\pi = 3/2^+$ would be a typical 1^- excitation and contain the largest number of adiabatic low lying states. The corresponding configuration must contain one neutron in an s-state and the other neutron in a p-state around the core. The 1^- excitation is basically lifting one of these neutrons from s to p or from p to s states. These excitations are strongly dependent on the spin splitting of the neutron-core interaction and therefore the finite spin of the core is essential.

We shall use $J^\pi = 3/2^+$ as illustration. The corresponding angular eigenvalue spectrum is first computed revealing an attractive pocket suggesting low-lying structures in this 1^- channel. The lowest pole of the S-matrix gives the energy $E = (0.68 - i0.33/2)$ MeV. The dominating component

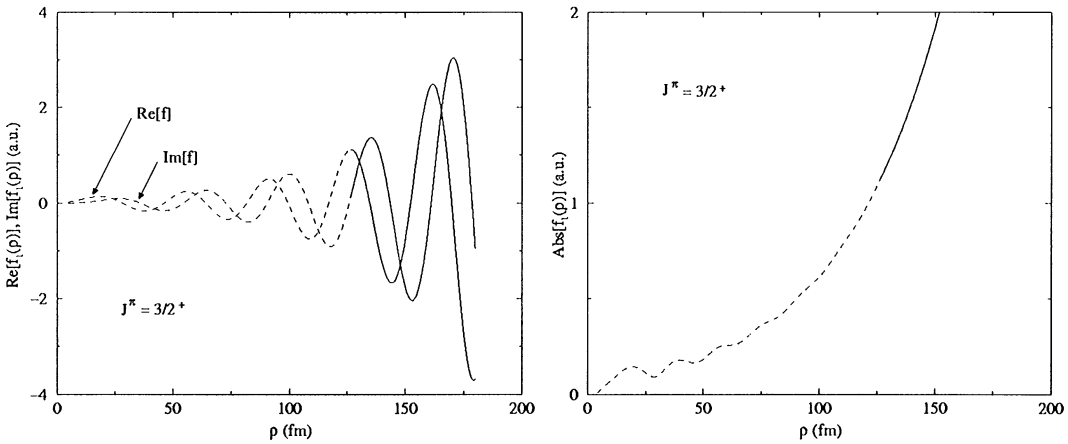

Fig. 20. Real and imaginary parts (left) and absolute square (right) of the radial wave function of ^{11}Li for $J^\pi = 3/2^+$ for the energy $E = (0.68 - i0.33/2)$ MeV, where the S-matrix has a pole. The dashed lines are full numerical calculations and the solid lines are the asymptotic Hankel functions $H_n^+(\kappa\rho)$. Courtesy of A. Cobis [160].

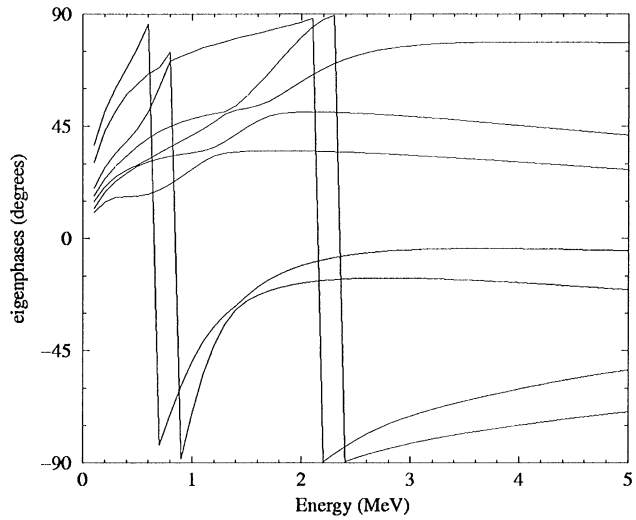

Fig. 21. The same as Fig. 19 for ^{11}Li for $J^\pi = 3/2^+$. Courtesy of A. Cobis [160].

of the radial wave function for this resonance is shown in Fig. 20. The concentration of probability in the pocket region is small reflecting the relatively large imaginary part of the energy. As for $J^\pi = 1^-$ in ^{6}He, the exponential growth sets in leaving only a small trace of small-distance structure. Still this small bump, combined with similar contributions from the continuum states of $J^\pi = 1/2^+, 5/2^+$, produce substantial effects in the low-energy dipole strength function [98].

The eigenphases obtained after computation and diagonalization of the S-matrix show relatively rapid variations and crossings of $\pi/2$ at about 0.7 MeV and 0.9 MeV, see Fig. 21. The two other crossings of $\pi/2$ at higher energies show much less energy variation. In all cases are complex energy

solutions unambiguously related. The near degeneracy is directly related to two similar attractive adiabatic potentials. The wave functions do not show pronounced probability peaks at small distances for these energies.

In conclusion the complex energy method allows relatively simple investigations of resonances in three-body systems. Resonances exhibit all the characteristic features found for two-body resonances, i.e. an increased probability in the pocket region of the potential and an asymptotic exponentially diverging tail. The eigenphases increase around the resonance energy and crosses $\pi/2$.

9.3. *Atomic recombination reactions*

The continuum properties may strongly influence scattering reactions. We shall here concentrate on the recombination or the dissociation process involving three helium atoms, i.e. $^4\mathrm{He} + {}^4\mathrm{He}_2 \leftrightarrow 3{}^4\mathrm{He}$. If we aim at the process from left to right we can numerically integrate Eq. (13), match the solution to the form in Eq. (121) and extract the S-matrix. We use the Gaussian two-body potentials in Section 7 and the two lowest adiabatic channels.

The transition probability for breakup of the two-body bound state producing the lowest three-body continuum state, where all three atoms at $\rho = \infty$ are non-interacting, is then given by $P(E) = |S_{12}|^2 = |S_{21}|^2$. The calculated transition probability in Fig. 22 behaves as $P(E) \propto E^2$ at low energy and grows smoothly until approximately $9|E_2|$, where a striking dip of about two orders of magnitude appears. This process is the prototype of one of the mechanisms of decay of Bose–Einstein condensates and it is therefore of practical importance to understand whether this behaviour is specific to the helium atoms or perhaps a general phenomenon. This problem is discussed in [107].

9.3.1. *The WKB approximation: hidden crossing theory*

The hyperspherical version of the *hidden crossing* theory is used in [106] for positronium formation in positron–hydrogen collisions and in [161] to give both an approximate expression for

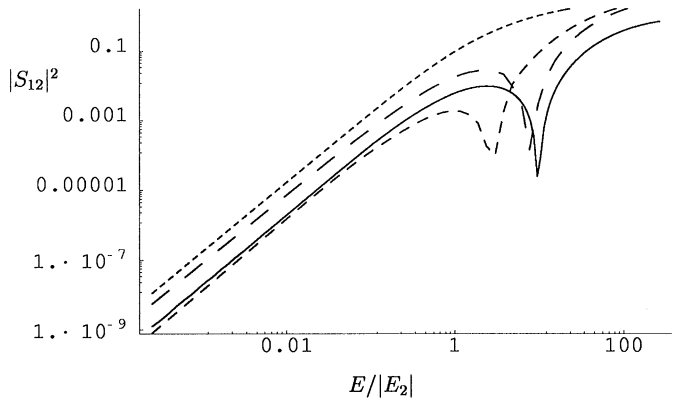

Fig. 22. The transition probability $|S_{12}|^2$ for the reaction $^4\mathrm{He}_2 + {}^4\mathrm{He} \to 3{}^4\mathrm{He}$ using different methods: The solid line is for coupled channels, the dotted line is the upper limit from hidden crossing theory for the zero-range model, the short and long-dashed lines are the mixed Gaussian and short-range model with and without the Langer correction, respectively. The energy unit is chosen to be $E_2 = -1.3\,\mathrm{mK}$.

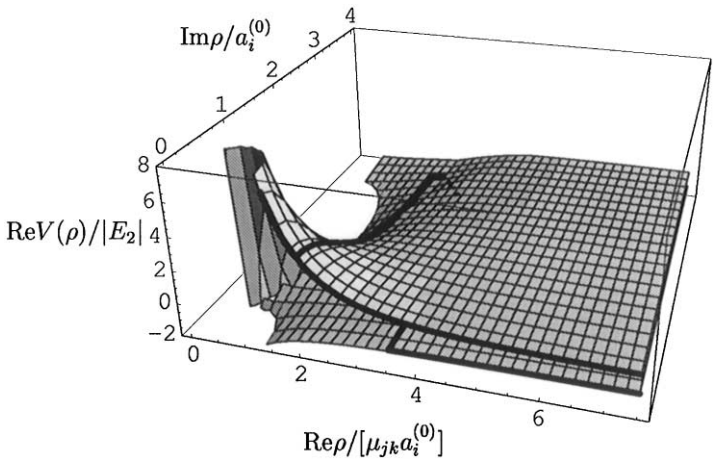

Fig. 23. The real part of $V(\rho)$ in Eq. (125) as a multi-valued function of ρ in the complex plane for three identical bosons in three dimensions interacting with zero-range potentials with positive scattering length $a_i^{(0)}$. The energy unit is again $E_2 = -1.3$ mK. We show only the two lowest branches, which asymptotically ($\rho \to +\infty$) represent the two-cluster state and the lowest three-body breakup channel. Also shown is one of the two paths, which contributes to the breakup reaction in the hidden crossing approach by going around the branch point at $\rho = (2.5918 + 2.9740\mathrm{i})\mu_{jk}a_i^{(0)}$.

Wannier's threshold law and a rigorous derivation for Coulomb interacting particles. We shall here only consider three dimensions and three identical bosons with total angular momentum 0 and zero-range two-body interactions. We assume that the three scattering lengths $a_i^{(0)}$ are identical and positive such that there is one bound state in each two-body subsystem. Therefore, the angular eigenvalues are given by Eq. (100), where ρ is understood as an analytic single valued complex function of ν with first order poles at all integers, except for $\nu = \pm 1$ where the function is finite.

Eq. (100) implicitly defines the *multi-valued* function $\nu(\rho)$ in the entire complex plane. The diagonal potentials in Eq. (17) ($\lambda = 4\nu(\nu+2)$, $\lambda_0 = 0$, $Q_{nn} \approx 0$)

$$\frac{2m}{\hbar^2}V(\rho) = \frac{4\nu(\nu+2)+15/4}{\rho^2} = \frac{4(\nu+1)^2-1/4}{\rho^2} \tag{125}$$

is therefore also a multi-valued function of ρ. On the positive real axis each of these values or *branches* corresponds to the adiabatic potentials in Eq. (13), which for asymptotically large ρ correspond to initial or final states for the reaction. The two lowest branches of this function are shown in Fig. 23.

The function $V(\rho)$ has a branch point $\rho = \rho_0 \equiv (2.5918 + \mathrm{i}2.9740)\mu_{jk}a_i^{(0)}$ found by Taylor expansion of Eq. (100), $\rho(\nu) \simeq \rho(\nu_0) + (\partial\rho/\partial\nu)(\nu-\nu_0) + \frac{1}{2}(\partial^2\rho/\partial\nu^2)(\nu-\nu_0)^2$, with $\nu = \nu_0 = 0.46719 + \mathrm{i}0.86782$ as the solution to $\partial\rho/\partial\nu = 0$. Then $\nu(\rho) \approx \nu_0 \pm \sqrt{2(\partial^2\rho/\partial\nu^2)^{-1}(\rho-\rho_0)}$, where $\rho_0 \equiv \rho(\nu_0)$ and the second derivative is for $\nu = \nu_0$. Going around the branch point ρ_0 changes the branch of $\nu(\rho)$, the sign in front of the square root, and through Eq. (125) $V(\rho)$ changes accordingly.

The breakup reaction corresponds to a "particle" in an initial state at large ρ moving towards smaller values on the lowest branch of $V(\rho)$. The final state is this particle moving from small towards larger ρ-values on the second branch of $V(\rho)$. The transition probability is in the

hidden-crossing theory obtained as an integral along a continuous path connecting the corresponding points by going around the branch point. Let ρ_{t1} and ρ_{t2} denote the classical turning points, $V(\rho_{ti}) = E$, on lower and upper branch. Then we have [161]

$$S_{12} = \sum_c \exp(\mathrm{i}Q_c(E) + \mathrm{i}\gamma_c), \quad Q_c(E) = \int_c \mathrm{d}\rho \sqrt{\frac{2m}{\hbar^2}(E - V(\rho))}\,, \tag{126}$$

$$Q_c(E) = \mathrm{i}S(E) + \Delta(E)/2\,, \tag{127}$$

where S and Δ are real, $\gamma_c = \pm\pi/2$ is the *topological phase* [162]. The sum is over all possible continuous paths c connecting $\rho = \infty$ on first and second branches.

There are basically two such paths: one of them connects $\rho = \infty$ on the first branch with $\rho = \mathrm{Re}\,\rho_0$, continues away from the real axis and around the branch point and back to the real axis at $\rho = \mathrm{Re}\,\rho_0$ on the second branch, then up to the classical turning point $\rho = \rho_{t2}$ and finally to $\rho = \infty$ on the second branch, see Fig. 23. The second path connects $\rho = \infty$ on the first branch with the classical turning point at $\rho = \rho_{t1}$, continues back to $\rho = \mathrm{Re}\,\rho_0$ on the first branch, then up and around the branch point to $\rho = \mathrm{Re}\,\rho_0$ on the second branch and from there to $\rho = \infty$. The square root in the integrand of Eq. (126) changes sign when the path passes the classical turning points.

When $\rho_{t2} < \mathrm{Re}\,\rho_0$, i.e. $E \geq V(\mathrm{Re}\,\rho_0)$ on the second branch, only the part of the path, from $\rho = \mathrm{Re}\,\rho_0$ on the first branch and around the branch point to $\rho = \mathrm{Re}\,\rho_0$ on the second branch, contributes to S in Eq. (127). All other contributions are real, because then ρ is real and $V(\rho) < E$. The phase difference between the two possible paths contributing to Eq. (126) is Δ defined in Eq. (127), since the parts of the integrals outside $\mathrm{Re}\,\rho_0$ contribute equally to both paths and therefore cancel in the phase difference. Then c is the path that goes from $\rho = \rho_{t1}$, out to $\rho = \mathrm{Re}\,\rho_0$, around the branch point to $\rho = \mathrm{Re}\,\rho_0$ on the second branch and then up to $\rho = \rho_{t2}$. By adding coherently the two paths contributing in Eq. (126) we get the transition probability

$$|S_{12}|^2 = 4\exp(-2S(E))\sin^2(\Delta(E)/2) \leq 4\exp(-2S(E))\,, \tag{128}$$

where we used the relative topological phase of π between the two paths [162].

For small energies, $0 < E < V(\mathrm{Re}\,\rho_0)$, the classical turning point on the second branch is outside the position of the branch point, i.e. $\rho_{t2} > \mathrm{Re}\,\rho_0$. Then $V(\rho) > E$ for ρ-values between $\mathrm{Re}\,\rho_0$ and ρ_{t2}. This part of the integrals in Eq. (126) are then imaginary corresponding to tunneling and contributes therefore to $S(E)$ and not to $\Delta(E)$ in Eq. (128). As $E \to 0$ the main contribution to $S(E)$ arises from tunneling through this barrier, i.e.

$$S(E) \sim \int_{\mathrm{Re}\,\rho_0}^{\rho_{t2}} \mathrm{d}\rho \sqrt{\frac{2m}{\hbar^2}(V(\rho) - E)} \simeq v_0 \log\left(\frac{\rho_{t2}}{\mathrm{Re}\,\rho_0}\right), \tag{129}$$

where we used $2mV(\rho)/\hbar^2 \simeq v_0^2\rho^{-2}$ with $v_0^2 = 15/4$ on the second branch for large distance. Since $\rho_{t2}^2 = v_0^2\hbar^2/(2Em)$, we get $|S_{12}|^2 \propto E^{v_0}$ from Eq. (128).

This low-energy dependence is only nearly correct as seen by integrating over all final states, constraint by energy conservation, in the breakup channel, i.e.

$$|S_{12}(E)|^2 \propto \int \mathrm{d}^3\boldsymbol{p}_x\, \mathrm{d}^3\boldsymbol{p}_y\, \delta\left(\frac{p_x^2 + p_y^2}{2m} - E\right) \propto \frac{E^2}{E_2^2} = E^2\frac{m_i^2}{\hbar^4}[a_i^{(0)}]^4\,, \tag{130}$$

where $\boldsymbol{p}_x$ and $\boldsymbol{p}_y$ are the conjugated momenta of the Jacobi coordinates, see [157] p. 500. Therefore, we must have $v_0^2 = 4$ instead of $\frac{15}{4}$ as used above. The discrepancy is removed by adding $V_L(\rho) = \hbar^2/(8m\rho^2)$, the *Langer correction* to the potential $V(\rho)$ [163]. This extra term arises automatically in the rigorous derivation in [161]. It is a general correction providing substantial improvements in WKB calculations [164,165].

The energy E_2 in Eq. (130) must for zero-range potentials be the only available energy, i.e. the two-body binding energy $E_2 = \hbar^2/(m_i[a_i^{(0)}]^2)$, see Eq. (C.9). To find the proportionality constant in Eq. (130) we could turn to Eq. (128). However, according to Eq. (102) the lowest branch of $V(\rho)$ diverges as $V(\rho) = -1.26\rho^{-2}$ for $\rho \to 0$ and there is therefore no classical turning point on the first branch. Consequently, $\Delta = \infty$ in a zero-range model and $\sin^2(\Delta(E)/2)$ is undetermined and in this way we can only find the upper limit given in Eq. (128), see the dotted curve in Fig. 22 exceeding all the other results.

The phase difference Δ can only be computed by use of a finite range potential. We use the Gaussian potentials from Section 7 to provide adiabatic potentials when ρ is on the real axis, while we maintain the potentials of the zero-range model with the same scattering length when ρ is away from the real axis. We thereby get a classical turning point on the lower branch and Δ is calculated as function of energy with and without the Langer correction, see Fig. 24. Both curves passes through 3π, i.e. at $E = 2.8|E_2|$ and $E = 7.9|E_2|$, where the calculated transition probabilities in Eq. (128) vanish due to this destructive interference between the two paths. This gives the origin of the dip in Fig. 22.

The computed hidden crossing transition probabilities in Eq. (128) are shown in Fig. 22. The position of the minimum only coincides with the coupled channel result without the Langer correction. This is unfortunate, since then neither the correct amplitude nor the correct threshold law is obtained. On the other hand, the results are very good with the Langer correction for energies below $0.2|E_2|$, but the dip then occurs at too small an energy. The fairly good agreement is somewhat surprising as the model is rather crude.

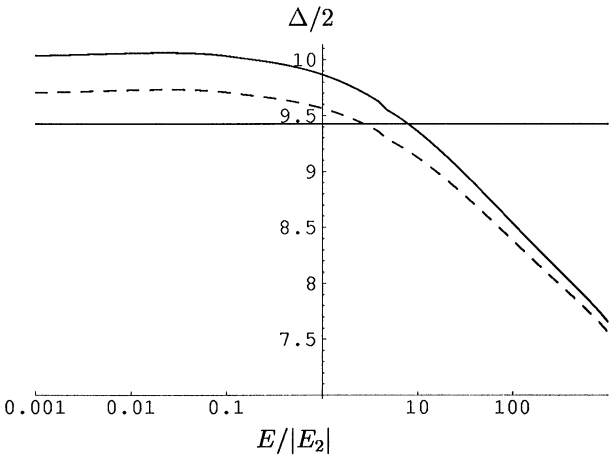

Fig. 24. Half of the phase difference in Eq. (128) as function of energy in units of $|E_2|$. The two-body interaction is the Gaussian found in Section 7 with the same scattering length and effective range as LM2M2 [130]. The dashed line is with and the solid line is without the Langer correction.

9.3.2. The three-body recombination rate

The three-body recombination rate at zero temperature is given by [157]

$$R_{\rm rec} = 2(2\pi)^2 3^{3/2} n^3 \frac{\hbar}{m_i} [a_i^{(0)}]^4 \lim_{E\to 0} \frac{|S_{12}(E)|^2}{(E/|E_2|)^2}$$
$$= 8(2\pi)^2 3^{3/2} n^3 \frac{\hbar}{m_i} [a_i^{(0)}]^4 \lim_{E\to 0} \left[\frac{\exp(-2S(E))}{(E/|E_2|)^2}\right] \sin^2\left(\frac{\Delta(0)}{2}\right). \quad (131)$$

where n is the atomic density [105] and Eq. (128) was used for $|S_{12}(E)|^2$. If $a_i^{(0)}$ is large compared to the range of the potential we can use the zero-range model, i.e. Eq. (129), $v_0^2 = 4$ and $\mathrm{Re}\,\rho_0 = 2.5918\mu_{jk} a_i^{(0)}$. This gives [107]

$$R_{\rm rec} = 68.4 \frac{\hbar}{m_i} a_i^{(0)^4} n^3 \sin^2\left(\frac{\Delta(0)}{2}\right) = 7.38 \frac{\hbar}{m_i} a_i^{(0)^4} n^3 \,, \quad (132)$$

where we inserted the computed $\Delta(0)/2$, which is fairly close to 3π, see Fig. 24. Therefore a 3% decrease in $\Delta(0)/2$ would shift the result to exactly 3π and change the recombination rate by 100% to zero. This sensitivity is perhaps better appreciated by the comparison in Table 5 of ground state energies for Gaussian and LM2M2 potentials amounting to a 20% relative difference.

We have from Eq. (102) that the potential behaves as $V(\rho) = -1.26\rho^{-2}\hbar^2/2m$ when ρ is between ρ_{t1}, which is comparable to the range of the two-body potential, and ρ_{t2}, which is about the scattering length $a_i^{(0)}$. We may divide the integral in Eq. (127) into three contributions, i.e. from short range ($\rho < \rho_{t1}$), middle range ($\rho_{t1} < \rho < \rho_{t2}$) and long range ($\mathrm{Re}\,\rho > \rho_{t2}$), where the latter also includes the path around the branch point.

Let us now imagine a system, where the two-body potential can be tuned around the point of infinite scattering length. The short-distance contribution Δ_1 must be nearly constant for relatively small variations of the potentials. At zero energy this also holds for the large-distance contribution Δ_2 as everything in this region scales with the scattering length. All lengths and energies must be proportional to respectively $a_i^{(0)}$ and $[a_i^{(0)}]^{-2}$ leaving the integral in Eq. (126) invariant. With the Langer correction we therefore get from Eq. (127)

$$\Delta(E=0) = \Delta_1 + 2\int_{\rho_{t1}}^{\rho_{t2}} \mathrm{d}\rho \sqrt{1.01\rho^{-2}} + \Delta_2 = 2.01 \ln a_i^{(0)} + \text{constant}. \quad (133)$$

Thus in a tuning experiment [166] the recombination rate should behave as

$$R_{\rm rec} = 68.4 \frac{\hbar}{m_i} [a_i^{(0)}]^4 n^3 \sin^2(1.01 \ln(a_i^{(0)}) + \delta) \,, \quad (134)$$

where δ is an unknown phase, nearly independent of small variations of the potential when $a_i^{(0)}$ is positive and large. This phase depends on the other hand on the adiabatic potentials at short distance and thereby on the radial shape of the two-body potentials. This is analogous to the Efimov states, located in the interval between ρ_{t1} and ρ_{t2}, but still depending on the boundary condition provided by the shape of the potentials for $\rho < \rho_{t1}$, see Section 5.

We now consider negative scattering lengths, where the zero-range model is insufficient for estimates of recombination rates due to the lack of bound states. For large negative $a_i^{(0)}$, the

large-distance behaviour of the adiabatic potentials, corresponding to three-body continuum states, equals that of the zero-range potential, but for finite range potentials there may be lower lying adiabatic potentials corresponding to two-body bound states. Branch points connecting two-body and continuum branches must therefore be within a few times the range of the two-body potentials. Thus, the hidden crossing result for recombination rates must be highly sensitive to the shape of the two-body potentials.

However, as noticed in [167], the lowest adiabatic potential corresponding to a three-body continuum state has a barrier at large distance, see the dashed curve in Fig. 5. At very low energies the system has to tunnel through this barrier and we can use the WKB approximation to estimate this penetration probability. We first add the Langer correction to the potential in Eq. (125) effectively removing $-\frac{1}{4}$. The inner turning point ρ_{t1} of the barrier, where $V(\rho_{t1}) = E$, is for very low energies close to the point where $V(\rho_{t1}) = 0$ and therefore $v = -1$, i.e. $\rho_{t1} = \rho(v = -1) = -0.903\mu_{jk}a_i^{(0)}$ as found from Eq. (100). At large distance $v \simeq 0$ and the outer turning point is then about $\rho_{t2} \simeq 2\hbar/\sqrt{mE}$. The tunneling probability in the limit of zero energy is then

$$P = \exp\left(-2\int_{\rho_{t1}}^{\rho_{t2}} \mathrm{d}\rho \sqrt{\frac{4(v+1)^2}{\rho^2} - \frac{2m}{\hbar^2}E} \right) \simeq 69.5\frac{m_i^2}{\hbar^4}[a_i^{(0)}]^4 E^2 \,, \tag{135}$$

which has both the E^2 behaviour and the factor $[a_i^{(0)}]^4$, see Eq. (134).

Thus in an experiment, where the potentials are tuned around the point where the scattering length is infinitely large, we must again find the behaviour expressed in Eq. (134), but with a different proportionality factor. In fact, the proportionality constants for negative and positive scattering lengths are entirely independent as the recombination processes are completely different.

10. Summary and conclusions

We have investigated quantum mechanical three-body problems with short-range interactions in d dimensions. We have formulated and discussed a general method, derived a number of useful analytical properties, extracted occurrence conditions for the exotic but interesting Efimov structures, applied the method in realistic numerical computations of bound states and scattering properties.

The distinguished features of the method are the efficient treatment of large distances allowing analytical deduction of universal conclusions about spatially extended and weakly bound systems, the formulation of how to deal with bound and scattering states on the same footing and the possibility of high accuracy when both small and large distances turn out to be important.

The method combines hyperspherical adiabatic expansion with the Faddeev equations. This expansion divides the degrees of freedom into hyperradial and hyperangular parts. For fixed hyperradius we solve the angular part of the Faddeev equations and obtain a complete basis set of eigenfunctions. The corresponding discrete eigenvalues are functions of hyperradius and related to one of the adiabatic potentials. We eliminate a priori states of unwanted symmetries and spurious

solutions with zero norm by diagonalizing the kinematic rotation operator and subsequently removing the eigenstates corresponding to the eigenvalue 0. An optimal incomplete basis is used for small hyperradii whereas simplified equations are used at intermediate distances when at least one particle is not interacting with both the other two. Analytical behaviour of the adiabatic potentials are extracted at very large distances.

The mathematical formulations are tested on physical systems in realistic numerical calculations. First the atomic helium trimers where the interaction has a strongly repulsive core. The ground state of $^4He_3$ is a state of a size comparable to the effective range of the interactions. The ground state of $^3He^4He_2$ is a weakly bound halo system. The excited state of $^4He_3$ is the first (and last) Efimov state. It could be classified as a halo state on top of a Efimov state. These trimers are investigated in two dimensions where all asymmetric trimers have one bound state and the symmetric bosons have two bound states. We use the method for the breakup reaction, $^4He + {}^4He_2 \to 3{}^4He$, since this type of process is relevant for the stability of Bose–Einstein condensates.

The second set of examples are the nuclear three-body halos of the hypertriton and the Borromean nuclei ^6He and ^{11}Li. The hypertriton structure is basically a two-cluster system with the Λ-particle and a deuteron far apart and weakly bound. We derive limits for the Λ-nucleon singlet s-wave scattering length. The bound and continuum state structure of the Borromean nuclei are surveyed. The Pauli principle are accounted for by phase equivalent potentials. The peaks of the density distributions correspond roughly to a distance of 2 fm between the particles. Low-lying 1^- continuum structure increase the Coulomb dissociation cross sections substantially.

We discuss the Thomas and Efimov effects existing when the s-wave scattering length divided by the effective range is an infinitely large number. We derive occurrence conditions for arbitrary angular momenta and dimensions. For three identical bosons the effects are only possible for dimensions between 2.3 and 3.8. We use an external electric field to tune to the conditions. For $^4He^3He_2$ the field strength needed to reach the Efimov limit is 2.7 V/Å.

A number of the conclusions in this report are universal in the sense that they are independent of the details of the short-range two-body potentials. Beyond a few times the range of the potentials the angular spectrum only depends on the logarithmic derivatives of the radial two-body wave functions for energies given by the angular eigenvalues and the hyperradius. In other words two-body potentials with the same low-energy scattering properties produce identical intermediate and large-distance behaviour.

For $d < 4$ the lowest part of the angular spectrum only depends on the s-wave scattering lengths and the two-body binding energies provided the hyperradius is a few times the range of the potentials. For $d \geq 4$ and hyperradii much larger than the absolute values of the scattering lengths these determine exclusively the adiabatic potentials. At smaller hyperradii, still larger than the ranges of the potentials, the eigenvalues depend on the shapes of the potentials.

For $d = 2, 3$, but not for $d \geq 4$, there may in addition exist a region in hyperradius ρ where the low energy part of the angular spectrum is model independent but still not converged to the free spectrum. This region extends from a few times the range of the potentials up to the absolute values of the scattering lengths. Thus in such cases the large-distance behaviour of the angular spectrum is independent of the exact shapes of the potentials and only depends on the low energy scattering properties. However, even then the wave function is not necessarily positioned at the

corresponding large hyperradii. For $d = 3$ the energies and wave functions of the Efimov states depend upon the behaviour at short distance, because the long-range model independent part of the adiabatic potentials does not provide a repulsive barrier that would keep the wave function in this long-distance region. Instead the lowest adiabatic potential is attractive and proportional to $-1/\rho^2$ in the region between the range of the two-body potentials and the absolute values of the scattering lengths.

In contrast for $d = 2$ a repulsion proportional to $+1/\rho^2$ is present. The two bound states, always existing for three identical particles and overall attractive two-body potentials, are independent of the details of the potential in the limit of weak binding. Their energies and root mean square radii are then proportional to the two-body bound state energy and the two-body scattering length, respectively. The large proportionality constant related to the three-body ground-state energy reminds us about the non-existing, but still not very distant, Thomas effect. The radius of the excited state is close to the scattering length reminding about the also non-existing Efimov effect. For three different particles and $d = 2$ this type of model independence remains but the number of bound states may be reduced to one.

The three-body recombination processes in three dimensions also depend on the shapes of the two-body potentials, since the lack of repulsion in the lowest adiabatic potential allows the scattering wave function in the inner region, where the lowest adiabatic potentials are model dependent. For positive scattering length, still in the low-energy regime, the recombination rate is proportional to the fourth power of the scattering length. The influence of the details of the potentials on this rate is an oscillating factor depending on the shapes of the potentials. For negative scattering length the process of recombination can only take place at small distance, where the adiabatic potentials and the couplings are strongly dependent on the shapes of the two-body potentials. On the other hand, for $d = 2$ and very large scattering length, there is a centrifugal barrier effectively screening off the short-distance region. Therefore, the zero-temperature recombination rate should be independent of the shape of the two-body potentials even in the limit of large scattering length.

Our method may be extrapolated to more complicated systems. First, it could be extended explicitly to 4, 5 or 6 particles. This is again most appealing when the large distances are decisive. Second, the large-distance treatment may be exploited for many-body systems described by appropriate generalized hyperspherical coordinates. This seems to be most interesting for processes like chemical reactions where large distances are essential.

Third, it is possible to use the method in descriptions of few-body correlations within genuine many-body systems. Vaguely speaking, this could be two correlated particles interacting with the average of all remaining, possibly many, particles. Fourth, with hyperspherical coordinates for many particles the centrifugal barrier term maintains the usual form, but with a different strength, i.e. $l(l+1)$ is replaced by $(f-1)(f-3)/4$, where $f = d(N-1)$ is the number of intrinsic degrees of freedom for N particles in d dimensions.

Fifth, apart from three dimensions, two dimensions attract in particular increasing interest especially in condensed matter physics. Three-body correlations in two dimensions differ substantially from those of three dimensions. It is quite conceivable that large-distance correlations, the hall mark of our method, could mediate otherwise very unlikely reactions and thereby exhibit catalytic behaviour. In conclusion, we find many specific applications of our method and in addition a number of possible extensions.

Appendix A. Jacobi functions

The Jacobi functions, $P_\nu^{(a,b)}(x)$ and $Q_\nu^{(a,b)}(x)$, as well as the Jacobi polynomials repeatedly appear in this report. We shall here collect some of their basic properties derived from [124]. They are solutions to the differential equation

$$(1-x^2)y'' + [b-a-(a+b+2)x]y' + \nu(\nu+a+b+1)y = 0\,, \tag{A.1}$$

where a and b are real constants, ν is a complex number, and primes denote derivatives with respect to the variable $x \in]-1, 1]$. The Jacobi functions P and Q are regular and irregular at $x = 1$, respectively. We can express P as

$$\begin{aligned} P_\nu^{(a,b)}(x) &= \frac{\Gamma(\nu+a+1)}{\Gamma(\nu+1)\Gamma(a+1)}[1+\mathcal{O}(1-x)] \\ &= \frac{\Gamma(\nu+a+1)}{\Gamma(\nu+1)\Gamma(a+1)} F\left(-\nu, \nu+a+b+1; a+1; \frac{1}{2}(1-x)\right), \end{aligned} \tag{A.2}$$

defining normalization of P as $\mathcal{O}(t)/t$ is a function remaining finite for $t \to 0$. Here F is the hypergeometric function expressed as a power series in x, i.e.

$$F(a,b;c;x) = 1 + \frac{ab}{1!c}x + \frac{a(a+1)b(b+1)}{2!c(c+1)}x^2 + \cdots\,, \tag{A.3}$$

where the convergence radius is 1 unless either a or b is a non-positive integer, in which cases the series terminates and the resulting $P_n^{(a,b)}(x)$ is simply a polynomial of order n with the orthogonality relation

$$\int_{-1}^{1} \mathrm{d}x(1-x)^a(1+x)^b P_{n'}^{(a,b)} P_n^{(a,b)} = \delta_{nn'} \frac{2^{a+b+1}\Gamma(n+a+1)\Gamma(n+b+1)}{(2n+a+b+1)n!\Gamma(n+a+b+1)}\,. \tag{A.4}$$

We want to rewrite P in a more suitable form around $x = -1$. First

$$\begin{aligned} P_\nu^{(a,b)}(x) &= \frac{\Gamma(-b)}{\Gamma(\nu+1)\Gamma(-\nu-b)} F\left(-\nu, \nu+a+b+1; b+1; \frac{1}{2}(1+x)\right) \\ &\quad + \frac{\Gamma(b)\Gamma(\nu+a+1)}{\Gamma(\nu+1)\Gamma(-\nu)\Gamma(\nu+a+b+1)} \left(\frac{1+x}{2}\right)^{-b} \\ &\quad \times F\left(\nu+a+1, -\nu-b; 1-b; \frac{1}{2}(1+x)\right). \end{aligned} \tag{A.5}$$

Using $\Gamma(x)\Gamma(1-x) = \pi/\sin(\pi x)$ the irregular Jacobi function Q is given by

$$\begin{aligned} Q_\nu^{(b,a)}(-x) &= -\cot(\pi b) P_\nu^{(b,a)}(-x) + \frac{\Gamma(b)\Gamma(\nu+a+1)}{\pi\Gamma(\nu+a+b+1)} \\ &\quad \times F\left(\nu+a+1, -\nu-b; 1-b; \frac{1}{2}(1+x)\right)\left(\frac{1+x}{2}\right)^{-b} \end{aligned} \tag{A.6}$$

and we then obtain the simple relation

$$P_\nu^{(a,b)}(x) = \cos(\pi\nu)P_\nu^{(b,a)}(-x) - \sin(\pi\nu)Q_\nu^{(b,a)}(-x)\,, \tag{A.7}$$

which is valid even when b is a non-negative integer, where $\Gamma(x)$ has poles and Eqs. (A.5) and (A.6) invalid. This implies that

$$\begin{aligned} Q_\nu^{(b,a)}(-x) &= \frac{\Gamma(\nu+b+1)}{\pi\Gamma(\nu+1)\Gamma(b+1)} \\ &\sum_{n=0}^{\infty}\frac{(-\nu)_n(\nu+a+b+1)_n}{(b+1)_n n!}\Bigg[\psi_\Gamma(1+n)+\psi_\Gamma(b+1+n) \\ &-\psi_\Gamma(1+\nu-n)-\psi_\Gamma(\nu+a+b+n+1)-\ln\frac{1+x}{2}\Bigg]\left(\frac{1+x}{2}\right)^n \\ &-\begin{cases} 0 & \text{for } b=0\,, \\ \dfrac{\Gamma(b)\Gamma(\nu+a+1)}{\pi\Gamma(\nu+a+b+1)}\left(\dfrac{1+x}{2}\right)^{-bb-1}\displaystyle\sum_{n=0}^{}\frac{(-\nu-b)_n(\nu+a+1)_n}{(1-b)_n n!}\left(\frac{1+x}{2}\right)^n & \text{for } b\geq 1\,, \end{cases} \end{aligned} \tag{A.8}$$

where $(x)_n \equiv x(x+1)\ldots(x+n-1)$ and ψ_Γ is the di-gamma function, i.e. the logarithmic derivative of the gamma function.

The function $Q_\nu^{(b,a)}(-x)$ diverges for $x\to -1$, as $(1+x)^{-b}$ for $b>0$ and as $\ln(1+x)$ for $b=0$. Thus $P_\nu^{(a,b)}(x)$ is only regular for $x=-1$ when ν is an integer. If ν is a negative integer then $P_\nu^{(a,b)}$ vanishes due to the pole in $\Gamma(\nu+1)$, see Eqs. (A.2) and (A.5). Then the term $\Gamma(\nu+1)\sin(\pi\nu)Q_\nu^{(b,a)}(-x)$ does not vanish when $\nu\to -n$, see Eq. (A.7) and $\Gamma(\nu+1)P^{(a,b)}(x)$ still diverges at $=-1$. Thus only solutions to Eq. (A.1) with $\nu=-n$ are regular at $x=\pm 1$.

For large absolute values of ν and $0<|\arg\nu|<\pi$ we approximate F and find

$$\begin{aligned} P_\nu^{(a,b)}(\cos\gamma) &= \frac{1}{\sqrt{\pi}}\mathrm{e}^{-\mathrm{i}\pi a}2^{a+b}(1-\mathrm{e}^{-\mathrm{i}\gamma})^{-a-1/2}(1+\mathrm{e}^{-\mathrm{i}\gamma})^{-b-1/2} \\ &\quad(-\nu)^{-1/2}(\mathrm{e}^{-\mathrm{i}(\nu+a+b+1)\gamma}+\mathrm{e}^{\mathrm{i}\pi(a+(1/2))}\mathrm{e}^{\mathrm{i}\nu\gamma})(1+\mathcal{O}(|\nu|^{-1}))\,. \end{aligned} \tag{A.9}$$

We need $a=(d-2)/2+l_x$, $b=(d-2)/2+l_y$, $x=\cos(2\alpha)$, where d is the spatial dimension, l_x and l_y are the partial angular momenta and α is the hyperangle, see Section 2. From Eqs. (A.2), (A.6) and (A.8) we then get that

$$P_\nu^{((d-2)/2+l_x,\,(d-2)/2+l_y)}(\cos 2\alpha) = \frac{\Gamma(\nu+d/2+l_x)}{\Gamma(\nu+1)\Gamma(d/2+l_x)}(1+\mathcal{O}(\alpha^2)) \tag{A.10}$$

$$Q_\nu^{((d-2)/2+l_x,\,(d-2)/2+l_y)}(\cos 2\alpha)$$

$$= \begin{cases} -\dfrac{1}{\pi}(2\gamma_\Gamma + \psi_\Gamma(1+v) + \psi_\Gamma(1+v+l_y) + 2\ln\alpha) & \\ \quad + \mathcal{O}(\alpha^2 \ln\alpha) & \text{for } d + 2l_x = 2\,, \\ \dfrac{\Gamma\left(\dfrac{d-2}{2} + l_x\right)\Gamma\left(v + \dfrac{d}{2} + l_y\right)}{\pi\Gamma(v + d - 1 + l_x + l_y)}\alpha^{2-d-2l_x}(1 + \mathcal{O}(\alpha^2)) & \\ \quad + \mathcal{O}(\ln\alpha) & \text{for } d \text{ even and } d + 2l_x \geq 4\,, \\ \dfrac{\Gamma\left(\dfrac{d-2}{2} + l_x\right)\Gamma\left(v + \dfrac{d}{2} + l_y\right)}{\pi\Gamma(v + d - 1 + l_x + l_y)}\alpha^{2-d-2l_x}(1 + \mathcal{O}(\alpha^2)) & \\ \quad - \cot\left(\pi\dfrac{d}{2}\right)\dfrac{\Gamma\left(v + \dfrac{d}{2} + l_x\right)}{\Gamma(v+1)\Gamma\left(\dfrac{d}{2} + l_x\right)}(1 + \mathcal{O}(\alpha^2)) & \text{else}\,, \end{cases} \tag{A.11}$$

where $\gamma_\Gamma = -\psi_\Gamma(1)$ is Euler's constant. A case of special interest is $d = 3$, $l_x = l_y = 0$ and therefore $a = b = \frac{1}{2}$. The corresponding $P_v^{(1/2,1/2)}$ is given by

$$P_v^{(1/2,1/2)}(\cos 2\alpha) = \frac{\Gamma(v+\frac{3}{2})}{\Gamma(v+1)\Gamma(\frac{3}{2})}\frac{\sin(2(v+1)\alpha)}{(v+1)\sin(2\alpha)}\,. \tag{A.12}$$

Appendix B. Spherical coordinates in *d* dimensions

We shall here give some pertinent details and derive key formulae for an integer dimension $d \geq 2$, see [108] for the details. We divide the Cartesian coordinates $(x_1, \ldots, x_d)$ into the first $d-1$ coordinates $(x_1, \ldots, x_{d-1})$ and the last coordinate x_d. We define angles θ_k and radii r_k recursively by $r_d = \sqrt{x_d^2 + r_{d-1}^2} = \sqrt{x_1^2 + \cdots + x_d^2}$ and $\theta_d = \arctan(r_{d-1}/x_d) \in [0, \pi]$. Thus

$$\begin{aligned} x_d &= r_d \cos\theta_d\,, \\ x_{d-1} &= r_{d-1}\sin\theta_{d-1} = r_d \sin\theta_d \cos\theta_{d-1}\,, \\ &\vdots \\ x_3 &= r_3 \cos\theta_3 = r_d \sin\theta_d \ldots \sin\theta_4 \cos\theta_3\,, \\ x_2 &= r_d \sin\theta_d \ldots \sin\theta_3 \sin\theta_2\,, \\ x_1 &= r_d \sin\theta_d \ldots \sin\theta_2 \cos\theta_1\,. \end{aligned} \tag{B.1}$$

The parity transformation is given by $r_d \mapsto r_d$, $\theta_i \mapsto \pi - \theta_i$ for $3 \leq i \leq d$ and $\theta_2 \mapsto \pi + \theta_2$. The Laplace operator is

$$\nabla_d^2 = \frac{\partial^d}{\partial r_d^2} + \frac{d-1}{r_d}\frac{\partial}{\partial r_d} - \frac{\hat{\Lambda}_d^2}{r_d^2}\,, \tag{B.2}$$

where the square of the angular momentum operator for $d \geq 2$ is given by

$$\hat{\Lambda}_d^2 = -\frac{\partial^2}{\partial\theta_d^2} - (d-2)\cot\theta_d \frac{\partial}{\partial\theta_d} + \frac{1}{\sin^2\theta_d}\hat{\Lambda}_{d-1}^2, \quad \hat{\Lambda}_1^2 = 0 \,. \tag{B.3}$$

The angular eigenfunctions to $\hat{\Lambda}_2^2 = -\partial^2/\partial\theta_2^2$ can be chosen as $(1/\sqrt{2\pi})\exp(-\mathrm{i}l_2 s\theta_2)$, where l_2 is a non-negative integer and $s = \pm 1$ correspond to the two degenerate solutions related to angular momentum projections of opposite sign. Then the eigenvalues of $\hat{\Lambda}_2^2$ are l_2^2 and the parity of the eigenfunctions are $(-1)^{l_2}$.

For $d > 2$ we now assume the recursive form of the eigenfunction to be

$$Y^{(d)}_{l_d \ldots l_2, s}(\theta_d, \ldots, \theta_2) = f(\theta_d) Y^{(d-1)}_{l_{d-1} \ldots l_2, s}(\theta_{d-1}, \ldots, \theta_2) \,, \tag{B.4}$$

where $Y^{(d-1)}_{l_{d-1} \ldots l_2, s}(\theta_{d-1}, \ldots, \theta_2)$ is an eigenfunction of $\hat{\Lambda}_{d-1}^2$ with the eigenvalue $l_{d-1}(l_{d-1} + d - 3)$. We then get the eigenvalue equation and the solutions as

$$\left[-\frac{\partial^2}{\partial\theta_d^2} - (d-2)\cot\theta_d \frac{\partial}{\partial\theta_d} + \frac{l_{d-1}(l_{d-1} + d - 3)}{\sin^2\theta_d} \right] f(\theta_d) = \lambda f(\theta_d) \,, \tag{B.5}$$

$$f(\theta_d) = \sin^{l_{d-1}}\theta_d P_n^{((d-3)/2 + l_{d-1},\, (d-3)/2 + l_{d-1})}(\cos\theta_d) \,, \tag{B.6}$$

$$\lambda = (n + l_{d-1})(n + l_{d-1} + d - 2) = l_d(l_d + d - 2) \,, \tag{B.7}$$

where n is a non-negative integer and $l_d \equiv n + l_{d-1}$. The parity of this solution is $(-1)^n(-1)^{l_{d-1}} = (-1)^{l_d}$. Thus the eigenvalues of $\hat{\Lambda}_d^2$ are $l_d(l_d + d - 2)$, where l_d are non-negative integers, and the parity of the eigenfunctions are $(-1)^{l_d}$.

The complete set of (unnormalized) angular eigenstates in d dimensions are

$$\begin{aligned} Y_\nu(\Omega) &\equiv Y_{l_d, l_{d-1}, \ldots, l_2, s}(\theta_d, \ldots, \theta_2) \\ &= \exp(-\mathrm{i}sl_2\theta_2) \prod_{i=3}^{d} \sin^{l_{i-1}}\theta_i P^{((d-3)/2 + l_{i-1},\, (d-3)/2 + l_{i-1})}_{l_i - l_{i-1}}(\cos\theta_i) \,, \end{aligned} \tag{B.8}$$

where $l_d \geq l_{d-1} \ldots \geq l_2 \geq 0$ and $s = \pm 1$. The two quantum numbers of three dimensions lm $(l = l_3, m = sl_2)$, are in d dimensions generalized to $d-1$ quantum numbers $l\bar{m}$, where $l = l_d$ and $\bar{m} = (l_{d-1}, l_{d-2} \ldots, l_2, s)$.

The two angular momenta $\hat{l}_x$ and $\hat{l}_y$ associated with the Jacobi vectors $\boldsymbol{x}$ and $\boldsymbol{y}$ couple to a total angular momentum $\hat{L} = \hat{l}_x + \hat{l}_y$. For $d = 3$ the simultaneous eigenfunctions of $\hat{l}_x^2, \hat{l}_y^2$ and $\hat{L}^2$ are given by

$$[Y_{l_x}(\Omega_x) \otimes Y_{l_y}(\Omega_y)]_{LM} \equiv \sum_{m_x + m_y = M} C^{LM}_{l_x m_x l_y m_y} Y_{l_x m_x}(\Omega_x) Y_{l_y m_y}(\Omega_y) \,, \tag{B.9}$$

where $C^{LM}_{l_x m_x l_y m_y}$ are the Glebsch–Gordan coefficients.

For $d = 2$ the eigenfunctions of the two angular momentum operators $\hat{l}_x$ and $\hat{l}_y$ are $(1/\sqrt{2\pi})\exp(-\mathrm{i}s_x l_x\theta_x)$ and $(1/\sqrt{2\pi})\exp(-\mathrm{i}s_y l_y\theta_y)$, where l_x and l_y are non-negative integers and

s_x and s_y both are ± 1. The total angular wave function Ψ_A is an eigenfunction of $\hat{l}_x^2, \hat{l}_y^2$ and $\hat{L} = \mathrm{i}\partial/\partial\theta_x + \mathrm{i}\partial/\partial\theta_y$ (eigenvalue $s_x l_x + s_y l_y$), i.e.

$$\Psi_A = \frac{1}{2\pi}\exp(-\mathrm{i}s_x l_x\theta_x - \mathrm{i}s_y l_y\theta_y)$$
$$= \frac{1}{2\pi}\exp\left[-\mathrm{i}(s_x l_x + s_y l_y)\frac{1}{2}(\theta_x + \theta_y) - \mathrm{i}\frac{1}{2}(s_x l_x - s_y l_y)(\theta_x - \theta_y)\right]. \tag{B.10}$$

We can now assign the quantum numbers LS where $L = |s_x l_x + s_y l_y|$ and $S = \mathrm{sign}(s_x l_x + s_y l_y)$. For each $l_x \geq 0$, $l_y \geq 0$ and $L \geq 1$ there is a degeneracy of 2, $S = \pm 1$, corresponding to the same size of L. Thus, S plays the same role for $d = 2$ as the projection quantum number M for $d = 3$. For each $L = 0$ and $l_x, l_y \geq 1$ the degeneracy is still 2, namely arising from $s_x = -s_y = 1$ and $-s_x = s_y = 1$. These two states belong to the same eigenspace of the total angular momentum $\hat{L}$ and even rotationally invariant two-body potentials may therefore couple them. For $L = l_x = l_y = 0$ there is no degeneracy.

We can generalize Eq. (B.9) to $d > 3$, see [120] for details. The corresponding summations over the two sets of the $d-2$ projection quantum numbers, $\bar{m}_x$ and $\bar{m}_y$, each related to a partial angular momentum, then produce the state of total angular momentum quantum number L with $d-2$ projections $\bar{M}$.

Appendix C. Basic properties of two-body systems in *d* dimensions

The Schrödinger equation for two particles of masses m_1 and m_2 described by the relative coordinates $\boldsymbol{r}$ and interacting via a central potential $V(|\boldsymbol{r}|)$ is

$$\left[\frac{-\hbar^2}{2\mu}\sum_i \frac{\partial^2}{\partial x_i^2} + V(r) - E\right]\psi(\boldsymbol{r}) = 0\,, \tag{C.1}$$

where $\mu = m_1 m_2/(m_1 + m_2)$ and x_i is the ith component of the relative coordinate.

Expanding the wave function in angular momentum eigenfunctions gives

$$\psi(\boldsymbol{r}) = \sum_\nu \psi_\nu(r) Y_\nu(\Omega)\,, \tag{C.2}$$

where $\nu = (l_d, l_{d-1}, \ldots, l_2, s)$ and Ω are defined in Eq. (B.8). By use of Eqs. (B.2) and (B.7) we then obtain the equation

$$\left[-\frac{\partial^2}{\partial r^2} - \frac{(d-1)}{r}\frac{\partial}{\partial r} + \frac{l_d(l_d + d - 2)}{r^2} + \frac{2\mu}{\hbar^2}(V(r) - E)\right]\psi_\nu(r) = 0\,, \tag{C.3}$$

where we from now on shall use $l = l_d$ rather than ν to label the wave functions.

Introducing $R_l(r) \equiv r^{(1/2)(d-1)}\psi_l(r)$ leads to the equation

$$\left[\frac{\partial^2}{\partial r^2} - \frac{\frac{1}{4}(d-3)(d-1) + l(l+d-2)}{r^2} - \frac{2\mu}{\hbar^2}(V(r) - E)\right]R_l(r) = 0\,, \tag{C.4}$$

where the centrifugal barrier for $d = 2$ and $l = 0$ is *negative*.

Let us define the following moments of the potential:

$$I_l \equiv \int_{r_0}^{\infty} \mathrm{d}r\, |V(r)|r^{d-1+2l}\,. \tag{C.5}$$

The *maximum short-range angular momentum* l_{sh} is now defined as the maximum angular momentum l for which I_l exists and can be made arbitrarily small by increasing r_0 to a sufficiently large value. The potential is of short range if $l_{\mathrm{sh}} \geq 0$. For $l \leq l_{\mathrm{sh}}$ the effect on a plane wave from such potentials is small in the region $r > r_0$. For potentials falling of exponentially we must have $l_{\mathrm{sh}} = -\infty$. The definition of short range in [116] is equivalent to $l_{\mathrm{sh}} = \infty$.

Assuming that $V(r) = 0$ for $r > r_0$ we find for $E > 0$ that ψ_l is a linear combination of the Bessel functions $r^{(2-d)/2}J_{(d-2)/2+l}(kr)$ and $r^{(2-d)/2}Y_{(d-2)/2+l}(kr)$, where $k = \sqrt{2\mu E/\hbar^2}$. For $E = 0$ we get r^l and r^{2-l-d} (1 and $\ln r$ for $d = 2$, $l = 0$).

The *scattering length* $a^{(l)}$ is defined by $\psi_l(r)$ for large r for $E = 0$ by

$$\psi_l(r) \propto r^l\left(1 - \left(\frac{a^{(l)}}{r}\right)^{d-2+2l}\right), \quad \psi_0(r) \propto \ln\left(\frac{r}{a^{(0)}}\right) \quad \text{for } d = 2\,, \tag{C.6}$$

where $a^{(0)}$ is positive for $d = 2$. Thus, the scattering length is the node in the zero-energy wave function outside the potential. If $a^{(l)} \in]r_0, \infty[$ the zero-energy wave function has a node and the system must have at least one bound state with angular momentum l. If the system for $d = 2$ and $l = 0$ does not have any bound state, $a^{(0)}$ must be in the interval $[0, r_0]$. A more detailed discussion of scattering length and effective range for $d = 2$ can be found in [168].

The perturbative effect of the non-zero potential for $r > r_0$ is

$$\int_{r_0}^{\infty} \mathrm{d}r\, r^{d-1}|\psi_l(r)|^2 V(r)\,, \tag{C.7}$$

which diverges for $l > l_{\mathrm{sh}}$, see Eq. (C.6). However, if we assume $V(r) = 0$ for $r > r_0$, we redefine a short-range potential for all l. Then the scattering length $a^{(l)}$ looses any direct physical meaning as it diverges for $r_0 \to \infty$ when $l > l_{\mathrm{sh}}$.

A bound state of energy $E < 0$ must for $r > r_0$ have the wave function

$$\psi_l(r) = r^{(2-d)/2}K_{(d-2)/2+l}(\kappa r)\,, \tag{C.8}$$

where $\kappa = \sqrt{-2\mu E/\hbar^2}$ and K_ν is the modified Bessel function of the second kind. When $\kappa r_0 \ll 1$ the logarithmic derivatives of Eqs. (C.8) and (C.6) must for $d + 2l < 4$ approximately be equal at r_0, i.e.

$$E = -\frac{4\hbar^2}{2\mu a^{(l)2}}\left[\frac{\Gamma^2\left(l + \dfrac{d}{2}\right)\sin\left(\pi\left(l + \dfrac{d-2}{2}\right)\right)}{\pi\left(l + \dfrac{d-2}{2}\right)}\right]^{2/(d-2+2l)}, \tag{C.9}$$

which is valid for zero-range potentials with $r_0 \equiv 0$. For $d + 2l \geq 4$ the bound state energy depends on both $a^{(l)}$ and r_0.

Let us define a *zero-range* potential $V_0(r) = \lim_{t\to\infty} f(t)V(tr)$ as the limit of an arbitrary potential $V(r)$, where the function $f(t)$ is adjusted to maintain a constant scattering length independent of the parameter t. This limiting procedure in general only allows one constraint: the scattering length fully defining $V_0(r)$. The mean square radius for $l = 0$ and $d < 4$ is given by

$$\langle r^2\rangle = \frac{\int_0^\infty \mathrm{d}r\, r^{d+1}(r^{(2-d)/2}K_{(d-2)/2}(\kappa r))^2}{\int_0^\infty \mathrm{d}r\, r^{d-1}(r^{(2-d)/2}K_{(d-2)/2}(\kappa r))^2} = \frac{(4-d)d}{6}\frac{\hbar^2}{2\mu(-E)} \tag{C.10}$$

in the zero-range approximation. This expression is therefore more generally valid in the limit of very weakly bound systems, where $2\mu(-E)\hbar^{-2}r_0^2 \ll 1$. It is interesting that $\langle r^2\rangle$ as function of d has its minimum for $d = 2$.

References

[1] M.C. Gutzwiller, Rev. Mod. Phys. 70 (1998) 589.
[2] M.J. Holman, N.W. Murray, Astron. J. 112 (1996) 1278.
[3] H.A. Bethe, E.E. Salpeter, Quantum Mechanics of One- and Two-electron Atoms, Springer Verlag, Berlin, New York, 1957.
[4] J.M. Richard, Phys. Rep. 212 (1992) 1. **
[5] M.V. Zhukov, B.V. Danilin, D.V. Fedorov, J.M. Bang, I.J. Thomson, J.S. Vaagen, Phys. Rep. 231 (1993) 151. **
[6] W. Glöckle, H. Witala, D. Hüber, H. Kamada, J. Golak, Phys. Rep. 274 (1996) 107.
[7] J. Carlson, R. Schiavilla, Rev. Mod. Phys. 70 (1998) 743.
[8] C.D. Lin, Phys. Rep. 257 (1995) 1. **
[9] G. Tanner, K. Richter, J.M. Rost, Rev. Mod. Phys. 72 (2000) 497.
[10] J. Adamowski, B. Szafran, S. Bednarek, B. Stébe, Few-Body Systems 10 (Suppl.) (1998) 189.
[11] V.M. Efimov, Com. Nucl. Part. Phys. 19 (1990) 271. *
[12] A.S. Jensen, A. Cobis, D.V. Fedorov, E. Garrido, E. Nielsen, Few-Body Systems 10 (Suppl.) (1999) 19.
[13] K. Riisager, Rev. Mod. Phys. 66 (1994) 1105.
[14] P.G. Hansen, A.S. Jensen, B. Jonson, Ann. Rev. Nucl. Part. Sci. 45 (1995) 591.
[15] I. Tanihata, J. Phys. G 22 (1996) 157.
[16] B. Jonson, K. Riisager, Phil. Trans. R. Soc. Lond. A 356 (1998) 2063.
[17] B.D. Esry, C.D. Lin, C.H. Greene, Phys. Rev. A 54 (1996) 394. *
[18] F. Robicheaux, Phys. Rev. A 60 (1999) 1706. *
[19] Y. Li, C.D. Lin, Phys. Rev. A 60 (1999) 2009.
[20] D.V. Fedorov, A.S. Jensen, Phys. Rev. Lett. 71 (1993) 4103. ***
[21] A.S. Jensen, E. Garrido, D.V. Fedorov, Few-Body Systems 22 (1997) 193. **
[22] D.V. Fedorov, A.S. Jensen, Phys. Lett. B 389 (1996) 631. **
[23] E. Nielsen, D.V. Fedorov, A.S. Jensen, E. Garrido, The three-body problem with short-range interactions, preprint, IFA, University of Aarhus, 2000.
[24] R. Martin, J.M. Richard, T.T. Wu, Phys. Rev. A 52 (1995) 2557.
[25] J.M. Rost, J.S. Briggs, J. Phys. B 24 (1992) 4293. *
[26] J.M. Launay, M.Le. Dourneuf, J. Phys. B 15 (1982) L455.
[27] P. Honvault, J.M. Launay, Chem. Phys. Lett. 287 (1998) 270.
[28] J. Yuan, C.D. Lin, J. Phys. B 31 (1998) L637.
[29] T. Cornelius, W. Glöckle, J. Chem. Phys. 85 (1986) 3906.
[30] E. Nielsen, D.V. Fedorov, A.S. Jensen, J. Phys. B 31 (1998) 4085. ***
[31] T. Yamazaki, Few-Body Systems 10 (Suppl.) (1999) 151.
[32] Chi-Yu Hu, A.A. Kvitsinsky, Phys. Rev. A 46 (1992) 7301.
[33] L. Johannsen, A.S. Jensen, P.G. Hansen, Phys. Lett. B 244 (1990) 357. *

[34] J.M. Bang, I.J. Thompson, Phys. Lett. B 279 (1992) 201. **
[35] D.V. Fedorov, A.S. Jensen, K. Riisager, Phys. Rev. C 49 (1994) 201. *
[36] D.V. Fedorov, A.S. Jensen, K. Riisager, Phys. Rev. C 50 (1994) 2372. *
[37] D.V. Fedorov, A.S. Jensen, K. Riisager, Phys. Rev. Lett. 73 (1994) 2817. **
[38] S.K. Adhikari, A. Delfino, T. Frederico, L. Tomio, Phys. Rev. A 47 (1993) 1093.
[39] E. Nielsen, A.S. Jensen, D.V. Fedorov, Few-Body Systems 27 (1999) 15. ***
[40] E. Garrido, D.V. Fedorov, A.S. Jensen, Phys. Rev. C 53 (1996) 3159.
[41] L. Tomio, T. Frederico, A. Delfino, A.E.A. Amorim, Few-Body Systems 10 (Suppl.) (1999) 203.
[42] E. Garrido, D.V. Fedorov, A.S. Jensen, Nucl. Phys. A 650 (1999) 247. **
[43] K. Riisager, D.V. Fedorov, A.S. Jensen, Europhys. Lett. 49 (2000) 547. *
[44] J. Goy, J.-M. Richard, S. Fleck, Phys. Rev. A 52 (1995) 3511. *
[45] A.S. Jensen, K. Riisager, Phys. Lett. B 480 (2000) 39.
[46] V.M. Efimov, Phys. Lett. B 33 (1970) 563. **
[47] L.H. Thomas, Phys. Rev. 47 (1935) 903. **
[48] R.N. Barnett, K.B. Whaley, Phys. Rev. A 47 (1993) 4082.
[49] B.S. Pudliner, V.R. Pandharipande, J. Carlson, S.C. Pieper, R.B. Wiringa, Phys. Rev. C 56 (1997) 1720.
[50] J. Boronat, J. Casullera, Phys. Rev. B 59 (1999) 8844.
[51] D. Blume, M. Mladenović, M. Lewerenz, K.B. Whaley, J. Chem. Phys. 110 (1999) 5789.
[52] V.R. Pandharipande, Nucl. Phys. A 654 (1999) 157c.
[53] C.J. Joachain, Quantum Collision Theory, North-Holland Physics Publishing Company, Amsterdam, 1983.
[54] E. Garrido, D.V. Fedorov, A.S. Jensen, Phys. Rev. C 59 (1999) 1272. ***
[55] E. Garrido, E. Moya de Guerra, Nucl. Phys. A 650 (1999) 387.
[56] L.D. Faddeev, Sov. Phys. JETP. 12 (1961) 1014. **
[57] M.I. Haftel, T.K. Lim, J. Chem. Phys. 77 (1982) 4515.
[58] O.A. Yakubovsky, Yad. Fiz. 5 (1967) 1312 [Sov. J. Nucl. Phys. 5 (1967) 937.]
[59] Ch. Elster, W. Glöckle, Phys. Rev. C 55 (1997) 1058.
[60] S.P. Merkuriev, S.L. Yakovlev, Teor. Mat. Fiz. 56 (1984) 60 [Theor. Math. Phys. 56 (1984) 673]. **
[61] F. Ciesielsky, J. Carbonell, Phys. Rev. C 58 (1998) 58.
[62] N. Barnea, M. Viviani, Phys. Rev. C 61 (2000) 034003.
[63] E. Nielsen, D.V. Fedorov, A.S. Jensen, Phys. Rev. C 59 (1999) 554.
[64] A.A. Kvitsinsky, J. Carbonell, C. Gignoux, Phys. Rev. A 51 (1995) 2997.
[65] A.A. Kvitsinsky, C-Y. Hu, J.S. Cohen, Phys. Rev. A 53 (1996) 255.
[66] C.R. Chen, G.L. Payne, J.L. Friar, B.F. Gibson, Phys. Rev. 44 (1991) 50.
[67] E.A. Kolganova, A.K. Motovilov, Yad. Fiz. 62 (1999) 1253 [Phys. At. Nucl. 62 (1999) 1179.]
[68] B.V. Danilin, I.J. Thompson, J.S. Vaagen, M.V. Zhukov, Nucl. Phys. A 632 (1998) 383.
[69] L.V. Grigorenko, B.V. Danilin, V.D. Efros, N.B. Shul'gina, M.V. Zhukov, Phys. Rev. C 60 (1999) 044312.
[70] J.W. Humberston, P. van Reeth, M.S.T. Watts, W.E. Meyerhof, J. Phys. B 30 (1997) 2477.
[71] A. Kievsky, S. Rosati, M. Viviani, Phys. Rev. Lett. 82 (1999) 3759.
[72] A. Kievsky, M. Viviani, S. Rosati, Nucl. Phys. A 551 (1993) 241. ***
[73] M. Viviani, A. Kievsky, S. Rosati, Few-Body Systems 18 (1995) 25. **
[74] A. Kievsky, Few-Body Systems 10 (Suppl.) (1999) 27.
[75] J. Macek, J. Phys. B 1 (1968) 831. **
[76] B.L. Christensen-Dalsgaard, Phys. Rev. A 29 (1984) 470.
[77] Jz. Tang, S. Watanabe, M. Matsuzawa, Phys. Rev. A 46 (1992) 2437.
[78] A. Igarashi, I. Shimamura, Phys. Rev. A 58 (1998) 1166.
[79] L. Wolniewicz, J. Hinze, A. Alijah, J. Chem. Phys. 99 (1993) 2695.
[80] A. Igarashi, I. Toshima, Phys. Rev. A 50 (1994) 232.
[81] Y. Zhou, C.D. Lin, J. Phys. B 28 (1995) 4907.
[82] P.O. Fedichev, M.W. Reynolds, G.V. Shlyapnikov, Phys. Rev. Lett. 77 (1996) 2921.
[83] M. Lewerenz, J. Chem. Phys. 106 (1997) 4596.
[84] J.L. Bohn, B.D. Esry, C.H. Greene, Phys. Rev. A 58 (1998) 584.

[85] K.C. Engvild, Fusion Technol. 34 (1998) 253.
[86] E. Nielsen, D.V. Fedorov, A.S. Jensen, Phys. Rev. A 56 (1997) 3287. **
[87] D.V. Fedorov, A.S. Jensen, K. Riisager, Phys. Lett. B 312 (1993) 1.
[88] K. Riisager, A.S. Jensen, P. Møller, Nucl. Phys. A 548 (1992) 393. *
[89] E. Nielsen, A.S. Jensen, D.V. Fedorov, Few-Body Systems 10 (Suppl.) (1999) 277.
[90] E. Garrido, D.V. Fedorov, A.S. Jensen, Nucl. Phys. A 617 (1997) 153.
[91] A. Cobis, D.V. Fedorov, A.S. Jensen, J. Phys. G 23 (1997) 401. ***
[92] P.G. Hansen, A.S. Jensen, K. Riisager, Nucl. Phys. A 560 (1993) 85.
[93] K. Riisager, A.S. Jensen, Phys. Lett. B 301 (1993) 6.
[94] A.S. Jensen, D.V. Fedorov, K. Langanke, H.-M. Müller, in: M. de Saint Simon, O. Sorlin (Eds.), Int. Conf. ENAM 95, Edition Frontieres, 1995, p. 677. *
[95] A.S. Jensen, K. Riisager, Phys. Lett. B 264 (1991) 238.
[96] A.S. Jensen, K. Riisager, Nucl. Phys. A 537 (1992) 45.
[97] E. Garrido, A. Cobis, D.V. Fedorov, A.S. Jensen, Nucl. Phys. A 630 (1998) 409c.
[98] A. Cobis, D.V. Fedorov, A.S. Jensen, Phys. Rev. C 58 (1998) 1403. ***
[99] A. Cobis, D.V. Fedorov, A.S. Jensen, Phys. Rev. Lett. 79 (1997) 2411. *
[100] A. Cobis, D.V. Fedorov, A.S. Jensen, Phys. Lett. B 424 (1998) 1. *
[101] D.V. Fedorov, A. Cobis, A.S. Jensen, Phys. Rev. C 59 (1999) 554.
[102] E. Garrido, D.V. Fedorov, A.S. Jensen, Europhys. Lett. 36 (1996) 497.
[103] E. Garrido, D.V. Fedorov, A.S. Jensen, Europhys. Lett. 43 (1998) 386.
[104] E. Garrido, D.V. Fedorov, A.S. Jensen, Phys. Rev. C 58 (1998) R2654.
[105] E. Nielsen, D.V. Fedorov, A.S. Jensen, Phys. Rev. Lett. 82 (1999) 2844. ***
[106] S.J. Ward, J.H. Macek, S.Yu. Ovchinnikov, Phys. Rev. A 59 (1999) 4418.
[107] E. Nielsen, J. Macek, Phys. Rev. Lett. 83 (1999) 1566. ***
[108] D.R. Herschbach, J. Avery, O. Goscinsky, Dimensional Scaling in Chemical Physics, Kluwer Academic Publishers, Dordrecht, 1993.
[109] M. Dunn, D.K. Watson, Phys. Rev. A 59 (1999) 1109. *
[110] A. Gonzalez, Few-Body Systems 13 (1992) 105.
[111] G. Leibbrandt, Rev. Mod. Phys. 47 (1975) 849.
[112] L.M. Delves, Nucl. Phys. 9 (1959) 391; 20 (1960) 275.
[113] J. Raynal, J. Revai, Nuovo Cimento 68 (1970) 612. *
[114] S.I Vinitskii, S.P. Merkuriev, I.V. Puzynin, V.M. Suslov, Yad. Fiz. 51 (1990) 641 [Sov. J. Nucl. Phys. 51 (1990) 406].
[115] R.G. Littlejohn, K.A. Mitchell, Phys. Rev. A 58 (1998) 3705.
[116] A.A. Kvitsinsky, V.V. Kostrykin, J. Math. Phys. 32 (1991) 2802. **
[117] B.R. Johnson, J. Chem. Phys. 73 (1980) 5051.
[118] V.M. Efimov, Nucl. Phys. A 210 (1973) 157.
[119] P. Navrátil, B.R. Barrett, W. Glöckle, Phys. Rev. C 59 (1999) 611.
[120] M. Dunn, D.K. Watson, in: D.R. Herschbach, J. Avery, O. Goscinsky (Eds.), Dimensional Scaling in Chemical Physics, Kluwer Academic Publishers, Dordrecht, 1993, p. 375.
[121] Ya.A. Smorodinskii, V.D. Efros, Yad. Fiz. 17 (1973) 210 [Sov. J. Nucl. Phys. 17 (1973) 107]. **
[122] R.C. Whitten, F.T. Smith, J. Math. Phys. 9 (1968) 1103.
[123] D.V. Fedorov, E. Garrido, A.S. Jensen, Phys. Rev. C 51 (1995) 3052. ***
[124] A. Erdelyi, W. Magnus, F. Oberhettinger, F.G. Tricomi, Higher Transcendental Functions (Bateman Manuscript Project), McGraw-Hill, New York, 1953. **
[125] S.K. Adhikari, T. Frederico, I.D. Goldman, Phys. Rev. Lett. 74 (1995) 487.
[126] A.E.A. Amorim, L. Tomio, T. Frederico, Phys. Rev. C 56 (1997) R2378. *
[127] S.A. Vulgal'ter, G.M. Zhislin, Teor. Mat. Fiz. 55 (1983) 269 [Theor. Math. Phys. 55 (1983) 493.]
[128] T.K. Lim, P.A. Maurone, Phys. Rev. B 22 (1980) 1467.
[129] S.K. Adhikari, A. Delfino, T. Frederico, I.D. Goldman, L. Tomio, Phys. Rev. A 37 (1988) 3666.
[130] R.A. Aziz, M.J. Slaman, J. Chem. Phys. 94 (1991) 8047. *

[131] T. González-Lezana, J. Rubayo-Soneira, S. Miret-Artés, F.A. Gianturco, G. Delgado-Barrio, P. Villarreal, Phys. Rev. Lett. 82 (1999) 1648.
[132] W. Schöllkopf, J.P. Toennies, J. Chem. Phys. 104 (1996) 1155. *
[133] F. Lou, C.F. Giese, W.R. Gentry, J. Chem. Phys. 104 (1996) 1151. *
[134] C.A. Parish, C.E. Dykstra, J. Chem. Phys. 101 (1994) 7618.
[135] I. Roeggen, J. Almlöf, J. Chem. Phys. 102 (1995) 7095.
[136] A. Griffin, D.W. Snoke, S. Stringari (Eds.), Bose–Einstein Condensation, Cambridge University Press, Cambridge, 1995.
[137] Ph. Courteille, R.S. Freeland, D.J. Heinzen, F.A. van Abeelen, B.J. Verhaar, Phys. Rev. Lett. 81 (1998) 69.
[138] J. Stenger, S. Inouye, M.R. Andrews, H.J. Miesner, D.M. Stamper-Kurn, W. Ketterle, Phys. Rev. Lett. 82 (1999) 2422.
[139] E. Nielsen, B.D. Esry, submitted for publication.
[140] P.M.M. Maessen, T.A. Rijken, J.J. de Swart, Phys. Rev. C 40 (1989) 2226.
[141] I. Tanihata, H. Hamagaki, O. Hashimoto, Y. Shida, N. Yoshikawa, K. Sugimoto, O. Yamakawa, T. Kobayashi, Phys. Rev. Lett. 55 (1985) 2676.
[142] P.G. Hansen, B. Jonson, Europhys. Lett. 4 (1987) 409. **
[143] C.A. Bertulani, G. Baur, Nucl. Phys. A 480 (1988) 615.
[144] E. Garrido, D.V. Fedorov, A.S. Jensen, Phys. Lett. B 480 (2000) 33.
[145] E. Garrido, D.V. Fedorov, A.S. Jensen, Europhys. Lett. 50 (2000) 735.
[146] T. Kobayashi, O. Yamakawa, K. Omata, K. Sugimoto, T. Shimoda, N. Takahashi, I. Tanihata, Phys. Rev. Lett. 60 (1988) 2599.
[147] G. Audi, A.H. Wapstra, Nucl. Phys. A 595 (1995) 409.
[148] B.M. Young et al., Phys. Rev. Lett. 71 (1993) 4124.
[149] B.M. Young et al., Phys. Rev. C 49 (1994) 279.
[150] S.N. Abramovich, B.Ya. Guzhovskij, L.M. Lazarev, Phys. Part. Nucl. 26 (1995) 423.
[151] J.A. Caggiano, D. Bazin, W. Benenson, B. Davids, B.M. Sherill, M. Steiner, J. Yurkon, A.F. Zeller, B. Blank, Phys. Rev. C 60 (1999) 064322.
[152] E. Garrido, D.V. Fedorov, A.S. Jensen, Phys. Rev. C 55 (1997) 1327.
[153] G.F. Bertsch, K. Hencken, H. Esbensen, Phys. Rev. C 57 (1998) 1366.
[154] L.V. Chulkov, B.V. Danilin, V.D. Efros, A.A. Korsheninnikov, M.V. Zhukov, Europhys. Lett. 8 (1989) 45.
[155] I. Tanihata et al., Phys. Lett. B 287 (1992) 307.
[156] B.D. Esry, private communication, 1999.
[157] R.G. Newton, Scattering of Waves, Particles, Springer-Verlag, New York, 1982.
[158] J.R. Taylor, Scattering Theory, Wiley, New York, 1972 (Chapter 20).
[159] F. Ajzenberg-Selove, Nucl. Phys. A 490 (1988) 1.
[160] A. Cobis, Ph.D. Thesis, IFA, University of Aarhus, 1997.
[161] J.H. Macek, S.Yu. Ovchinnikov, Phys. Rev. A 54 (1996) 544. ***
[162] R.K. Janev, J. Pop-Jordanov, E.A. Solov'ev, J. Phys. B 30 (1997) L353.
[163] R.E. Langer, Phys. Rev. 51 (1937) 669.
[164] L.D. Landau, E.M. Lifschitz, Quantum Mechanics, 3rd Edition, Pergamon Press, Oxford, 1977 (Chapter VII).
[165] H. Friedrich, J. Trost, Phys. Rev. A 59 (1999) 1683.
[166] S. Inouye, M.R. Andrews, K. Stenger, H.J. Miesner, D.M. Stamper-Kurn, W. Ketterle, Nature 392 (1998) 151.
[167] B.D. Esry, C.H. Greene, Y. Zhou, C.D. Lin, J. Phys. B 29 (1996) L51.
[168] B.J. Verhaar, J.P.H.W. van den Eijnde, M.A.J. Voermans, M.M.J. Schaffrath, J. Phys. A 17 (1984) 595.